Reconstructing Late Quaternary environmental change on the southern Cape coast of South Africa: A 30,000-year geochemical record from Pearly Beach

WITS UNIVERSITY

100 1922 2022

Rachel Tess Mey

Supervisors: Prof Marc Humphries and Dr. Lynne Quick

Dissertation submitted in fulfilment of the academic requirements for the degree of Master of Science

School of Chemistry

University of the Witwatersrand, Johannesburg

November 2023

Declaration

I declare that this thesis is my own, unaided work. It is being submitted for the Degree of Master of Science at the University of the Witwatersrand, Johannesburg. It has not been submitted before for any degree or examination at any other University.

R. Mey

2 November 2023

Abstract

The southern Cape coast of South Africa has undergone complex and dynamic climate changes due to its position at the boundary of major atmospheric and oceanic systems. However, climate changes that occurred in the region during the Last Glacial Maximum (30,000 – 18,000 cal yr BP) and the deglaciation period that followed (18,000 – 11,000) are still not fully understood. Climatic change along the southern Cape coast is of archaeological, cultural and environmental significance given the ecological diversity and hominin fossil richness of the region. Moreover, predictions of future climate change and water scarcity management issues in the southern Cape make it vital to understand and response to future climate scenarios.

To address this gap, this study investigated the geochemical composition of a 5.42 m sediment record (KSV-1) extracted from a freshwater coastal wetland near Pearly Beach on the southern Cape coast. The wetland, situated in the winter rainfall zone, is influenced by the southern westerly storm track, the South Atlantic anticyclone, and Agulhas-Benguela interactions, making it an ideal location to investigate changes to large-scale atmospheric and oceanic circulation systems. Using a combination of inorganic elemental (X-ray fluorescence, XRF) and stable carbon isotope ($\delta^{13}C$) analysis, this study presents a 30,000 year record of palaeoenvironemental change from Pearly Beach and considers these in relation to broad-scale climatic perturbations that occurred in southern Africa over this period.

A chronology for the core was derived from radiocarbon dating of 8 bulk sediment samples. Sedimentation rates over the record averaged 0.02 cm/yr, giving the XRF analyses which were conducted at 2 cm intervals, an average temporal resolution of ~ 110 years. Sediments deposited 30,000 – 15,000 cal yr BP consist primarily of quartz-rich (60 – 90% SiO_2) silt and fine sand with relatively low quantities of clay material. An increase in the relative proportion of Al_2O_3 from ~15,000 cal yr BP, coupled with a rise in sedimentation rate, marks an increase in the accumulation of fine-grained material within the wetland that is associated with a rise in global sea levels following deglaciation. A distinct shift to higher $\delta^{13}C$ values around this time points to a change in vegetation community, with an increase in contribution from C_4 drought-tolerant plants. The presence of calcium carbonate in sediments provides a strong indicator for marine intrusions at site and a pronounced increase in marine influence is inferred from ~8,500 cal yr BP, corresponding with the stabilisation of sea levels near to present-day levels.

Variations in elements typically associated with heavy minerals (titanium and zirconium) are used to infer changes in depositional energy at the site. Enrichments in Ti and Zr suggest a period of enhanced transport energy between 18,800 and 14,500 cal yr BP. This is coupled with an increase in the Si/Al ratio and linked to enhanced aeolian activity. An increase in wind intensity during this period is attributed to the intensification in the Southern Hemisphere westerly winds at this time. This corresponds with available fossil pollen records, which suggest an increase in moisture at Pearly Beach 18,500 to 15,000 cal yr BP that was possibly linked to a slowdown in the Atlantic Meridional Overturning Circulation (AMOC) and build-up of heat in the southeast Atlantic. It is possible that a build-up of heat in the southeast Atlantic brought on by a slowdown in the AMOC increased moisture uptake in the frontal storms, resulting in stronger low-pressure systems and intensified storms, as reflected in the KSV-1 record. Comparisons with other records from South Africa, including Mfabeni, Cold Air Cave and Cango Caves, indicate that the central and eastern parts of the country experienced a cooling event ~18,500 and 14,500 cal yr BP. New geochemical data from Pearly Beach suggests that this cooling may have been linked to intensification of westerly winds at this time. An apparent lag effect in the warming of South Africa after deglaciation may be attributed to the enhanced influence of westerly winds during the glacial-interglacial period, which pushed cold air masses across the interior of the country. The complex interplay between local sea level changes, westerly wind dynamics, and regional climatic conditions underscores the significance of the geochemical record from Pearly Beach in understanding past environmental changes and their broader implications for southern Africa.

Acknowledgements

Firstly, I would like to thank my supervisor Prof Marc Humphries for his guidance, support, and expertise throughout my research journey. His insights have been instrumental in shaping my understanding of the field. I am immensely grateful for his mentorship throughout this journey, fuelling my passion for Palaeostudies and growth in research. I would also like to extend my sincere appreciation to my co-supervisor, Dr. Lynne Quick for her valuable input and continuous support during the course of this study. Her expertise and feedback have been invaluable to the success of my research. I would also like to thank the members of the Enviro-Geochem research group for their collaboration, discussions, and moral support. Their input has enriched my work and broadened my perspective.

I would like to thank PAST (Paleontological Scientific Trust) for providing the necessary funding that enabled me to carry out this research. Their support has been crucial in facilitating the completion of my MSc thesis.

I would like to acknowledge and thank Nelson Mandela University Palaeoecology Laboratory for their work in splitting and subsampling the core for analysis. A huge thanks to Queens University for conducting the age analysis used in this study. I also would like to extend my gratitude to Stellenbosch University for their assistance in the isotope analysis conducted as part of my research.

To my friends and family, thank you for your encouragement and support throughout my academic pursuits. Your unwavering belief in my abilities has been a driving force behind my achievements.

I would lastly like to express my heartfelt gratitude to Mitchell for his unwavering support, patience, and understanding throughout all of my endeavours and this challenging, but rewarding journey. Your encouragement and belief in me have been a constant source of motivation.

I am deeply indebted to all the individuals and organizations mentioned above. Their contributions have been instrumental in shaping the outcomes of my research and academic journey.

Table of Contents

List of figures

List of tables

Chapter 1: Introduction

The southern Cape coast experiences a complex and dynamic climate due to its location at the convergence of major oceanic (the cold Benguela and the warm Agulhas currents) and atmospheric (South Atlantic Anticyclone, Subtropical Indian Anticyclone, southern westerlies, and subtropical easterlies) systems (Tyson and Preston-Whyte, 2000; Chase and Meadows, 2007). As a result, the region exhibits pronounced spatial and temporal climatic variations. Palaeoenvironemental studies play a crucial role in helping to develop climate models for past environmental change (e.g., Barrable et al., 2002; Holmgren et al., 2003; Chase and Meadows, 2007; Chevalier and Chase, 2015; Chase et al., 2015a, 2015b, 2017; Hahn et al., 2017; Chase and Quick, 2018; Engelbrecht et al., 2019), which serve to deepen our understanding of the climate systems in southern Africa and the driving forces behind them. This is especially important in southern Africa, where water scarcity is already a pressing issue (Donnenfeld et al., 2018). Moreover, southern Africa boasts diverse ecosystems that contain some of the world's most biodiverse flora, including ecological hotspots such as the Cape Floristic Region (Campbell, 1986; Cowling et al., 1988; Myers et al., 2000). Palaeoclimate data can provide insight into ecosystem responses to climate variations, aiding the development of conservation strategies to safeguard species richness and investigate ecosystem evolution (Cowling, 1990; Midgley et al., 2002). Additionally, southern Africa is home to numerous important archaeological sites, including Die Kelders (Avery, 1997), Pinnacle Point (Cawthra et al., 2019), Klassies River (Thackeray, 1988), Blombos Cave (Jacobs et al., 2006), and Nelson Bay Cave (Deacon, 1978), which hold valuable clues about the physical and behavioural evolution of modern humans (Marean et al., 2007).

The Quaternary period (2.58 Mya – present) represents a recent geological epoch characterized by pronounced climate variability and significant climate change (Gibbard and Cohen, 2008). Understanding the environmental shifts and interactions between the atmosphere, hydrosphere, and biosphere during this period is crucial as they serve as the closest analogues to present-day climates. In southern Africa, the availability of records extending beyond the Holocene is limited, with many records displaying discontinuities or lacking sufficient age-control (Chase and Meadows, 2007). Furthermore, long-term records from the winter rainfall zone (WRZ, *Sensu* Chase and Meadows, 2007) of the country predominantly focus on mountainous regions within the Cederberg and Swartbert (e.g., Chase et al., 2011, 2013; Valsecchi et al., 2013; Chase et al., 2015a, 2017, 2019a).

A variety of archives have been utilized to gain valuable insights into the climate history of southern Africa. These include the use of speleothems (Talma and Vogel, 1992; Bar-Matthews, 2010; Braun et al., 2019, 2020), rock hyrax middens (Quick et al., 2011; Chase et al., 2012, 2013, 2020), archaeological fossils (Faith et al., 2018; Sealy et al., 2020), and sedimentary cores (du Plessis et al., 2020; Humphries et al., 2020; Hahn et al., 2021; Quick et al., 2021). Sediment cores serve as valuable palaeoclimate archives, enabling the study of multiple proxies such as pollen, diatoms, foraminifera, microcharcoal, stable isotopes, and elemental geochemistry (Quick et al., 2021; Kirsten and Meadows, 2016; Kirsten et al., 2018; Humphries et al., 2020). These multi-proxy analyses provide nuanced insights into past climates and vegetation dynamics (Franke et al., 2020). Despite the arid climate of southern Africa limiting the availability of suitable sites (Chase et al., 2010), wetlands, peats, and lakes have proven to be useful palaeoclimate archives for sedimentary cores

(Wündsch et al., 2018; Humphries et al., 2019; Strobel et al., 2019; Humphries et al., 2020; du Plessis et al., 2020; Quick et al., 2021). Several studies have used geochemistry to infer information on transport processes (e.g., Humphries et al., 2017; Strobel et al., 2019), hydrological balances (e.g., Wündsch et al., 2016, 2018; Humphries et al., 2019, 2020), and chemical weathering of the study site (e.g., Norström et al., 2018; Hahn et al., 2021; Miller et al., 2020).

Stable isotope data from the organic fraction of sediment cores has been widely used for palaeoclimate studies (e.g., Carr et al., 2015; Baker et al., 2017; Norström et al., 2018; Kirsten et al., 2020). Organic matter from terrestrial and aquatic sources are deposited into wetlands and retain information of depositional conditions (Meyers, 2003). The concentration of total organic carbon (TOC), ^{13}C and ^{15}N signals, as well as the C/N ratio can be used to infer intra and extra basin productivity and to distinguish between sources of organic matter (Carr et al., 2015; Baker et al., 2017; Norström et al., 2018; Kirsten et al., 2020).

In this study, elemental and organic geochemical analysis of a sediment core retrieved from a wetland situated on the southern Cape coast is used to examine environmental changes that occurred in the region over the past 30,000 years. The study site is located on the Agulhas Plain, a large coastal plain stretching from Gansbaai to Struisbaai (Fig. 1A; Kraaij et al., 2009). The Agulhas Plain experienced multiple sea-level fluctuations during the late Quaternary, shaping its present coastal morphology (Marker and Holmes, 2010). At the onset of the last interglacial, rising sea levels resulted in the submergence of a significant section of the Agulhas Plain (Compton, 2001). Sea level changes throughout the late Quaternary and Holocene have shaped the coastal landforms observed today (Cowling and Holmes, 1991) and contributed to the diverse geology and remarkable botanical diversity found in the region (Thwaites and Cowling, 1988). The Agulhas Plain supports various vegetation types, including fynbos, strandveld thicket, southern coastal forest, renosterveld, and coastal grasslands (Mucina and Rutherford, 2006).

Aims and Objectives:

This study aims to examine the geochemical composition of a 30,000-year sediment record extracted from a freshwater coastal wetland near Pearly Beach on the southern Cape coast. The site is situated in the winter rainfall zone and is strongly influenced by the southern westerly storm track, the South Atlantic anticyclone and Agulhas-Benguela interactions (Chase and Meadows, 2007). The site therefore offers the potential for investigating changes in the strength and position of these large-scale atmospheric circulation systems over the last glacial-interglacial transition (18,000 – 11,000 cal yr BP). The wetland has not previously been studied from a palaeoenvironemental perspective and builds on previous work conducted on a nearby wetland site by Quick et al. (2021) (Fig. 1B).

The study wetland (34°40’10.54’’S, 19°31’39.95’’E) is a shallow wetland system with an average water depth of ~1 m spanning an area of ~32,000 m^2. The system is slightly raised, ~2 – 3 m above sea level, and is shielded from the coastline, ~650 m away, by coastal dunes. The wetland is fed by the Haelkraal River and connects with the Atlantic Ocean via a small channel during significant wet seasons (Avery, 1974).

The main objectives of this study are to:

- Examine changes in sediment deposition and source using inorganic elemental analysis and stable isotopes (^{13}C, ^{15}N).
- Use the geochemical changes recorded in the sedimentary record to reconstruct palaeoenvironments at the site over the last 30,000 years.
- Place the results of this study into context by comparing palaeoenvironemental information from the site with other regional and global climate datasets.

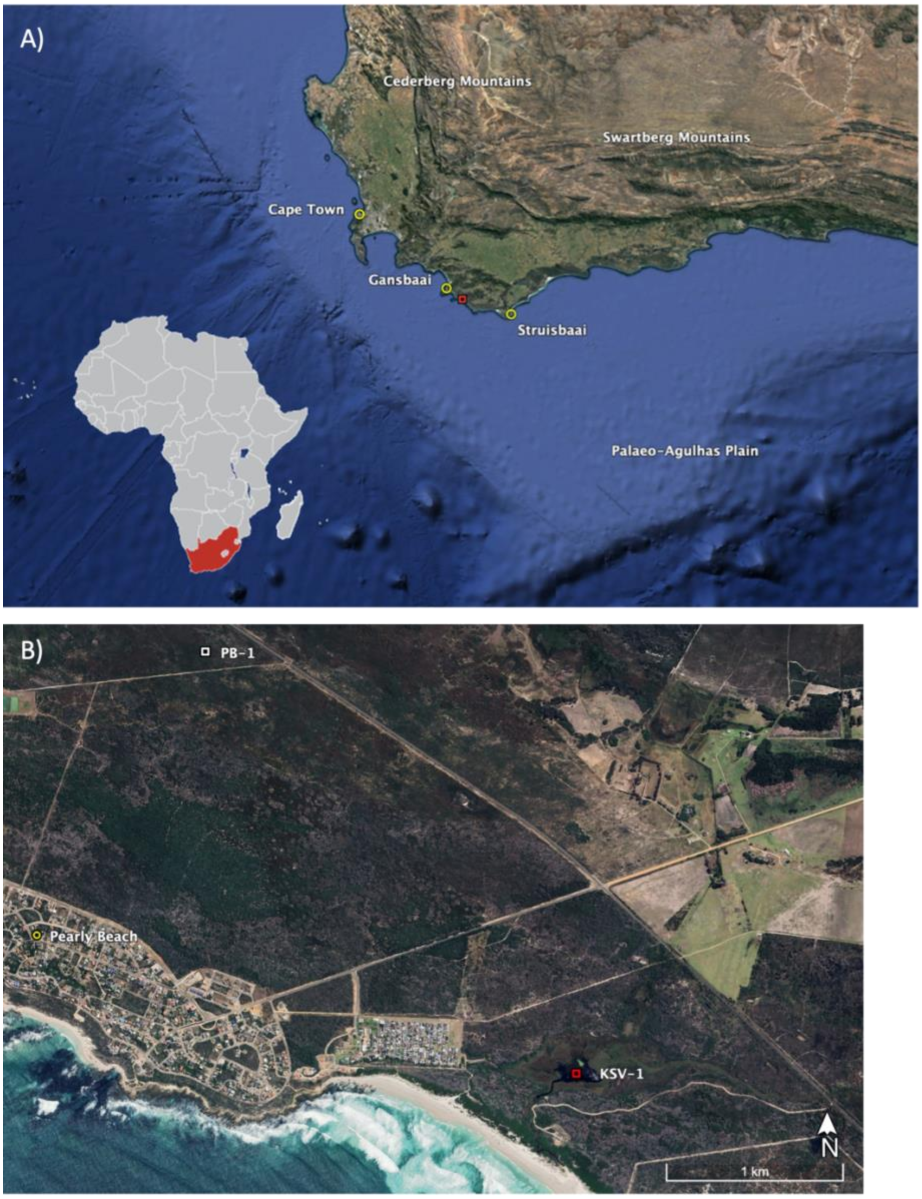

Figure 1: *A) A map of the study site (red square) situated along the southern Cape coast of South Africa, B) Location of the core site (KSV-1) in relation to a nearby pollen record, PB-1 (Quick et al., 2021).*

Chapter 2: Contemporary and Palaeo- Environmental Setting

The geological features, atmospheric patterns, and oceanic systems along the southern Cape coast have exerted substantial influence on the climatic variability and diverse vegetation found within the Agulhas Plain, as well as on the development and mobility of early humans (Myers et al., 2000; Cawthra et al., 2019; Marean et al., 2020). This chapter provides a brief overview of the Agulhas Plain, including its formation, contemporary geology, and vegetation. Furthermore, it outlines the characteristics of present-day climatic conditions and provides an overview of existing palaeoclimate studies.

2.1 Sea level change and development of the Agulhas Plain

The southern Cape coast is surrounded by a broad continental shelf that extends up to 250 km south of Cape Agulhas (Fig. 2a). This submerged continental shelf represents the Paleo-Agulhas Plain (PAP) which formed during the break-up of the supercontinent Gondwana, around 155 – 135 Myr ago (Marker and Holmes, 2010). The southern African coastline experienced down faulting and uplift during the later stages of Gondwana's fragmentation, leading to the formation of the Great Escarpment, which separates the interior plateau from the coastal platform (Partridge and Maud, 1987). The coastal platform was subsequently shaped during the hot and humid conditions of the Cretaceous Period, with further erosion of the Great Escarpment inland (Partridge and Maud, 1987; Marker and Holmes, 2010). During the Quaternary period, southern Africa has exhibited tectonic stability and changes in the Agulhas Plain during this time are primarily attributed to sea-level fluctuations (Partridge and Maud, 1987).

Features observed on the continental shelf primarily reflect the geological substrate and Pleistocene sea-level changes (Cawthra et al., 2015). From approximately 120,000 to 95,000 cal yr BP, sea levels similar to modern-day levels submerged the PAP (Fig. 2b). As sea levels receded between 95,000 and 45,000 cal yr BP, offshore sediment deposits became exposed, significantly extending the southern African coastline (Cowling and Holmes, 1991). The exposed continental shelf underwent erosion, and Pleistocene aeolianite was redistributed by wind and water. This period of low sea levels witnessed substantial aeolian deposition on the PAP (Cawthra et al., 2019). A major regression occurred at approximately 18,000 cal yr BP when sea levels dropped to around 120 - 130 meters below present-day levels, significantly expanding the coastal plain by a factor of five (Ramsay and Cooper, 2002; Compton, 2011; Marean et al., 2020). The exposure of the PAP during intervals between major regression events allowed for the development of fertile soils. During this time, it is believed that the PAP comprised of extensive floodplains and wetlands, in contrast to the infertile and undulating landscape of the modern-day Agulhas Plain (Cawthra et al., 2019). As sea levels rapidly rose during Termination I (starting from ~18,000 cal yr BP), the coastline migrated inland once again (Cooper et al., 2018). This led to the formation of various coastal features such as beaches, dunes, and estuaries. Over time, sand deposits were shaped by wind and wave action, resulting in distinct parallel dune cordons primarily formed by the prevailing westerly winds (Cawthra et al., 2019).

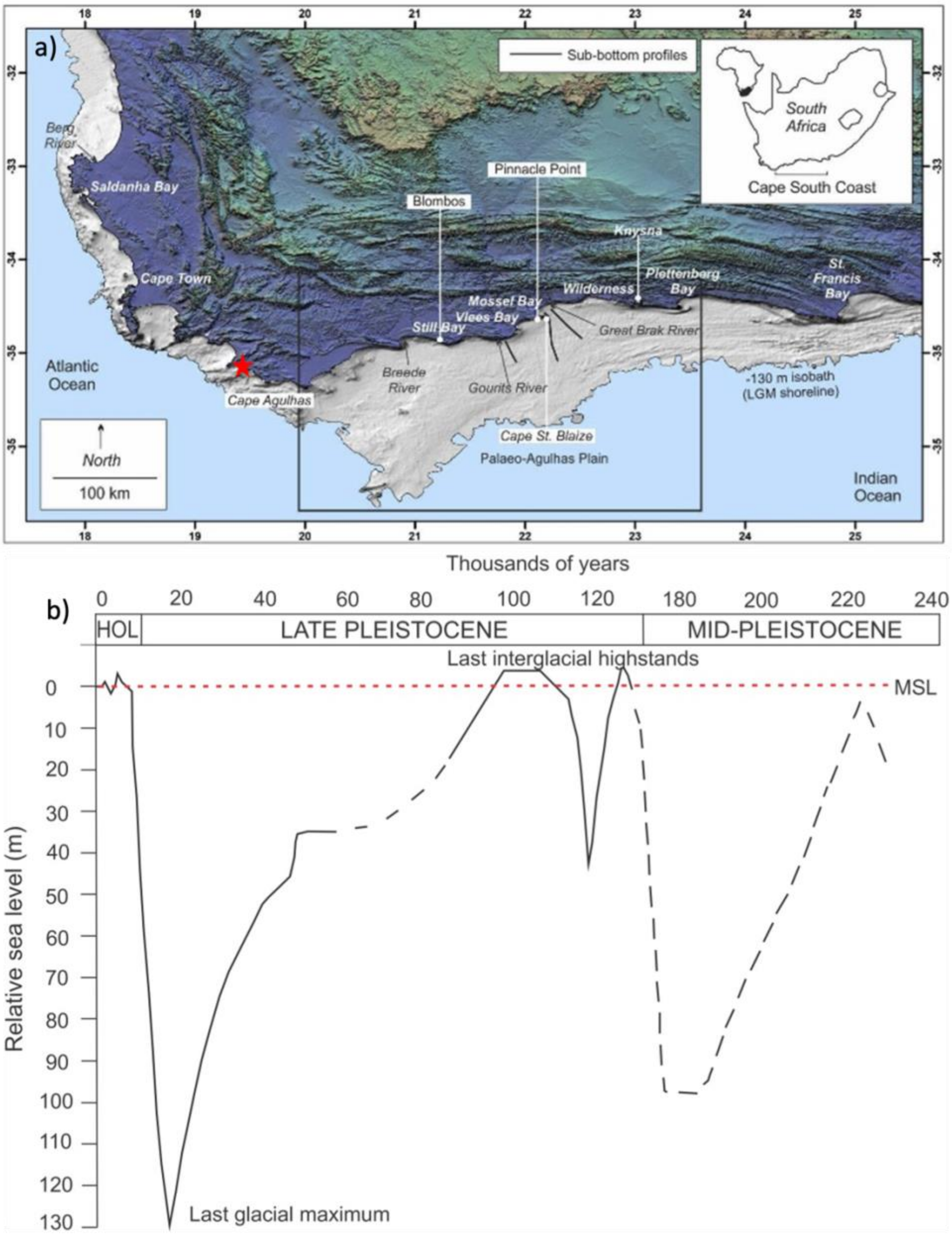

__Figure 2:__ a) A map showing the extent of the Palaeo-Agulhas Plain with the study site shown by a red star (from Cawthra et al., 2020) b) Relative sea level changes over the last 240,000 years (Ramsey and Cooper, 2002).

2.2 Geology and vegetation of the Agulhas Plain

The complex history of the Agulhas Plain has resulted in a geologically diverse region, contributing to the vast floral biodiversity in the region (Thwaites and Cowling, 1988). The predominant rock groups within the southern Cape coastal region fall under the Cape and Karoo Supergroups (Miller, 2020). The uplift and erosion of Malmesbury Group rocks, along with granitic intrusions of Igneous Cape Granite Suite during the Precambrian Era, resulted in Cape Supergroup sedimentary rocks being deposited in a passive margin basin during the Paleozoic Era (Partridge and Maud, 2000). The Cape Supergroup comprises the Table Mountain, Bokkeveld, and Witteberg Groups, which formed during the Paleozoic Era (Fig. 3; Marker and Holmes, 2010).

The Agulhas Plain is characterized by the presence of Bredasdorp limestone and Table Mountain sandstone and quartzites (Malan, 1989). The low mountains and coastal ridges, derived from the Table Mountain Group rocks are acidic and highly infertile (Cowling and Holmes, 1991). On the narrow coastal plain (1.5 – 5 km wide), the Bredasdorp Group limestones unconformably overlie the Cape Supergroup and consist of limestones, calcarenites, calcirudites, conglomerates, coquinites, and calcareous sandstones (Malan, 1989). The coastal plain consists of rocky and sandy beaches, backed by sand dunes (Heydorn and Tinley, 1980; Tinley, 1985). These Quaternary dunes are composed of unconsolidated aeolian calcareous quartz and shelly sand (Cawthra et al., 2020). These soils are poorly developed alkaline sands, which exhibit moderate fertility under thicket and forest vegetation (Cowling and Holmes, 1991). Inland of these dunes is a sandy, flat coastal plain scattered with vleis (seasonally flooded depressions) and pans (shallow, temporary lakes), representing the youngest identifiable surfaces. These soils are duplex, with alluvial or colluvial acidic topsoils overlaying residual or transported clays (Cowling and Holmes, 1991).

Limestone formations of the Bredasdorp Group, which are also from the Paleozoic era, form distinct relief features along the coast, with calcareous sands covering the bedrock (Cowling and Holmes, 1991). Limestone hills surround the coastal plain and rise to a maximum of 500 m above the coastal plain and have vertical cliff faces with a range of slope and aspect combinations (Cowling and Bond, 1991). Surrounding the limestone hills are colluvial sands, creating weakly acidic and infertile soils (Cowling and Holmes, 1991). A series of small limestone outcrops occur which are lanceolate in shape with the long axis running north to south. Outcrops of siliceous ferricrete can also be found across the Agulhas Plain (Cowling and Holmes, 1991). Inland of these mountains are fertile undulating plains (Cowling and Witkowski, 1994). The broad valleys and surfaces between the mountain ridges are underlain by Bokkeveld Group Shales which have non-hydromorphic and duplex soils. These are overlain by an acidic topsoil and a sodic, clayey B horizon (Cowling and Holmes, 1991).

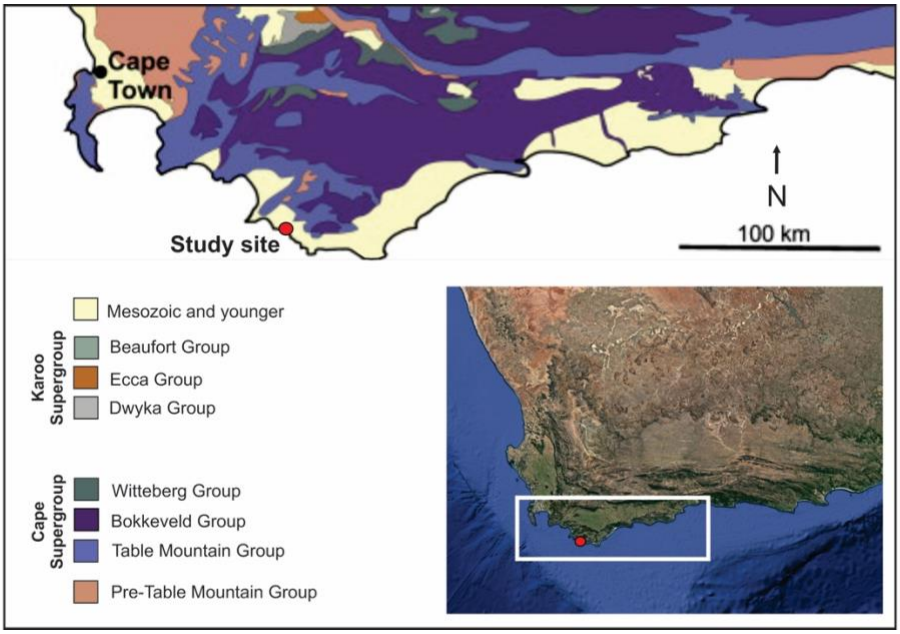

***Figure 3**: The geological setting of the study site in the southern Cape coastal Plain (Flint et al., 2011)*

The Agulhas Plain holds significant botanical importance as part of the Cape Floristic Region (CFR) (Campbell, 1986; Cowling et al., 1988). The dominant vegetation types in the area include fynbos (including limestone fynbos, sand fynbos, sandstone fynbos), shrublands, and renosterveld (Goldblatt, 1997; Cowling et al., 1988; Musina & Rutherford, 2006).

Edaphic factors, particularly soil characteristics, play a crucial role in shaping the vegetation of the Agulhas Plain. Limestone fynbos is endemic to the alkaline soils of the Bredasdorp Group limestones and aeolianites (Thwaites and Cowling, 1988). Asteraceous, restoid, and proteid fynbos species dominate the limestone fynbos community (Mucina and Rutherford, 2006). Limestone fynbos is typically found in patches within sand fynbos areas, surrounded by thicket vegetation (Mucina and Rutherford, 2006). Sand fynbos, the largest group of fynbos in the Agulhas region, thrives in weakly acidic and infertile soils, as well as in colluvial sands surrounding the limestone hills (Cowling, 1990). The distribution of sand fynbos and thicket vegetation is influenced by fire frequency and the topography of the coastal dunes (Thwaites and Cowling, 1988). Strandveld thicket consists of a mosaic of asteraceous or restoid fynbos and subtropical thicket, found on the calcareous coastal dunes of the Agulhas Plain (Cowling et al., 1988). Sandstone fynbos occurs in high-relief areas of the plain, where coarse-grained, nutrient-poor substrates derived from Table Mountain Group sandstones are present (Cowling, 1990). Dune fynbos thrives on deep, well-drained, alkaline sands of dune ridges (Cowling, 1990). Coastal forest is sparsely distributed along the coast, growing on nutrient-rich sandy soils overlaying Bredasdorp aeolianite or limestone (Mucina and Rutherford, 2006). Renosterveld, a non-fynbos shrubland, occurs on moderately fertile clays and silts derived from the Malmesbury and Bokkeveld Groups (Low and Rebelo, 1966). Additionally, thicket and coastal grasslands can be found along the coast and in low-lying areas of the Agulhas Plain, respectively (Mucina and Rutherford, 2006).

2.3 Contemporary climate and climatic drivers

Southern Africa can be divided into three zones according to modern day rainfall seasonality (Tyson, 1986). The summer rainfall zone (SRZ) receives more than 66% of its precipitation during the austral summer months (October – March) and the winter rainfall zone where 66% of its precipitation occurs in the austral winter months (April – September) (Fig. 4; Chase and Meadows, 2007). Found in between these two regions is a zone where precipitation is received during both summer and winter seasons, this is referred to as the year-round or aseasonal rainfall zone (YRZ or ARZ, Chase and Meadows, 2007).

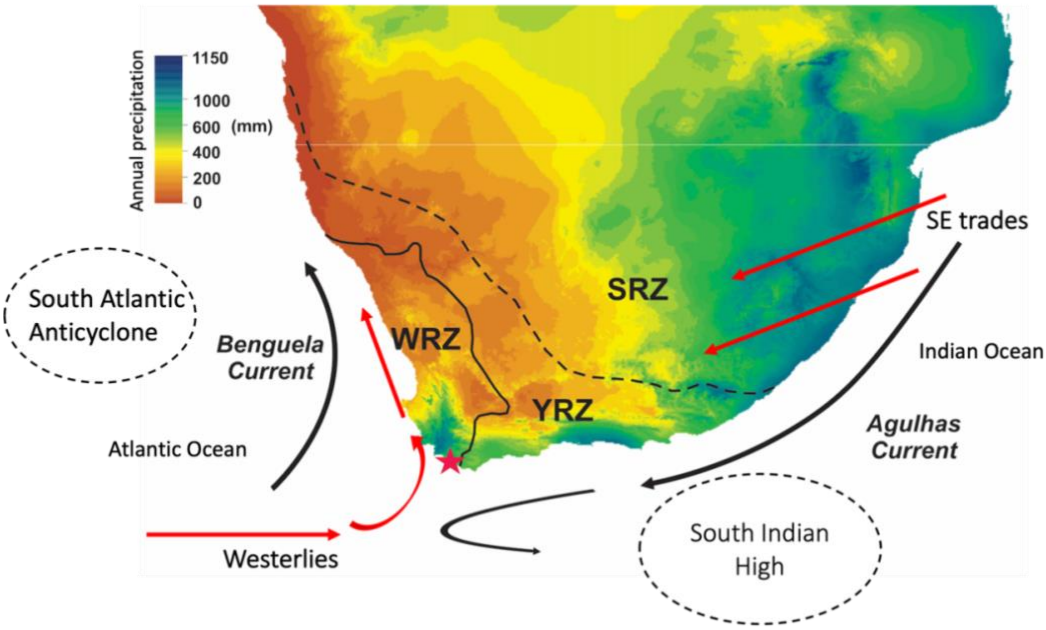

Figure 4: *Map of the modern rainfall zones and climate drivers of southern Africa during Austral summer months in relation to the study site (red star)*

The winter rainfall zone (WRZ), located in the west and southwestern coast of southern Africa, exhibits a Mediterranean-type climate characterized by cool, wet winters and warm, dry summers (Tyson, 1986). The majority of rainfall in the WRZ is associated with low pressure systems embedded in the circumpolar westerly winds (Tyson, 1986). These systems, known as cold fronts, are characterized by distinctive cloud bands, backing winds, and changes in wind speeds, leading to increased precipitation and lower temperatures (Tyson and Preston-Whyte, 2000). Coastal lows, which are synoptic-scale features associated with the westerlies, are formed when air descends from the escarpment and moves onto the coastal platform, resulting in warm offshore adiabatic flow ahead of the system and cool onshore air behind it, often leading to light mist or drizzle (Tyson and Preston-Whyte, 2000). Another important synoptic-scale feature is the South Atlantic Anticyclone, which is associated with ridging anticyclones and blocking highs (Tyson, 1986). Ridging anticyclones extend from the South Atlantic Anticyclone and are found on the Agulhas Bank (Hunter, 1987). The South Atlantic Anticyclone influences the Southern Cape Coast by pushing cool, dry air towards the region during the austral summer months, resulting in dry and sunny conditions. In winter, this anticyclone shifts northwards, reducing its influence and allowing moisture from westerly frontal systems to reach the coastline (Kruger, 2004). At the southern tip of South Africa, the convergence of two major ocean currents, the cold Benguela Current and the warm Agulhas Current, plays a significant role in moisture availability and global ocean circulation (Scott and Lee-Thorp, 2004; Carr et al., 2006b; Kirsten, 2014). The Benguela Current, a cold ocean current flowing northwards along the west coast of southern Africa, brings cool, dry air to the southern Cape coast (Tyson, 1999). During the summer months when the Benguela Current is strongest, dry and sunny conditions prevail in the region due to upwelling of cold water. However, in winter, when the current weakens, warmer and more humid air can move into the region, leading to increased rainfall and cooler temperatures. Sea surface temperatures (SSTs) also play a role in atmospheric circulation, as warmer SSTs can create low-pressure areas and a pressure gradient that affects onshore or offshore winds, depending on continental pressures (Tyson, 1999). Additionally, the increased evaporation resulting from warmer SSTs contributes to increased moisture in the air and can lead to increased precipitation on the continent (Chase and Meadows, 2007).

The climate in the summer rainfall zone (SRZ) of southern Africa is primarily influenced by the South Indian Anticyclone, which is located over the southern Indian Ocean. This anticyclone leads to the divergence of air, inhibiting cloud formation and precipitation (Tyson and Preston-Whyte, 2000). During the austral summer, the South Indian Anticyclone moves eastwards, allowing moisture from the Agulhas Current to reach the continent (Kruger, 2004). As a result, the interior and east coast of the SRZ experience clear, dry winters and humid, wet summers (Tyson, 1986). Disturbances in the tropical easterlies, such as easterly waves and thermal low pressures, account for most of the precipitation received in the SRZ (Tyson and Preston-Whyte, 2000). These disturbances trigger tropical convection and the formation of the tropical rain belt, as well as an increase in warm moist air from the Indian Ocean (Reason et al., 2006). During the austral summer months, easterly flow is enhanced due to a southerly shift in the South Indian Anticyclone and the development of a semi-stationary low-pressure system over the continent, resulting in increased rainfall (Tyson and Preston-Whyte, 2000). The Agulhas Current, which flows southward along the east coast, transports warm, salty water at high velocities from the South Equatorial Current and the East Madagascar Current to the polar region (Lutjeharms et al., 2001). It is mainly driven by high-latitude climate mechanisms and wind stress curl between the westerlies and easterlies (Beal et al., 2011; Caley et al., 2011). The Agulhas Current provides a source of moisture, contributing to the humid conditions experienced along the south coast (Tyson, 1999). Leakage of this current system into the southeast Atlantic increases evaporation and moisture advection, resulting in localized precipitation systems along the southern Cape coast (Jury et al., 1993, 1997). The year-round rainfall zone (YRZ) receives precipitation from both the westerlies and easterlies and is influenced by the Kalahari Anticyclone, which blocks moisture from the interior during the austral winter months (Tyson, 1999; Scott and Lee-Thorp, 2004; Chase and Meadows, 2007). This anticyclone affects the rainfall patterns in the YRZ, leading to a more balanced distribution of precipitation throughout the year.

Interactions between the westerlies and the tropical easterlies or subtropical anticyclones in southern Africa are associated with southern meridional flow and the formation of tropical-temperate troughs (TTTs) (Chase and Meadows, 2007). Southern meridional flow occurs when the South Atlantic Anticyclone extends behind the westerly trough, creating a ridging anticyclone that produces southerly onshore airflow (Lindesay, 1998). This airflow pattern leads to rainfall along the coast and cold conditions during winter, with occasional snowfall on the Cape Fold Belt mountains (Tyson, 1999). During the austral summer, when tropical convergence is at its maximum, the interaction between the easterlies and westerlies can result in the formation of TTTs, which bring increased precipitation over the interior regions (Harrison, 1984). The occurrence and intensity of TTT events can be influenced by elevated sea surface temperatures (SSTs) in the southeast Atlantic and/or Indian Ocean. When SSTs are higher than normal, it can lead to a shift in the location of temperate and tropical systems, with a poleward (equatorward) shift of the temperate (tropical) systems. This enhanced interaction between the climate systems can increase the frequency and intensity of TTT events (Chase et al., 2015b).

2.4 Palaeoclimate studies

Long-term climate changes are significantly influenced by variations in orbital forcing through their impact on insolation (Knight, 2020). The amount and distribution of insolation is influenced by the tilt of the Earth's axis of rotation relative to its orbital plans (obliquity) and the direction of axial tilt (precession) (Kurtzbach, 1981; Kurtzbach et al., 2008). The combined effect of insolation and precession can cause significant changes in Earth's climate. For example, when Earth's axis is tilted more towards the sun, the Northern Hemisphere receives more solar radiation, which can lead to warmer summers and winters. Variations in solar insolation influence both oceanic and atmospheric climate drivers. For example, solar insolation controls the extent of Antarctic Sea ice, which influences the latitudinal position of the westerlies. The expansion of Antarctic Sea ice leads to an extension of the Antarctic vortex high pressure cell, which in turn shifts the westerlies equatorward and increases their influence on the southern Cape coast (Tyson and Preston-Whyte, 2000; Chase and Meadows, 2007; Mahlalela et al., 2019).

The Atlantic Meridional Overturning Circulation (AMOC) also plays a critical role in long-term climates. This system draws heat from the Southern Hemisphere into the North Atlantic thereby controlling southeast Atlantic SSTs (Broecker, 1988). During stadial events, there is reduced transport of ocean heat and a subsequent buildup of heat in the southern hemisphere, while interstadials are associated with an intensification in heat transport. This results in an alternating build-up and loss of heat in the Southern Hemisphere known as the bipolar seesaw (Broecker, 1988; Stocker, 1998; Stocker and Johnsen, 2003). The AMOC is thought to have been particularly sensitive to abrupt climate changes that occurred during the last ice age (Heinrich events), which released large amounts of freshwater into the North Atlantic Ocean. During Heinrich Stadial 1 (HS1 18,000 – 14,600 cal yr BP) evidence suggests there was an almost near shutdown of the AMOC (Broecker, 1998; McManus et al., 2004). A decrease in AMOC strength sees an increase in the southeast Atlantic SSTs, increasing moisture uptake of the westerlies as well as increasing Agulhas Current leakage and tropical influence in the region (Barker et al., 2009; Kim et al., 2003; Farmer et al., 2005).

Conventional explanations for climate changes in southern Africa since the Last Glacial (30,000 – 18,000 cal yr BP) proposed a coeval inverse relationship between summer and winter rainfall zones (van Zinderen Bakker, 1976; Tyson, 1986; Cockcroft et al., 1987; Chase and Meadows, 2007). This model suggests that during interglacial periods summer rainfall systems are more invigorated, while during glacial periods a northward shift of the westerlies would result in an intensified and expanded WRZ (Cockcroft et al., 1987). This led to the theory that an anti-phase relationship exists between the WRZ and SRZ, with the WRZ experiencing either cool and wet or warm and dry conditions, while the SRZ experienced cool and dry or warm and wet conditions (Tyson, 1986). Although initial data supported this paradigm, recent studies suggest more complex interactions between climate forcing mechanisms at varying spatial and temporal scales (e.g., Chase et al., 2017; Quick et al., 2021).

Recent studies (e.g., Chase et al., 2013; 2017; Chase and Quick, 2018; Chase et al., 2020) have further highlighted the subregional nature of climate change along the southern Cape coast. These studies demonstrate that climate changes can vary within small geographic areas, resulting in distinct climate subregions. The interaction between temperate and tropical circulation systems plays a significant role in shaping climate variability across the region. Key climate drivers, operating individually or in combination, influence climate patterns at different temporal scales, leading to unique climatic characteristics in the subregions. Understanding the interplay between these temperate and tropical systems is crucial for comprehending climate change dynamics. The complexity of climate change has been emphasized, with shifts in atmospheric circulation patterns and sea surface temperatures also contributing significantly to climate variability (Chase et al., 2020). The Agulhas Current, in particular, is a significant factor in shaping Holocene climate change, influencing sea surface temperatures, moisture availability, and atmospheric circulation patterns in the southern Cape (Chase and Quick, 2018). Changes in Southern Ocean sea surface temperatures and sea ice extent have substantial implications for climate variability, with sea surface temperatures, westerly wind systems, and shifts in atmospheric circulation driven by sea ice changes playing a significant role. The climate changes in the region are complex and multifaceted, requiring consideration of multiple climate drivers, their interactions, and spatial and temporal variability.

Paleoclimate studies in southern Africa have investigated various archives in hopes of understanding the history of southern Africa’s complex climate and mechanisms behind climate changes (Fig. 5). Rock hyrax (*Procavia capensis*) middens have provided some important long-term palaeo-records, particularly in the WRZ. Key hyrax midden sites include Pakhuis Pass (e.g., Scott and Woodborne, 2007; Chase et al., 2019a), De Rif (e.g., Chase et al., 2011, 2012, 2014, 2015a; Reason et al., 2006; Valsecchi et al., 2013; Zhao et al., 2016), and Seweweekspoort (Chase et al., 2017). Various archives found in caves are also widely used to look at climates spanning across the LGM and interglacial. These include records from Elands Bay Cave (e.g., Bovid tooth enamel (Stowe and Sealy, 2015) and pollen (Baxter, 1996)), Cango Caves (e.g., Speleothems (Talma and Vogel, 1992), and the Cold Air Caves (e.g., Stalagmites (Holmgren et al., 2003)). Sediment cores have also been useful in generating long-term records, extracting cores from wetlands and peatlands (e.g., Rietvlei-Still Bay (Quick et al., 2015), Vankervelsvlei (Strobel et al., 2019, Strobel et al., 2022), and Mfabeni (Baker et al., 2017; Miller et al., 2019; Fietz et al., 2023). It is important to note that sediment cores often contain hiatuses (e.g., Pearly Beach between 12,000 – 7800 cal yr BP, Rietvlei-Still Bay between 30,000 – 16,000 cal yr BP, and Vankervelsvlei between 28,000 – 8,000 cal yr BP) enhancing the need for continuous, long-term sediment records to be analysed (Quick et al., 2015; Strobel et al., 2019; Quick et al., 2021).

Several shorter records also exist providing valuable, high-resolution records for the WRZ and YRZ over the Holocene (11,000 cal yr BP - present). Such records include hyrax middens (e.g., Katbakkies Pass (Chase et al., 2015b), Seweweekspoort (Chase et al., 2013), Baviaanskloof (Chase et al., 2019b)), and sediment cores from coastal lakes (e.g., Verlorenvlei (Carr et al., 2015; Kirsten et al., 2020), Voëlvlei (Strobel et al., 2021), and Eilandvlei (Kirsten et al., 2018; Quick et al., 2018).

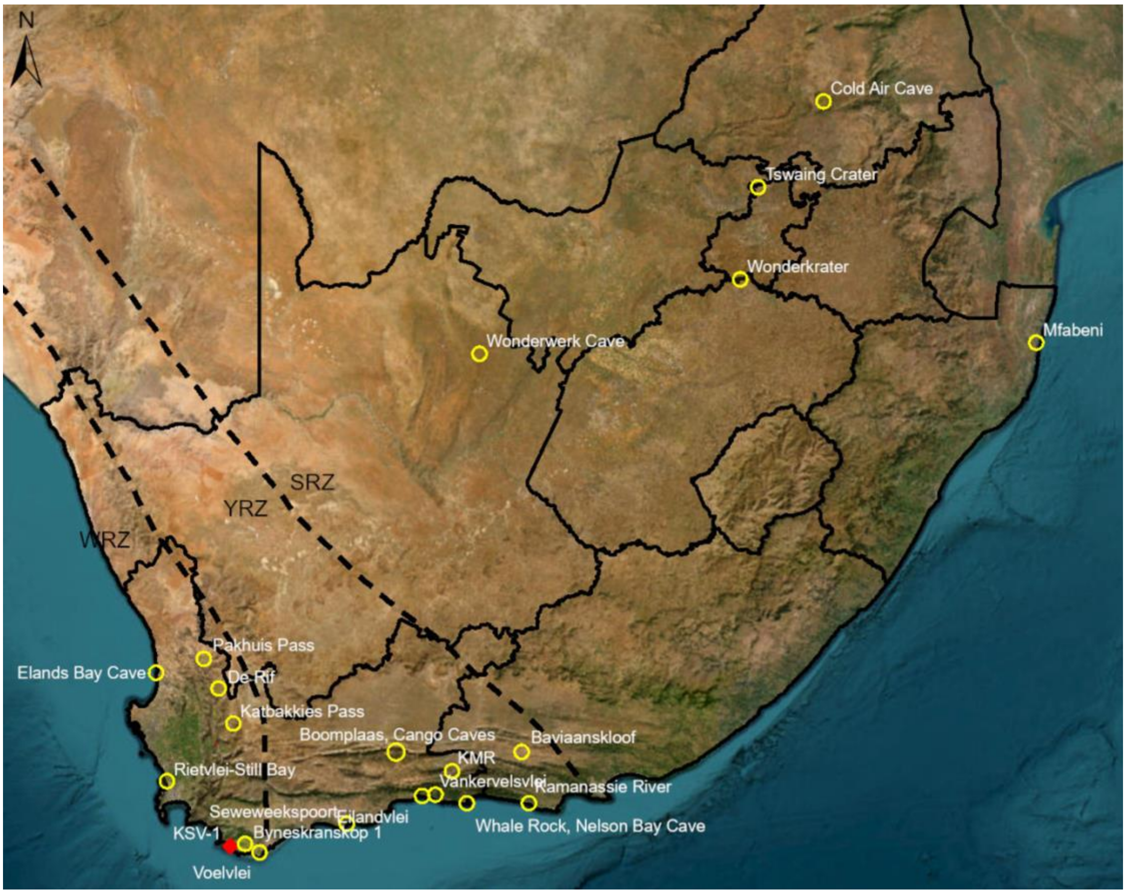

***Figure 5**: Map of southern Africa showing the location of the present study site (red diamond) in relation to other key palaeoclimate records referred to in the text. The extent of the modern winter (WRZ), year-round (YRZ), and summer (SRZ) rainfall zones are also indiacted.*

2.4.1 Last Glacial (30,000 – 18,000 cal yr BP)

Temperature reconstructions from the Mfabeni peatland and Cango Caves show Last Glacial Maximum (LGM; ~ 25,300 – 19,000 cal yr BP) temperatures were 4 – 6 °C cooler than Holocene temperatures (Talma and Vogel, 1992; Fietz et al., 2023).

Along the southwestern Cape coast, records generally reveal wetter conditions predominantly occurring during winter months. The Elands Bay Cave stable carbon isotope record indicates predominantly C_3 vegetation, suggesting winter rainfall dominated the last glacial (Stowe and Sealy, 2015). The Pearly Beach pollen and microcharcoal record revealed cool conditions during the LGM (Quick et al., 2021). This record shows that although moisture was present during the LGM, it was not in substantial amounts (Quick et al., 2021). Moving eastward along the coast, there is some variation in the observed climate trends during the last glacial.

Boomplaas and Nelson Bay Cave both record enhanced winter rainfall (Sealy et al., 2016; Thackeray and Fitchett, 2016; Faith et al., 2018). The Nelson Bay Cave bovid teeth enamel record also suggests the occurrence of summer rainfall, although in comparatively lower amounts (Sealy et al., 2020). However, there are several sites where dry conditions during last glacial have been inferred. Dry conditions were seen inland at the Cederberg Mountain range. The Pakhuis Pass pollen and stable nitrogen isotopes record revealed dry condition around 22,000 cal yr BP (Scott and Woodborne, 2007). The Pakhuis Pass record is thought to be influenced predominantly by changes in the westerly frontal systems indicating that while these systems brought increased precipitation to the coast, their influence did not extend inland (Chase et al., 2019a). Between 21,000 – 19,000 cal yr BP the Pakhuis Pass record did reveal increased precipitation as seen in coastal sites (Scott and Woodborne, 2007). Stable carbon and nitrogen stable isotopes from the De Rif record also found that relatively dry conditions prevailed towards the end of the last glacial and early interglacial (between 19,500 – 17,500 cal yr BP) (Chase et al., 2011). Similarly, the Vankervelsvlei record reveals cool, dry conditions during the last glacial (Strobel et al., 2019).

In the SRZ the last glacial period also shows general cool and dry conditions in various records. Sites such as Wonderkrater (Scott and Thackery, 1987; Chevalier and Chase, 2015, 2016), Wonderwerk Cave (Brook et al., 2010; Scott and Thackeray, 2015), Cold Air Caves (Holmgren et al., 2003), and Mfabeni (Baker et al., 2017; Miller et al., 2019) recorded dry conditions during this time. These dry conditions have been attributed to an increased extent of Antarctic Sea ice, which led to an equatorward shift of the westerlies and the South Atlantic Anticyclone, blocking the influence of tropical easterlies (Chevalier and Chase, 2015, 2016).

2.4.2 The Last Glacial – Interglacial Transition (18,000 – 11,000 cal yr BP)

The southwestern Cape coastal sites, such as Elands Bay Cave and Byneskranskop 1, indicate significantly increased moisture and winter rainfall regimes dominating between 17,000 – 11,000 cal yr BP (Stowe and Sealy, 2015; Faith et al., 2018). This is attributed to increased moisture flow from strong south-easterly trade winds and the influence of frontal systems on the site (Faith et al., 2018). The Pearly Beach record also indicates increased moisture until around 13,000 cal yr BP, but notes that this was associated with increased Benguela SSTs (Quick et al., 2021). This increase in rainfall is attributed to a slowdown in AMOC conditions, which may have resulted in increased precipitation from local precipitation systems and enhanced interaction between tropical and temperate moisture-bearing systems (Quick et al., 2021).

The De Rif record aligns with the observations from southwestern coastal sites, indicating increased water availability between 18,000 and 14,600 cal yr BP (Chase et al., 2011, 2015a). The increased humidity at De Rif has been attributed to a poleward shift of the South Atlantic Subtropical Front (STF) during Heinrich Stadial 1 (HS1, 18,500 – 14,600 cal yr BP), which reduced southeast trade winds and upwelling intensity, leading to increased sea surface temperatures (SSTs) of the Benguela current and greater moisture availability (Chase et al., 2011). It is postulated that the increased Agulhas leakage into the southeast Atlantic, reduced Atlantic Meridional Overturning Circulation (AMOC) conditions, and enhanced influence of the tropical easterlies during HS1 resulted in increased summer rainfall with shorter and less intense droughts (Reason et al., 2006; Chase et al., 2015a). Reduced precipitation during the interglacial period was recorded at De Rif between approximately 15,400 and 14,100 cal yr BP (Valsecchi et al., 2013; Chase et al., 2015a). Pakhuis Pass also showed some aridity during the interglacial period, with reduced precipitation and increased temperatures around 16,000 cal yr BP (Scott and Woodborne, 2007). Following the dry period at De Rif, pollen and microcharcoal data indicate a shift from dry conditions with higher fire frequencies to increased humidity, which is thought to indicate an increasing influence of the South Atlantic Anticyclone (Valsecchi et al., 2013; Chase et al., 2015a).

Along the southern Cape coast, increasing occurrence of summer rainfall is observed at sites such as Nelson Bay Cave and Boomplaas, where the records show that during the interglacial period, rainfall became progressively more summer-based (Faith et al., 2018; Sealy et al., 2020). This trend is also observed at some sites in the summer rainfall zone (SRZ), such as Wonderwerk Cave and Tswaing Crater, indicating warm and humid conditions after approximately 15,000 cal yr BP (Kirsten et al., 2007; Bramford, 2016). However, between approximately 15,000 and 12,000 cal yr BP, the Boomplaas record shows increasing aridity, and from around 13,000 cal yr BP into the Holocene, the records indicate increasing winter rainfall (Faith et al., 2018). The Vankervelsvlei record, which experienced a hiatus during the interglacial period, further suggests drought conditions (Strobel et al., 2022). This may be attributed to the increased continentality of the site due to lower sea levels and exposure of the Paleo-Agulhas Plain, as well as increased evapotranspiration due to rising temperatures (Faith et al., 2018; Strobel et al., 2022). In contrast, the Rietvlei-Still Bay record does not show a clear increase in summer rainfall or severe aridity but attributes increased moisture to winter rainfall (Quick et al., 2015).

Inland of the coastal sites, the Seweweekspoort stable carbon and nitrogen record also indicates wet conditions during the interglacial transition (Chase et al., 2017). This period of increased precipitation has been attributed to the slowdown of the Atlantic Meridional Overturning Circulation (AMOC) during Heinrich Stadial 1 (HS1) and the increase in southwestern Indian Ocean sea surface temperatures (SSTs) (Chase et al., 2017). Chase et al., 2017 explain that while the influence of the westerly storm track may have been diminished after HS1, the increased evaporation from warmer oceans would have stimulated temperate-tropical interactions (TTIs), leading to enhanced precipitation. The KMR record notes a period of aridity between approximately 14,000 and 11,000 cal yr BP, with some phases of humidity indicating mixed summer-winter rainfall conditions (Scott et al., 2021). The Seweweekspoort record also shows that around 14,200 cal yr BP, wet conditions abruptly diminish, similar to the aridity trends observed at the coast, concurrent with the strengthening of the AMOC and the onset of the Antarctic Cold Reversal (Chase et al., 2017). During this period, as Antarctic sea ice expanded and shifted the westerly storm track equatorward, decreased TTI occurrence resulted in aridification (Chase et al., 2017). However, the period of aridity comes to an end, as indicated by the Seweweekspoort $\delta^{15}N$ record showing wetter conditions between approximately 13,300 and 11,000 cal yr BP, unlike the predominantly dry transition into the Holocene observed at Boomplaas (Chase et al., 2018). The humid conditions at Seweweekspoort correspond with a sharp decline in sea ice extent in the Atlantic and the subsequent increase in interglacial temperatures (Chase et al., 2017).

2.4.3 Holocene (11,000 cal yr BP – present)

Throughout the Holocene, the modern rainfall zones exhibited significant variability and heterogeneity. During the early Holocene, the WRZ experienced generally warm and dry conditions. Byneskranskop 1 recorded limited moisture availability, and the Pearly Beach record indicated a hiatus, suggesting drought conditions (Faith et al., 2018; Quick et al., 2021). This arid phase in the WRZ may have been influenced by a decrease in sea ice extent and subsequent southerly shift in the westerlies (Chase et al., 2013; Zhao et al., 2016). Similar dry conditions were observed in other sites, such as Voëlvlei, Eilandvlei, and Baviaanskloof (Quick et al., 2018; Chase et al., 2020; Strobel et al., 2021). On the other hand, increased moisture was observed in some sites in the SRZ and YRZ, attributed to declining sea ice extent, interglacial temperature rise, and enhanced tropical influence (Chase et al., 2017; Faith et al., 2018). The Mfabeni record also indicated warm and wet conditions associated with rising sea surface temperatures and a southward shift of the westerlies, allowing for increased tropical influence (Baker et al., 2017; Humphries et al., 2017; Fietz et al., 2023). A sudden arid period at Seweweekspoort and the Kamanassie River during an intensified tropical system, suggests that variations in the southern westerlies led to limited development of temperate-tropical interactions, resulting in decreased precipitation (Valsecchi et al., 2013; Zhao et al., 2016; Chase et al., 2017).

A shift towards increased moisture in the WRZ occurs during the mid-Holocene potentially associated with enhanced westerly influence driven by Southern Ocean sea surface temperatures and sea-ice extent (Faith et al., 2018; Kirsten et al., 2020; Quick et al., 2021). Inland sites of the WRZ, such as Pakhuis Pass and Katbakkies Pass, revealed an increase in tropical influence with a rise in summer rains (Scott and Woodborne, 2007; Chase et al., 2015b; Chase et al., 2019b). Some sites within the YRZ, such as Vankervelsvlei, also recorded increased precipitation derived from the westerlies (Strobel et al., 2021). Meanwhile, in the SRZ, continental temperatures were elevated and the South African monsoon system was well-developed, leading to increased precipitation in areas like Tswaing Crater, Wonderkrater, and Mfabeni (Kirsten et al., 2007; Metwally et al., 2014; Truc et al., 2013; Baker et al., 2017).

Towards the end of the Holocene, periods of increased moisture and aridity were highly variable, with dry conditions prevailing among brief periods of intense precipitation. Records from Verlorenvlei, Elands Bay Cave, De Rif, and Pakhuis Pass displayed variations in water availability, with intervals of increased water availability separated by arid conditions (Scott and Woodborne, 2007; Valsecchi et al., 2013; Carr et al., 2014; Stowe and Sealy, 2015; Kirsten et al., 2020). The YRZ also generally experienced dry conditions, transitioning from humid to dry at sites like Vankervelsvlei, Eilandvlei, KMR, and Rietvlei-Still Bay (Quick et al., 2015; Quick et al., 2018; Scott et al., 2021; Strobel et al., 2022). Moisture in these regions was attributed to both tropical (Stowe and Sealy, 2015) and temperate (Hahn et al., 2017; Quick et al., 2018; Kirsten et al., 2020; Strobel et al., 2022) drivers.

Chapter 3: Geochemical Proxies

Past climate variability and natural climate change patterns can be studied using a variety of chemical indicators or proxies extracted from different archives. Chemical indicators studied in archives include elemental geochemistry (section 3.2.1); different stable isotopes, including inorganic carbon, oxygen, hydrogen, nitrogen, silicon, boron, and metal isotopes, as well as organic carbon and nitrogen isotopes (see Leng et al., 2006), as well as molecular indicators, such as plant waxes and biomarkers (Carr et al., 2015).

Archives that have been used to study palaeoclimates in southern Africa include speleothems (e.g., Talma and Vogel, 1992; McDermott, 2004; Braun et al., 2020), hyrax middens (e.g., Quick et al., 2011; Chase et al., 2012, 2013; Chevalier and Chase, 2015; Chase et al., 2020), shell middens (e.g. Parkington, 2003; Marean, 2014), corals (e.g., Gagan et al., 2004; Botha et al., 2013; Zinke et al., 2014), fossils (e.g., Kirsten and Meadows, 2016; Faith et al., 2018; Scott et al., 2012) and sedimentary cores from lakes (e.g., Kirsten et al., 2018; Wündsch et al., 2018; Humphries et al., 2019), wetlands (e.g., Humphries et al., 2020; du Plessis et al., 2020; Quick et al., 2021), and coastal marine environments (e.g., Zhao et al., 2016; Miller et al., 2020; Hahn et al., 2021). Sedimentary records from wetlands have proven very useful in palaeoclimate reconstructions, particularly as they allow for multiproxy analyses (Ellery et al., 2016; du Plessis, 2021).

Palaeoclimates in southern Africa have traditionally been examined using fossil and microfossil proxies. Fossil assemblages have been widely used due to the abundance of archaeological sites such as Blombos Cave (Deacon, 1978; Jacob et al., 2020), Nelson Bay Cave (Sealy et al., 2020), Boomplaas Cave (Scott et al., 2005), and shell midden sites in Pearly Beach (Avery, 1974). The faunal assemblages of mammals have been used to infer environmental conditions such as temperature and moisture availability based on modern habitat preferences as well as their relative sizes and proportions (Deacon and Lancaster, 1988; Faith et al., 2018). Deposits of shells or shellfish remains left over from prehistoric people, can be used to infer ocean temperature and the changing configuration of shorelines by looking at the changes in proportion of shellfish species (Avery, 1974).

Microfossils have been widely used to provide high resolution palaeo-data particularly about the vegetation of past ecosystems and their associated climates. Pollen data (e.g., Quick et al., 2018; Wündsch et al., 2018; du Plessis et al., 2020; Quick et al., 2021) can be used to examine for long-term changes in the local vegetation, thereby allowing for inferences into environmental and climatic conditions. Microcharcoal records (e.g., Valsecchi et al., 2013; Quick et al., 2016; Zhao et al., 2016; Quick et al., 2018, 2021) can be used in conjunction with pollen data to reconstruct fire-vegetation dynamics. Inferences on aquatic conditions can be made by looking at diatoms and forams. Diatoms respond to biotic and abiotic ecological processes, allowing for inferences of environmental conditions to be made (Denys and de Wolf, 1999; Julius and Therlot, 2010). Diatoms are abundantly found in aquatic environments and have widely been used to infer marine influence (e.g., Kirsten and Meadows, 2016; Kirsten et al., 2018; Humphries et al., 2019; Kirsten et al., 2020). Also used to study aquatic climates, foraminifera, are another useful microfossil used in palaeostudies. The composition and abundance of foraminifera species elucidates information on palaeo-sea surface temperatures, salinity, and relative sea level (e.g., Cooper et al., 2018; Kirsten et al., 2018; Wündsch et al., 2018).

Taphonomic and taxonomic limitations restrict the use of microfossils, with differential production, dispersal and preservation resulting in potential biases (Deacon and Lancaster, 1988; Davies, 2015; Scott and Neumann, 2018). Over representation is another limitation which may occur in a few ways, such as some plants producing larger quantitates of pollen, or transport of lighter pollen into or out of the study area (Deacon and Lancaster, 1988). Microfossils may also display low sensitivity to abrupt changes in climate and therefore may not indicate some important climatic events (Scott and Neumann, 2018). Inferences should therefore be supported using a multi-proxy approach, providing a need for geochemical analyses to be done on records in conjunction with microfossils.

3.1 Wetlands as sedimentary archives

Wetlands are important long-term archives as they accumulate sediment slowly, capturing multiple proxies of the environmental conditions at the time of deposition (Humphries, 2021). Most wetland deposits in southern Africa capture only the Holocene or part thereof (e.g., Verlorenvlei (Carr et al., 2015), Eilandvlei (Wündsch et al., 2018; Kirsten et al., 2018; Quick et al., 2018), Rietvlei (Quick et al., 2015), and Voëlvlei (Strobel et al., 2021)). Some long-term records do exist (e.g., Mfabeni (Humphries et al., 2017; Miller et al., 2019; Fietz et al., 2023), Tswaing Crater (Kirsten et al., 2007), Pearly Beach (Quick et al., 2021), Vankervelsvlei (Quick et al., 2016; Strobel et al., 2019, 2022)), however, the Pearly Beach and Vankervelsvlei records are characterised by discontinuities.

Wetlands are often classified according to their hydrology, namely, permanent (lakes, riparian edges), seasonal (pans), and ephemerally flooded wetlands (McCarthy and Hancox, 2000; Rowberry et al., 2011). The hydrology of a wetland influences sediment and solute inputs and controls the retention within wetlands (McCarthy and Hancox, 2000). Permanent wetlands often receive sediment input from upstream sources within their catchment, while seasonal and ephemerally flooded wetlands accumulate sediment during high rainfall or flood events and only retain them until the water recedes (Fritz, 2008). Similarly, solutes from rivers can continuously enter permanent wetlands, contributing to elevated solutes in these systems (Fritz, 2008). Solute levels of seasonally or ephemerally flooded wetlands, however, are more variable and depend on the surrounding landscape as well as the frequency of flood events (McCarthy and Hancox, 2000). Permanent wetlands tend to retain water longer, allowing for sediment settling and nutrient uptake by vegetation within the wetland. Seasonal and ephemerally flooded wetlands have more episodic retention (McCarthy and Hancox, 2000).

Wetlands and coastal lakes are sensitive to a combination of *in-situ* (e.g., hydrological, biogeochemical) and *ex-situ* (e.g., geological, geomorphic) controls that operate across different temporal scales (Foster and Walling, 1994; McCarthy et al., 2010; Zolistchka et al., 2015; Ellery et al., 2016). The sediments accumulated in wetlands can be classified according to their origin and typically comprise both allogenic (allochthonous) and authigenic (autochthonous) components. Allogenic material is transported to wetlands from the surrounding environment and typically comprises minerogenic sediments derived through catchment weathering. Authigenic material is produced within the wetland system itself and may include biogenic (plant-derived) material and/or chemical precipitates (Leng et al., 2006; Humphries, 2021). The sedimentary composition of a wetland therefore reflects internal processes as well as external inputs, both of which are influenced by climatic conditions and changes in the surrounding landscape (du Plessis, 2021; Humphries, 2021).

3.2 Geochemical proxies

Environmental processes can be inferred from the chemical analysis of both inorganic and organic sedimentary components. Inorganic geochemical proxies are derived from non-living components of the environment and can include certain isotopes (e.g., Leng, 206) and a range of elements (e.g., Kirsten et al., 2007; Humphries et al., 2016; Higgs, 2017; Francke et al., 2020; Humphries, 2020, 2021). Organic proxies are derived from organic materials, such as plant or animal remains, and can include isotopic signatures of bulk sedimentary organic matter (e.g., Carr et al., 2015; Miller et al., 2019; Strobel et al., 2022), microfossils (e.g., diatoms (Kirsten and Meadows, 2006; Humphries et al., 2019; Kirsten et al., 2020), foraminifera (Kirsten et al., 2018), pollen (Quick et al., 2015; du Plessis et al., 2020; Quick et al., 2021)) leaf wax biomarkers (e.g., Carr et al., 2015; Miller et al., 2019; Strobel et al., 2022), and stable isotopes in organic matter such as carbon and nitrogen (Leng, 2006).

3.2.1 Inorganic proxies

The geochemical composition of sediments is controlled by chemical processes that occur during weathering, transport, and deposition (Bjørlykke, 2010). Variations in the elemental geochemistry can therefore potentially be used to infer sediment sources, hydrological changes, catchment dynamics, biotic processes, and particle sorting (Dellwig et al., 2000; Kylander et al., 2011). However, often the relative change in abundance of certain elements is more informative than concentration changes. Elemental concentrations are influenced by potential dilution effects associated with changes in grain size or organic matter content. For this reason, elemental abundance is often expressed in ratio form and calculated relative to a conservative element (e.g., Al or K) which is not typically influenced by biological or post-depositional processes (Davies et al., 2015).

Sediment sources and transport mechanisms can be examined using elements typically associated with siliciclastic material (e.g., Si, Al, K) (Humphries, 2021). These elements are found mostly in quartz, clay minerals and accessory silicates, and the relative ratio between these elements (e.g., Si/Al, K/Al) can be used to infer temporal variations in minerogenic input and changes in sediment source (Haberzettl et al., 2008; Davies et al., 2015). In some cases, differences in the mobility of certain elements during weathering and erosion allows changes in chemical weathering intensity to be assessed (Gebregiorgis et al., 2019). For example, the ratios K/Al and K/Rb are often used to infer weathering since the larger and oftentimes more immobile cations (Al, Rb) remain in source rock, while the smaller, more chemically mobile cations (K, Sr, Na) are preferentially leached during weathering (Nesbitt and Markovics, 1980). Chemical weathering is governed by various parameters, but precipitation and temperature have the most pronounced influence. The elemental proxies of chemical weathering may therefore be used to infer palaeo-precipitation and/or temperature conditions (Norström et al., 2018; Hahn et al., 2016, 2021).

Sediments are transported into wetlands primarily through fluvial and aeolian processes. The energy required to transport sediment into a wetland can be inferred by examining changes in grain size, where increased grain size usually corresponds to higher energy conditions (Humphries, 2021). For example, Si is present as quartz in sediments and most commonly occurs in the silt and sand fractions (Calvert and Pedersen, 2007). This allows the Si/Al ratio to be used as a proxy for grain size since Al is found in finer clay minerals (Kylander et al., 2011). Similarly, Ti and Zr are commonly associated with heavy mineral phases (TiO_2 and ZrO_2, respectively) which are carried in silt and fine-sand fractions of sediment (Calvert and Pedersen, 2007). The ratios Ti/Al and Zr/Al are therefore commonly used as geochemical proxies for grain-size (Humphries et al., 2020).

In coastal environments, changes in marine influence can potentially be inferred using a variety of geochemical indicators as marine water is relatively enriched in certain chemical components (e.g., sulfates, calcium, strontium, and sodium) relative to freshwater. By looking at elements that are common in marine environments, but rare in freshwater environments (e.g., Br, Sr, Na), changes in marine influence can be inferred (e.g., Wündsch et al., 2016, 2018). Calcium carbonate is supersaturated in seawater and forms a key component of many marine organisms. In certain situations, therefore, the presence of calcium minerals within coastal deposits can be used as a proxy to infer changes in the degree of marine influence (e.g., Wündsch et al., 2016, 2018; Strobel et al., 2021).

3.2.2 Organic proxies

Organic material (OM) in a wetland may be produced in the system or transported into the system by fluvial or aeolian mechanisms (Leng et al., 200; Higginson and Gornitz, 2009). The amount of organic material in sediments is indicated by the concentration of total organic carbon (TOC), which signifies the portion of OM that did not re-mineralize during sedimentation (Meyers and Teranes, 2001; Meyers, 2003). The organic content of sediment is influenced by the production and degradation of biomass which can therefore be used to comment on post-depositional conditions and origin of organic matter (Snyder et al., 2004). Lakes preserve OM produced by plants in and around the wetland, allowing for the analysis of carbon and nitrogen isotopes which allow for deductions on source of the OM, intra and extra past productivity of the system, and changes in nutrient supply (Meyers, 1994; Meyers and Lallier-Verges, 1999; Meyers and Teranes, 2001).

Stable carbon isotopes (^{12}C and ^{13}C, $\delta^{13}C$) can be used to distinguish vegetation dominance of the wetland (influenced by temperature, precipitation, and atmospheric CO_2 concentrations) thereby providing a means to infer paleaoclimatic conditions (Fig 6; Ehleringer et al., 1977). Terrestrial plants use Calvin (C_3), Hatch-Slack (C_4), or Crassulacean acid metabolism (CAM) photosynthetic pathways, which all have different $\delta^{13}C$ values (Smith and Epstein, 1971). C_3 plants include trees, most shrubs, and most temperate grasses; tropical grasses are mostly classified as C_4 species, and CAM plants mainly include succulents (Lamb et al., 2006). In southern Africa, the WRZ consists of mainly C_3 plants, while C_4 species dominate the YRZ (Vogel et al., 1978, Scott, 2002). Terrestrial plants preferentially take up ^{12}C during CO_2 fixation which leads to ^{13}C depleted OM (Lamb et al., 2006). The $\delta^{13}C$ value of terrestrial C_3 plants ranges between - 32‰ and - 21‰, while C_4 terrestrial plants range from – 17‰ to – 9‰ (Fig. 6; Deines, 1980; Ehleringer et al., 1997). CAM photosynthesizers have $\delta^{13}C$ values which vary between C_3 and C_4 where obligate CAM plants or CAM plants under dry or saline environments resemble C_4 plants, but under moist conditions resemble C_3 plants (Farquhar et al., 1989a; Pate, 2001). CAM terrestrial plants therefore have a wide range of $\delta^{13}C$ values of between – 11 ‰ to – 28 ‰ (Fig. 6; Schleser, 1995).

The $\delta^{13}C$ value of aquatic plants is largely determined by whether the plant utilizes bicarbonate (HCO_3^-) or dissolved CO_2 (Benedict et al., 1980). The inorganic carbon isotopes available in wetland systems, mainly from total dissolved inorganic carbon, are introduced to the lake system with authigenic and biogenic carbonates which can include CO_2 release from organic material within the system, atmospheric CO_2, as well as from the interaction of water within the system and rocks and soils (Leng et al., 2006; Francke et al., 2020). Dissolved CO_2 has lower $\delta^{13}C$ values than HCO_3^- where the ratio of CO_2 to HCO_3^- is a function of pH, meaning that in marine environments plankton will have higher $\delta^{13}C$ values than freshwater plankton (Lamb et al., 2006). Marine plants in general have $\delta^{13}C$ values between – 19 and – 22‰, and freshwater aquatic plants have depleted $\delta^{13}C$ values between – 10 to – 22‰ (Fig. 6; Meyers, 1997; Mackie et al., 2005). Bacteria in marine environments have $\delta^{13}C$ values ranging from – 12‰ to – 27‰ (Coffin et al., 1989). C_3 marine algae tend to have higher $\delta^{13}C$ values than freshwater algae with the former ranging from – 16‰ to – 23‰ and the latter ranging from – 26‰ to – 30‰, while C_4 algae have higher $\delta^{13}C$ ^{values} of above – 16‰ (Haines, 1976; Schidlowski et al., 1983; Meyers, 1994; Chivas et al., 2001).

The carbon-nitrogen ratio can be used to infer the source of organic material distinguishing algal and terrestrial plant origins (Fig. 6; Meyers, 1994). Organic nitrogen is found mainly in proteins and nucleic acids which occurs more prominently in lower plants (Talbot and Johannessen, 1992). Aquatic organic matter (OM) (such as bacteria and algae) therefore has a lower C/N ratio of between four and ten, while OM of terrestrial sources have a ratio of more than 20 (Meyers, 1994; Leng et al., 2006; Meyers, 2003). C_3 vascular plants have a C/N ratio of 12 or more, while C_4 grasses have a ratio of more than 30 (Tyson, 1995; Meyers, 1994). The C/N ratio of aquatic plants may be lower due to bacterial action introducing nitrogen into the system (Rice and Hanson, 1984). Looking at this ratio in isolation may be misleading due to the selective degradation of OM nitrogen components as well as the large fluctuations of nitrogen content in plants (Meyers, 1994; Lamb et al., 2006).

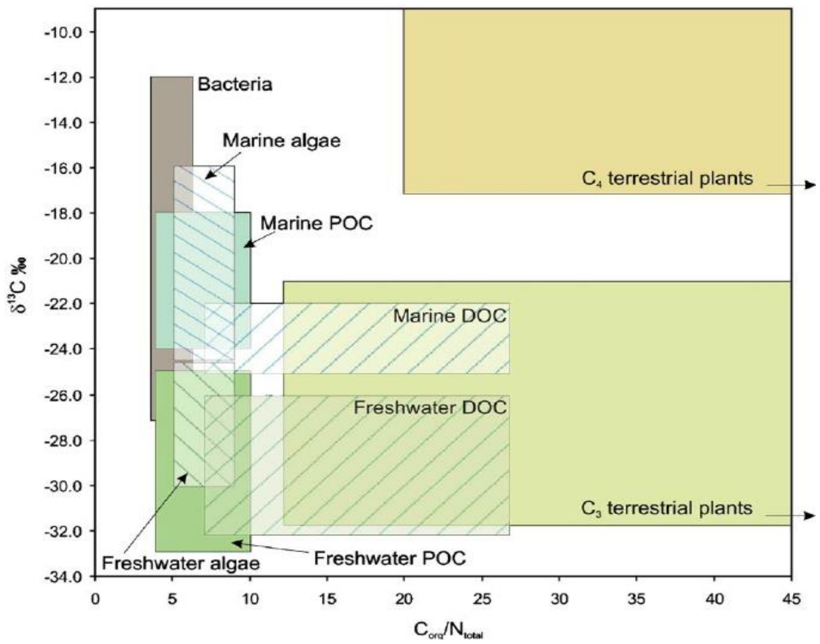

Figure 6: *A diagram illustrating the classification of plant material based on the $\delta^{13}C$ signals (relative to VPDB) and C/N ratio (from Lamb et al., 2006).*

3.2.3 Advantages and limitations of elemental geochemistry

Elemental geochemistry allows for quick, non-destructive data to be collected from sediment cores which provide information on transport processes, hydrological balances, and chemical weathering in an environment (Francke et al., 2020; Humphries, 2021). Elemental proxies have high spatial resolution, responding to abrupt climate events. This is particularly important for understanding rapid, or short-term climate events and allows for the development of highly resolved records with insight into the duration and intensity of past climate variations (Humphries, 2021). Elemental geochemistry typically involves analyzing multiple elements simultaneously. This multi-elemental approach provides a comprehensive view of the geochemical composition of samples, enabling researchers to examine the interplay between different elements and their responses to climate changes (Davies et al., 2015). This allows for the identification of complex climate signals and the differentiation of climate-related variations from other environmental influences. Elemental geochemistry is also suitable for a range of archives and is not limited to sediment cores alone. Elemental geochemistry complements other paleoclimate proxies, such as isotopic analyses, and pollen or microfossil assemblages (Humphries et al., 2019; du Plessis, 2020; Strobel et al., 2021). By combining different proxies, a more robust and nuanced understanding of past climate conditions can be made. The integration of elemental geochemistry with other techniques enhances the accuracy and reliability of paleoclimate reconstructions.

While elemental geochemistry provides a valuable tool to study palaeoclimates, it does have its limitations that must be taken into consideration. The interpretation of elemental geochemical data can be complex as many factors, such as geologic, geomorphic, biologic, and hydrologic, need to be considered to make comprehensive inferences (Davies et al., 2015). Data from wetlands is also limited by spatial heterogeneity where signals may be site specific, varying based on sediment sources, local environmental conditions, and biological processes

(Francke et al., 2020). Elemental interpretations are therefore not standardized, and many considerations must be taken into account before making deductions on palaeoclimates. Elemental interpretations are non-linear and the relationship between elemental composition and climate variables may respond differently to changes in climate conditions and their responses may vary depending on the specific context and environmental settings (Humphries, 2021). In some cases, the desired temporal resolution of records cannot be achieved due to factors such as low sedimentation rates, bioturbation, or the inability to obtain precise dating (Francke et al., 2020). This may make capturing short-term or abrupt climate events challenging. The preservation of elemental signals of sediments varies depending on post-deposition conditions, including environmental conditions and diagenetic processes such as microbial activity, redox, and temperature (Humphries, 2021). This may compromise the reliability of data as post-depositional processes such as dissolution, recrystallization, and mineralogical transformations may alter the original elemental composition, making it difficult to accurately interpret past climate conditions (Davies et al., 2015).

Chapter 4: Regional setting and Methods

4.1 Regional background

The study site (Fig. 7a) is a depression wetland located on the greater Agulhas Plain, which stretches from Gansbaai (34°35'S,19°21'E) to Struisbaai (34°49'S, 20°03'E). The Agulhas region has a variety of wetlands that occur within a relatively small area, including freshwater springs, rivers, floodplains, estuaries, lakes, vleis, and endorheic pans all characterized by alluvial deposits (Jones et al., 2000). The nearest town to the study site is Pearly Beach, located ~2 km away, and is primarily a holiday and retirement town, with a population of around 1000 people (Stats SA, 2011).

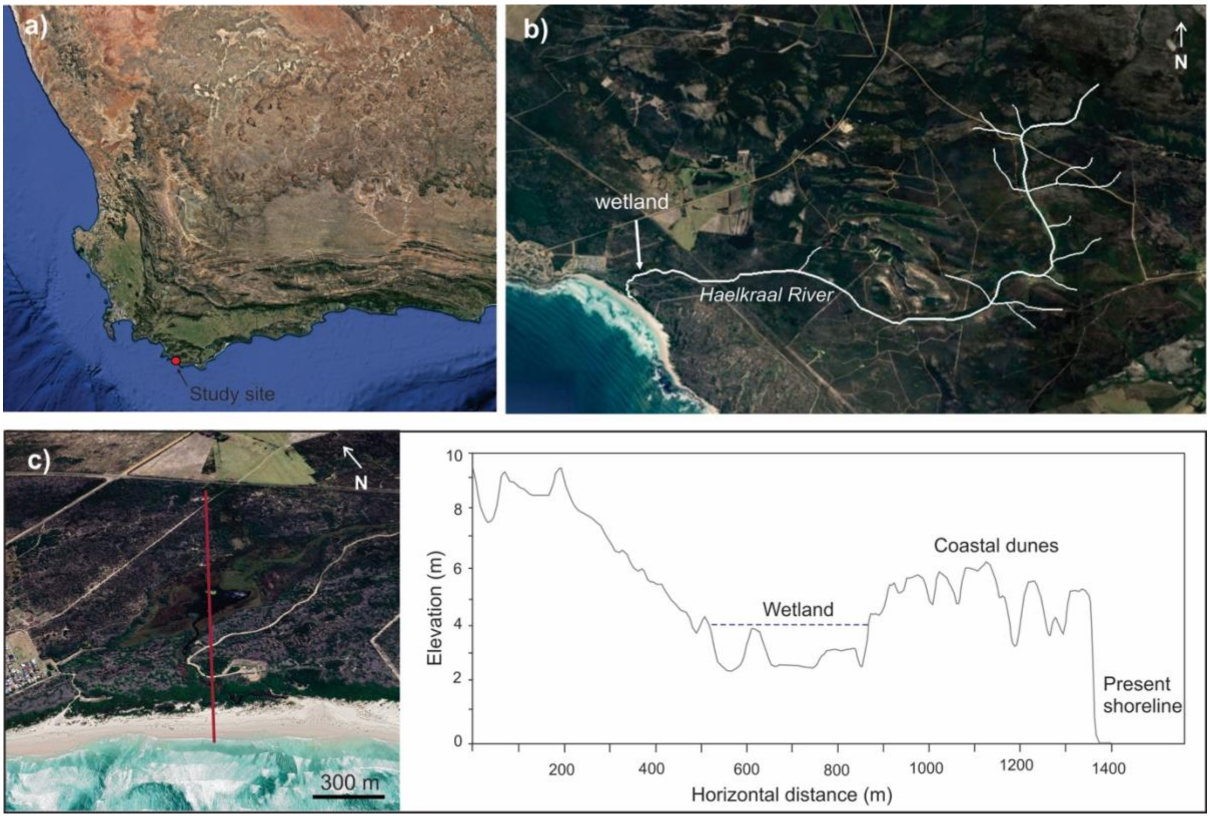

Figure 7: *a) A map of the study site located along the southern Cape coast, b) The location of the study wetland and Haelkraal River which represents the hydrological input, and c) A cross- section elevation profile generated using Google Earth, showing the location of the wetland within a interdunal depression.*

The wetland is located ~650 m from the coastline and is slightly perched (2 – 3 m) relative to sea level behind a ~6 m high vegetated coastal dune (Fig. 7c). The primary source of water into the wetland is from the Haelkraal River and through runoff from spring seeps (Fig. 7b; Kraaij et al., 2008). The Haelkraal River originates from limestone uplands northeast of the site and forms valley bottom wetlands and hill-slope seeps in the area (Avery, 1974). Water from the wetland drains out to the Atlantic Ocean via a sinuous, narrow channel. The

Haelkraal River only reaches the sea during very wet seasons, otherwise there is no surface outflow from the wetland (Avery, 1974).

Mean annual rainfall at Pearly Beach averages between 469 and 482 mm per annum (Climate Systems Analysis Group, 2012). The region falls within the modern WRZ (*Sensu* Chase and Meadows, 2007), with between 65% and 75% of the total annual rainfall occurring during the austral winter months (May – October). Temperate westerly low-pressure systems are responsible for winter rainfall in the region, while non-winter rainfall is the result of advection of moist air from the Indian Ocean by a high-pressure cell to the southeast (Deacon et al., 1992; Cowling et al., 1994; Carr et al., 2006a). Annual temperatures range between 8 °C and 28 °C (SAWS, 2001) with snow and frost not occurring in the region. The region experiences a bimodal wind regime with westerly winds prevailing in winter and easterly winds in summer (Tinley, 1985; Kraaij et al., 2006). Sea surface temperatures (SST) in the region range between 21 °C in summer and 14 °C in winter (Bolton & Stegenga 1990).

The Pearly Beach area has been the focus of two previous palaeoclimate studies. Avery (1974) looked at open station shell midden sites, along the coastline and within cave sites near Pearly Beach. This study looked at the patterns of coastal living and resource exploitation by communities that inhabited the region approximately 350 cal yr BP. More recently, Quick et al. (2021) studied a wetland known as Pearly Beach (PB-1). This study examined pollen and microcharcoal data of the core to reconstruct environmental conditions in the area from 25,000 cal yr BP. This study offered a new perspective on the long-term climatic changes in the Pearly Beach region and their teleconnections with extra-regional and hemispheric climate drivers.

4.2 Geology and vegetation

The wetland is situated on a low-lying undulating coastal plain bound to the north by Bredasdorp limestone ridges and Table Mountain Group sandstone outcrops of the Peninsula Formation (Malan, 1990). The coastal plain is underlain by unconsolidated aeolian calcareous sediments of the Strandveld Formation with partially consolidated calcrete lenses located in some patches along the coast and further inland (Gressa and Theron, 1992). The limestone ridges and sandstones are characterized by shallow, alkaline and calcareous soils, while more acidic, colluvial soils are found on the lower slopes with evidence of early stages of podsolidation (Cowling et al 1988; Rebelo et al., 1991). Along the southern and western boundaries of the wetland there are transverse coastal dunes adjacent to the ocean, while relict deflated Pleistocene parabolic dunes are found along the northwestern and southeastern boundaries of the site (Malan, 1990). The geology of the area surrounding the wetland consists of aeolian quartz and shelly sand (Thwaites and Cowling, 1988). Moving up the catchment sandstone and quartzite become more dominant with shale, phyllite and feldspathic sandstone occurring near the origin of the Haelkraal containing ferricrete fragments on the slopes in the region (Thwaites and Cowling, 1988).

The landscape surrounding Pearly Beach is dominated by three main vegetation types: fynbos, coastal thicket, and forest vegetation (Musina and Rutherford, 2006). The lowlands and uplands contain mainly Mediterranean type shrublands of the fynbos biome, with the lowlands also supporting riparian and wetland habitats where surface water allows (Mustart et al., 2003). There are three broad types of fynbos found within the study area, each characterised by their underlying geology (Thwaites and Cowling, 1988). Agulhas limestone fynbos is found over shallow, alkaline sands over Bredasdorp Group limestone pavements; Agulhas sand fynbos is found on the deep colluvial, neutral sands over the Bredasdorp Group limestones; and Overberg sandstone fynbos is found over Table Mountain Group sandstones with the deep colluvial, infertile acid sands (Thwaites and Cowling, 1988; Cowling et al., 1988; Mustart et al., 2003; Rebelo et al., 2006).

Coastal dunes are vegetated by Overberg dune strandveld, comprising grasses, succulent shrubs and herbaceous species (Cowling et al., 1988). Vegetation found within the wetlands of Pearly Beach are typically characterised by reeds and rushes, with sedges along the margins (Quick et al., 2021).

4.3 Sediment sampling

In November 2021, a 5.42 m sediment core (KSV-1) was retrieved from the center of the Haelkraal River wetland (34°40’10.54’’S, 19°31’39.95’’E) using an Uwitec piston coring system (Fig. 8B). The core was collected in 2 m sections within PVC liners of 63 mm diameter. Core sections were transported to the Nelson Mandela University Palaeoecology Laboratory where they were split longitudinally and subsampled for analysis.

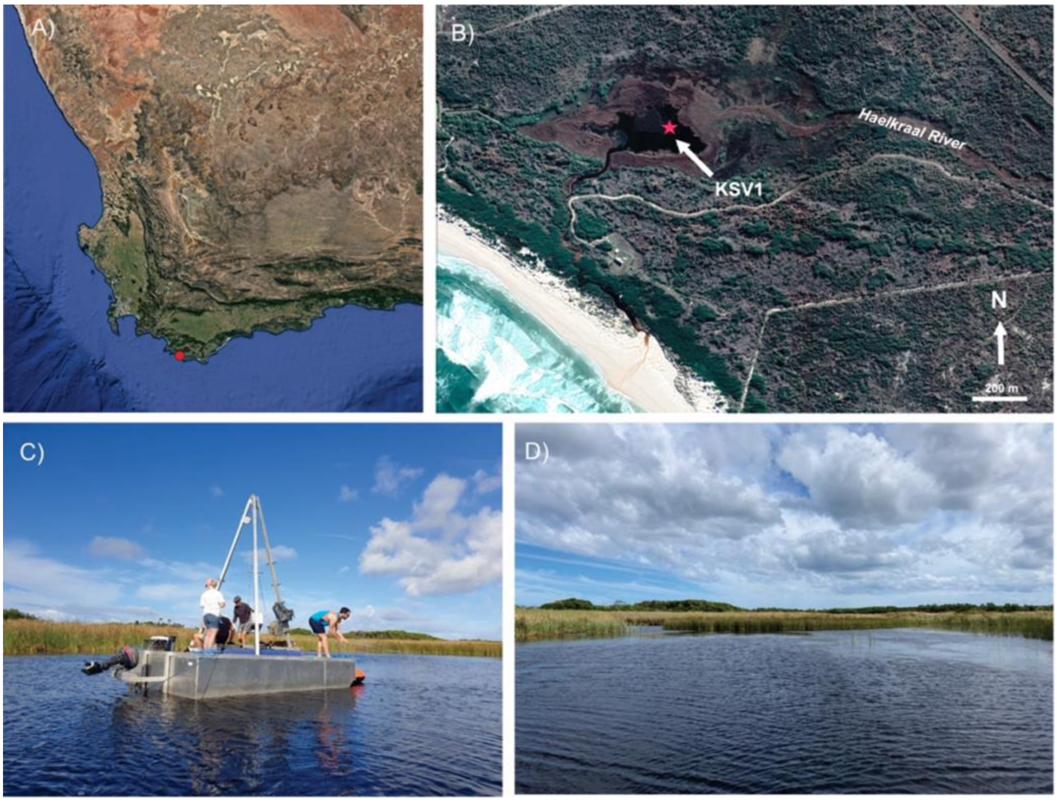

Figure 8: *A) Map of the study site in relation to the southern Cape B) A Google Earth image of the wetland and location of core KSV-1 C) Field image of the coring system used, and D) A field image of the wetland and surrounding vegetation.*

4.4 Analysis

An age-depth model for KSV-1 was established using radiocarbon. Eight bulk organic samples (1 cm intervals) were sent to Queens University (Belfast) for dating by Accelerator Mass Spectrometry (AMS). Radiocarbon ages were calibrated to calendar years using the Southern Hemisphere atmospheric curve SHCal.20 (Hogg et al. 2020) and a Bayesian age-depth model developed using the R software package Bacon (v2.2) (Blaauw and Christen, 2011).

The core was subsampled at 2 cm intervals for inorganic elemental analysis (a total of 250 samples). Material was dried at 105 °C overnight and milled into fine powder using a ball mill. Powders were then combusted at 550 °C for 4 hours and organic matter content matter was estimated based on the percentage weight loss on ignition (%LOI). Combusted residues were then analysed by X-ray fluorescence (XRF) using a Bruker S2 Ranger following calibration against a range of local (SARM) and USGS rock standards. Concentrations were found to be within 10% of the accepted values with analytical precision < 2% for all elements based on the repeat analysis of USGS rock standards AGV-2 and GSP-2.

The organic chemistry of sediments was investigated by measuring total organic carbon (%TOC), total nitrogen (%N) and stable isotope ($\delta^{13}C$ relative to VPDB and $\delta^{15}N$ relative to atmospheric Nitrogen) composition. Samples were taken at 5 – 10 cm intervals (a total of 66 samples) and treated with 10% HCl to remove inorganic carbonate. This material was then dried at 105 °C and milled to a homogenous powder for analysis. The samples were analysed at Stellenbosch University using a CNS elemental analyser (Vario Isotope Select Cube, Elementar) in line with a gas isotope ratio mass spectrometer (IRMS, IsoPrime). The measured analytical precision, based on the measurement of USGS rock standards (USGS40, USGS41a and USGS42) and two 'in-house' matrix-matched standards was <0.2%.

The mineralogy of selected samples was investigated by powder X-ray diffraction (XRD) using a Bruker D2 Diffractometer. Diffractograms were obtained for air-dried mounts (2θ in the range 5 – 60°) using monochromated CoKα radiation. Profex (4.3.6) was used to identify the mineral phases present.

Chapter 5: Results

5.1 Stratigraphy

The lithology of KSV-1 can be analysed based on changes in colour and texture (Fig. 9A). From 542 – 527 cm and 500 - 477 cm, the core primarily consists of dark brown, organic-rich sandy silt, with small amounts of clay and no shells present. Between 527 – 500 cm, the section is characterized by light brown sands, including lenses of coarse, light gravels. Moving up the core to 477 – 395 cm, there is sandy silt with mottles and alternating bands of dark and light-coloured coarser-grained silts, but without any shells. Subsequently, another dark brown, organic-rich sandy silt section follows. A sharp boundary separates this layer, and between 308 – 220 cm, we find brown-grey clayey silt containing an abundance of small shells, along with light-yellow sandy inclusions that have darker, organic-rich mottles. From 220 – 96 cm, the core contains organic-rich, dark brown silts with pockets of fine-grained sand and shells distributed throughout. A clear transition occurs at 96 cm, where a dark, organic-rich silt layer starts. This layer then shifts into sediment characterized by mottles and inclusions of coarse-grained, lighter-coloured sands, accompanied by the presence of shells between 95 – 50 cm. A gradual colour change is observed from brown silts to light-yellow sands, which characterizes the uppermost part of the core, from 50 – 10 cm.

5.2 Chronology

The results of the radiocarbon analysis are presented in Table 1. All age determinations were stratigraphically consistent, and the fitted age-depth model provided a chronology for the past ~30,000 years (Fig. 9B). Sedimentation rates averaged at ~0.01 cm/yr from ~ 30,000 to 20,000 cal yr BP, giving the XRF measurements a temporal resolution of 370 years. An increase of sedimentation rate to ~0.02 cm/yr occurs between ~ 20,000 and 10,000 cal yr BP. Between 10,000 and 5,000 cal yr BP sedimentation rates sharply increase to ~0.07 cm/yr (resulting in a sampling temporal resolution of ~40 years), after which sedimentation rates decrease to 0.03 cm/yr from ~ 5,000 cal yr BP to the top of the core.

Table 1: *Radiocarbon ages and calibration data using SHCal20*

Lab Code	Average Depth (cm)	^{14}C Age (yr BP)	95.4% prob. Range (cal yr BP)
UBA-43151	13	1198 ± 31	961-1103 (83.2%), 1135-1176 (16.8%)
UBA-43157	60	3467 ± 56	3489-3527 (4.06%), 3558-3844 (95.9%)
UBA-43158	109	5196 ± 54	5740-6011 (94.5%), 6080-6112 (3.93%)
UBA-43152	218	5711 ± 31	6318-6339 (2.11%), 6341-6371 (4.25%)
UBA-43159	288	7188 ± 58	7839-8044 (93.8%), 8090-8127 (3.12%)
UBA-43160	379	9697 ± 75	10785-11212 (100%)
UBA-43161	478	15673 ± 150	18658-19311 (100%)
UBA-43153	540	26154 ± 181	30047-30827 (100%)

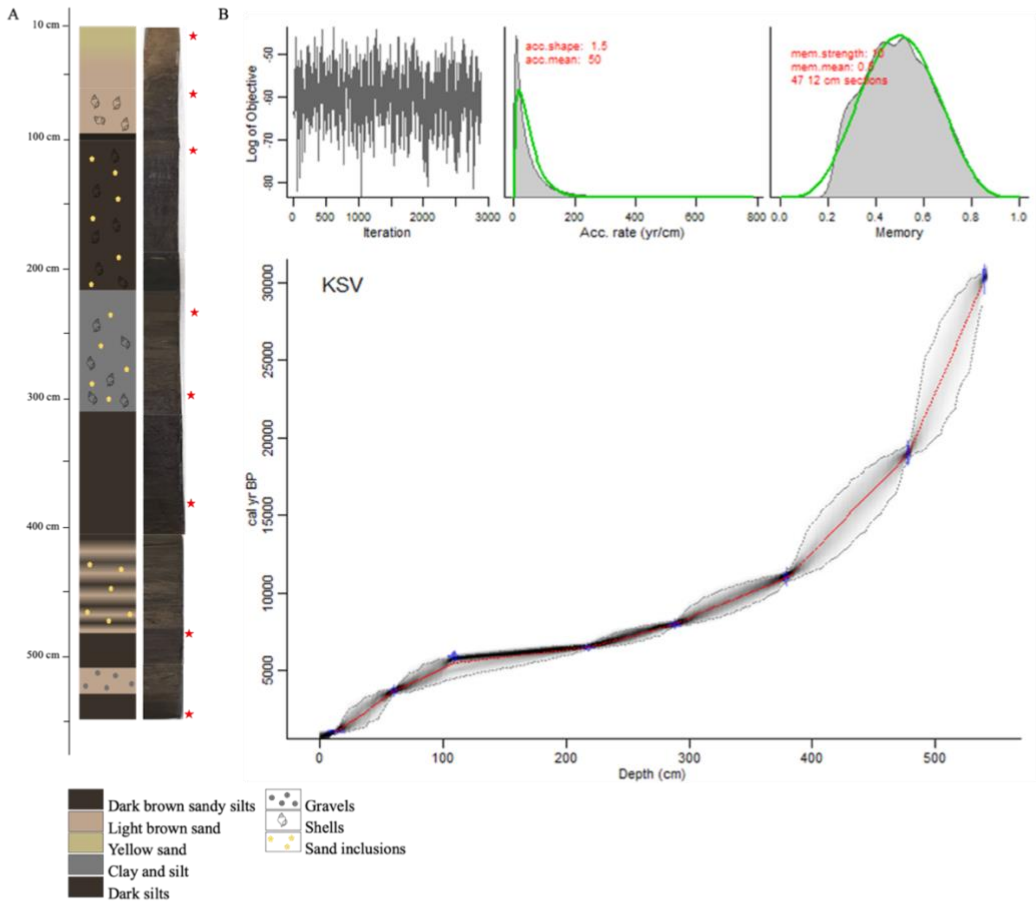

Figure 9: *A) Composition photograph of KSV-1 showing intervals where samples for ^{14}C dating were taken (red stars), B) The age-depth model for KSV-1 developed using the R software Bacon (V2.2) (Blaauw and Christen, 2011). The 2σ probability distribution of calibrated ^{14}C age is presented in blue and the 95% confidence intervals are represented by the grey dotted lines. The red line represents the best model according to the weighted mean age at each point.*

5.3 Inorganic geochemistry

Measured LOI varied considerably downcore ranging between 0.30% and 40.3% (Fig. 10a). Between 30,000 and 18,000 cal yr BP, LOI varied between 0 and 5%. A gradual increase in LOI is observed ~17,200 cal yr BP, although values remained relatively low (<10%) until ~10,900 cal yr BP where a rapid increase to 25% occurred. LOI values fluctuated between 15 and 25% until ~6,900 cal yr BP when a sharp increase is observed, peaking at 40% around 5,800 cal yr BP. Thereafter, LOI values decreased rapidly, with sediments deposited after ~3,500 cal yr BP characterised by low (<1%) LOI values.

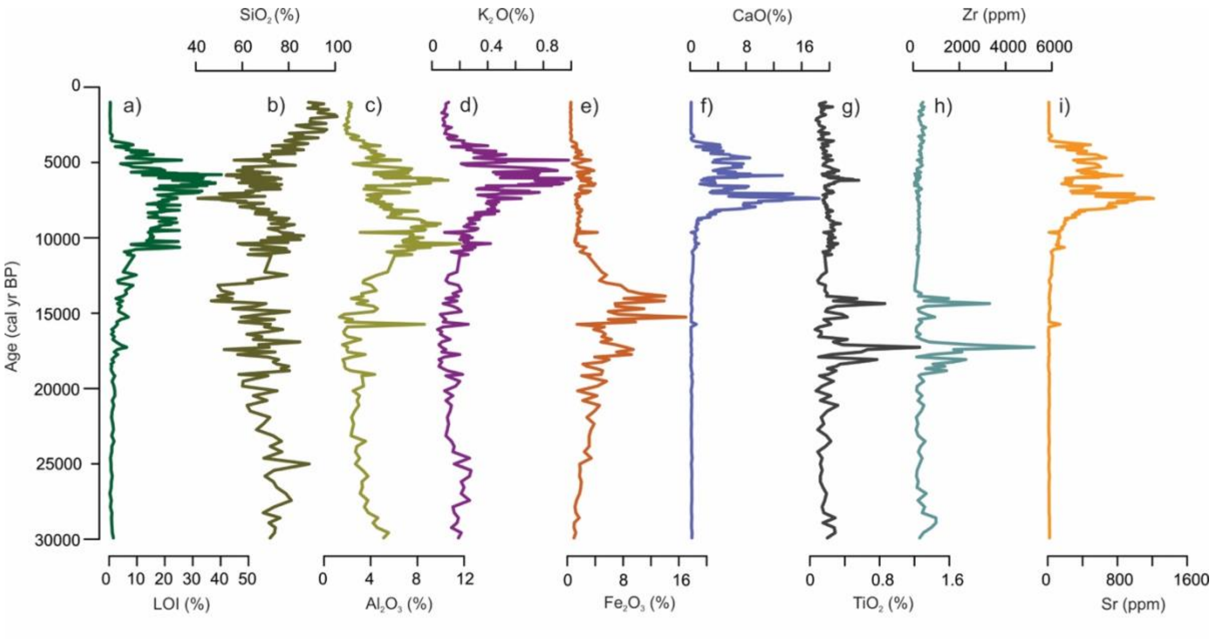

Figure 10: *Downcore variations in a) LOI, b) SiO2, c) Al2O3, d) K2O ,e) Fe2O3 f) CaO g) Ti2O h) Zr and i) Sr through core KSV-1. All XRF results are provided in Appendix 1.*

Concentrations of SiO_2 varied between 40 and 100%, and are typically inversely related to LOI (Fig. 10b). Although variable, %SiO_2 showed a general decreasing trend from 30,000 to 13,500 cal yr BP. The period 13,000 to 9,900 cal yr BP is characterised by increasing SiO_2 contents (up to 90%), after which a rapid decline is observed, with SiO_2 reaching 40% at 7,300 cal yr BP. A steady increase in %SiO_2 is observed from 7,300 cal yr BP to present, with sediments deposited over the last 2,500 years comprising almost entirely of quartz.

Abundance of Al_2O_3 (Fig. 10c) remained relatively low, typically ranging 2 – 5% between 30,000 and 15,000 cal yr BP. However, a marked increase in Al_2O_3 is observed from ~15,000 cal yr, with concentrations reaching 12% at 10,400 cal yr BP. Thereafter, Al_2O_3 concentrations fluctuated between 3 and 10%, before rapidly declining 6,200 cal yr BP to present. Variations in K_2O revealed a similar downcore trend (Fig. 10d), with concentrations increasing rapidly between 10,000 and 6,000 cal yr BP, before rapidly declining to present.

Concentrations in %Fe_2O_3 showed a gradual increase from ~1% at 30,000 cal yr BP to ~10% at 17,500 cal yr BP (Fig. 10e). The period 15,500 – 14,000 cal yr BP is characterised by particularly elevated Fe_2O_3 concentrations (up to 17%). Concentrations declined rapidly from ~14,000 to 11,000 cal yr BP, with sediments deposited after 100,00 cal yr BP being characterised by relatively low Fe_2O_3 abundances (<5%).

Variations in CaO (Fig. 10f) and Sr (Fig. 510i) showed similar downcore trends, with marked increases in concentration from ~8,200 cal yr BP. Strong enrichments in CaO and Sr are observed particularly at ~8,000 – 7,000 cal yr BP and 5,900 – 4,600 cal yr BP. Variations in TiO_2 and Zr show close correspondence, with downcore trends characterised by discrete abrupt increases in concentration (Fig. 10g, h). Two major events are observed at ~19,000 – 17,000 cal yr BP and at 15,000 – 14,000 cal yr BP.

Relationships between selected chemical components are shown in Figure 11. Correlation between K_2O and Al_2O_3 reveals a divergent trend, with samples clustering into two distinct groups (Fig. 11a). Correlation between K_2O and Al_2O_3 revealed a divergent trend, with samples clustering into two distinct groups (Fig. 11a). The first group, depicted in black, spans from 1,000 to 8,000 cal yr BP and is characterised by a potassium enrichment in the sediment. The second group from 8,000 cal yr BP onwards, represented in pink, showed a notable decline in K_2O content compared to Al_2O_3. Variations in CaO were strongly correlated with Sr (R^2 = 0.96, Fig. 11b) but showed no relationship with Al_2O_3 (Fig. 11c). A strong relationship is observed between TiO_2 and Al_2O_3 with the exception of a few samples that were enriched inTiO_2 (Fig. 11d). A similar pattern is observed between Zr and Al_2O_3, with several samples showing enrichment in Zr (Fig. 11e). Samples enriched in Zr were also enriched TiO_2 (Fig. 11f).

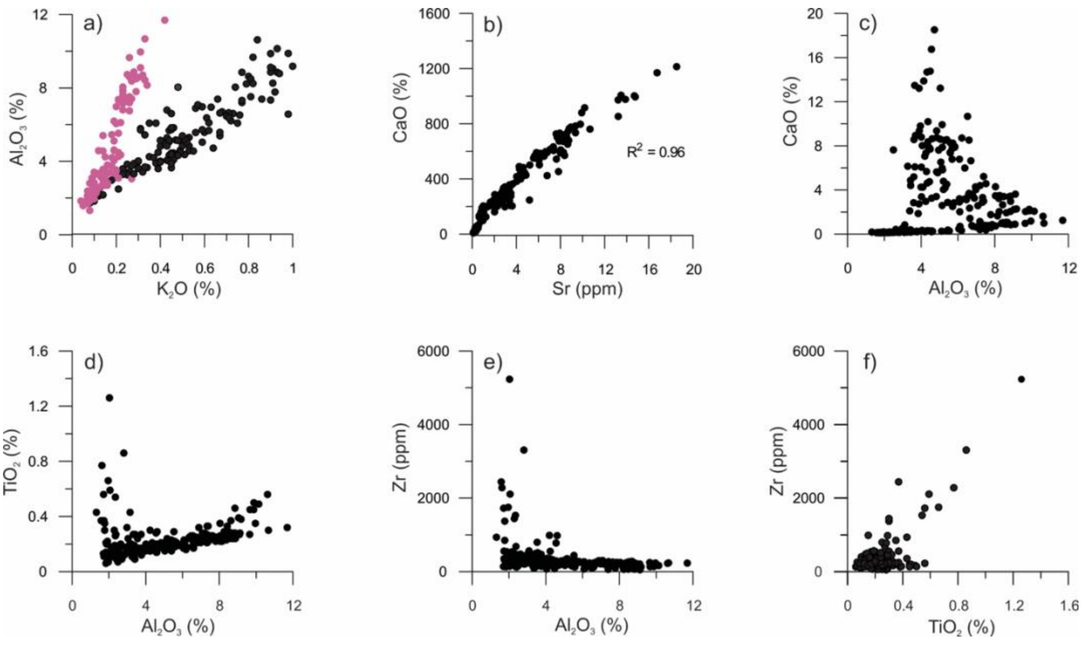

Figure 11: *Relationship between selected major chemical components of sediments from KSV-1*

5.4 Mineralogy

X-ray diffraction analysis reveals that high concentrations of calcium found between ~7,900 and 4,000 cal yr BP are present in the form of calcite ($CaCO_3$) (Fig. 12A). Enrichment in iron, evident between ~15,500 and 13,600 cal yr BP, is attributed to the presence of hematite (Fe_2O_3) (Fig. 12B). Both samples contained high amounts of quartz.

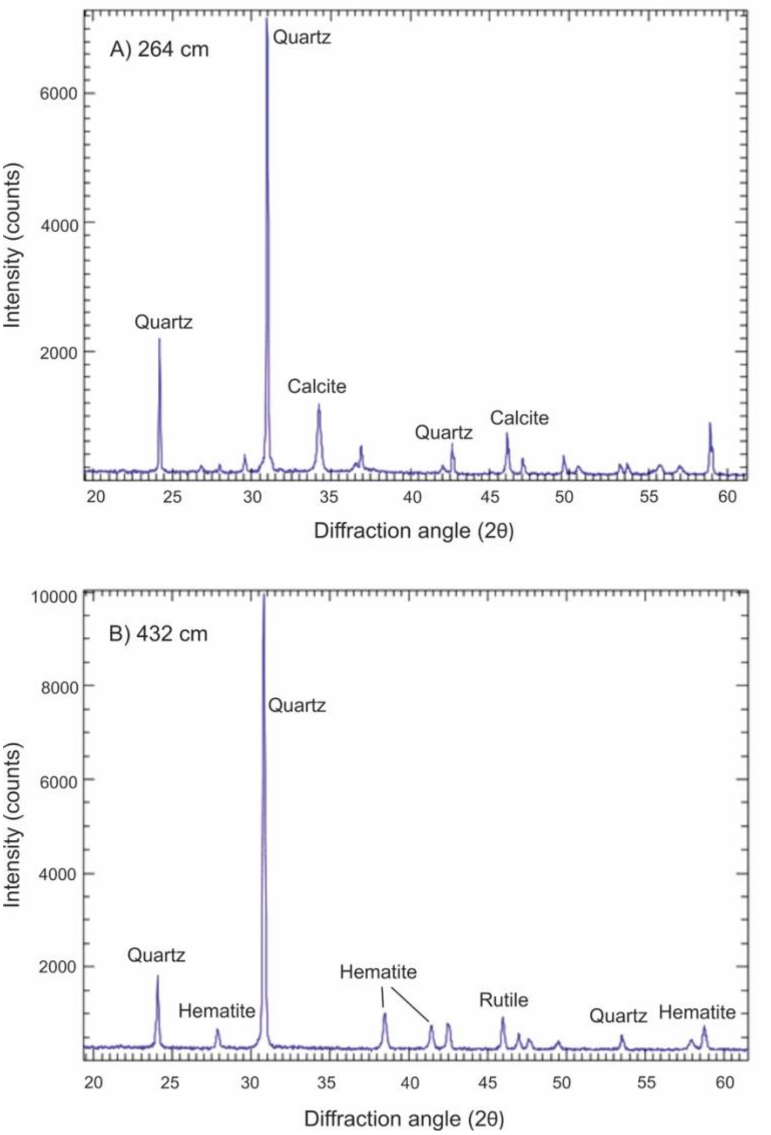

Figure 12: *X-ray diffraction (XRD) patterns and identified mineral phases for two samples A) 264 cm (7500 cal yr BP) and B) 432 cm (15,300 cal yr BP)*

5.5 Elemental ratios

Downcore variations in Si/Al ratios reveal marked fluctuations in sediment deposition over time (Fig. 13a). Between ~30,000 and 19,000 cal yr BP, a gradual increase in Si/Al ratios is observed, followed by sharp increase at ~19,100 cal yr BP. The period 19,100 – 15,000 cal yr BP is characterised by strong fluctuations in Si/Al ratios, which correspond with similar enrichments observed in Fe, Zr and Ti during the period (Fig. 13b, f, g). Fluctuations in Zr/Al and Ti/Al show very similar trends and suggest the occurrence of distinct episodic events centred at ~18,100; 17,200; 15,200 and 14,400 cal yr BP. A decline in Si/Al ratios is observed at ~14,700 cal yr BP and values remain relatively low until ~5,000 cal yr BP when a steady increase is observed. Sediments deposited over the last ~3,000 years are characterised by relatively high Si/Al ratios, although this does not correspond with similar enrichments in Fe, Zr or Ti.

Downcore fluctuations in K/Al reveal a significant shift at ~8500 cal yr BP, with sediments deposited after this time relatively enriched in K (Fig. 13c). A gradual decline in K/Al ratio is observed from around 4,000 cal yr BP to present. Similar trends are observed in Ca/Al and Sr/Al, with strong enrichment between ~8,500 and 3,800 cal yr BP (Fig. 13d).

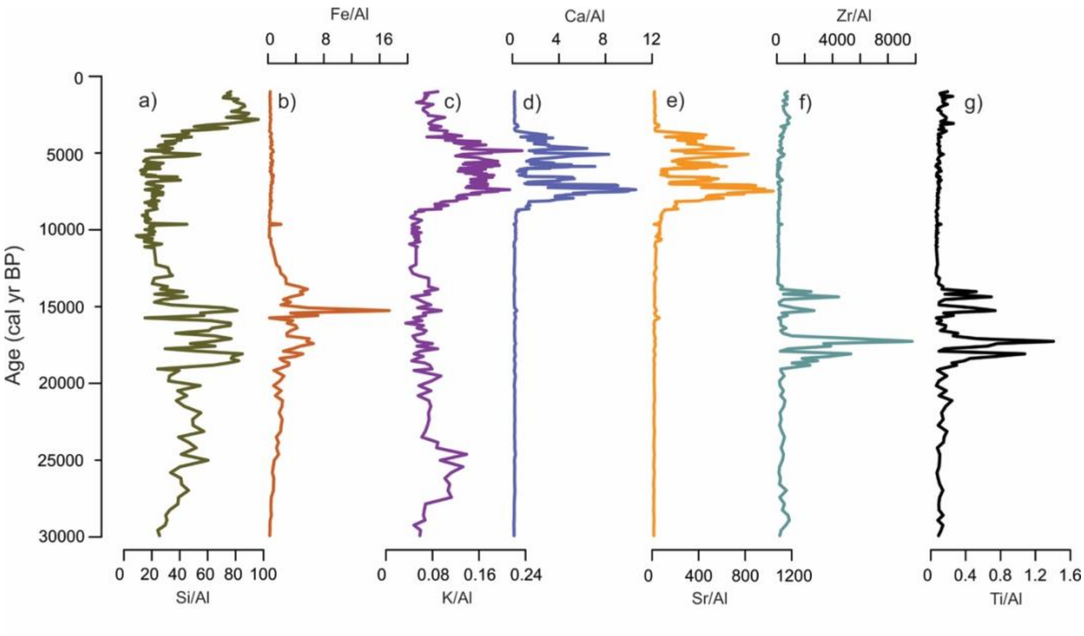

Figure 13: *Downcore variation in selected elemental ratios through core KSV-1*

5.6 Organic geochemistry

Total nitrogen sediment concentrations were too low for reliable $\delta^{15}N$ measurements to be obtained. The $\delta^{13}C$ signal varied between -22.4 and -27‰ (Fig. 14). Between 30,000 and 25,000 cal yr BP, $\delta^{13}C$ ranges between -26 and -27‰, followed by a gradual increase to -24.6‰ at ~21,400 cal yr BP. A steady decline in $\delta^{13}C$ is observed from 21,400 to 15,200 cal yr BP, followed by a pronounced shift to higher values at 14,500 cal yr BP. Thereafter, $\delta^{13}C$ fluctuates between - 26 and - 22‰, before declining sharply at ~3,400 cal yr BP. The last 3,000 years is characterized by relatively low $\delta^{13}C$ signatures, varying between -25 and -23.7‰.

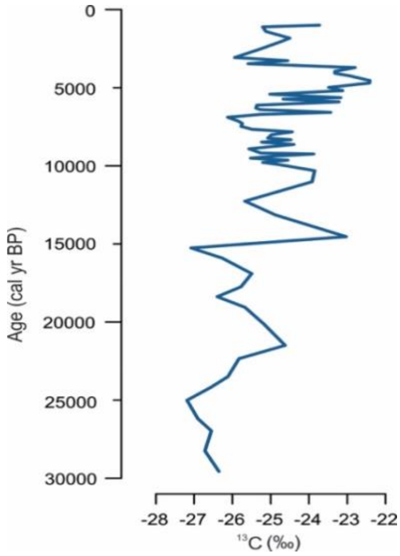

Figure 14: *Downcore variations in δ* ^{13}C *(relative to VPDB)*

Chapter 6: Discussion

6.1 Introduction

The sedimentary record recovered from a Pearly Beach wetland offers a valuable opportunity to investigate the complex depositional processes that have shaped the site over the past 30,000 years. Variations in the physical and chemical nature of the sedimentary infill reflect the dynamic interplay between local, regional, and global factors that drove changes in sea level, sediment supply and climate. This chapter aims to unravel the origins of these sediments and explore the transport and depositional processes that have shaped the landscape. Several geochemical proxies are used to provide insight into the geomorphological evolution of the wetland and associated palaeoenvironemental changes that have occurred along the southern Cape coast. By comparing the reconstructed changes at Pearly Beach with other palaeoclimate records from the region, findings from this study are considered in relation to broad-scale climatic perturbations that occurred in southern Africa over this period.

6.2 Proxy Interpretation

6.2.1 Sea level and change wetland evolution

The core site is located ~0.6 km from the modern coastline and ~22 km from the LGM coastline (Fig. 2; Marean et al., 2020). Most modern coastal lakes and estuaries found along the South African coast originated as river valleys incised during Quaternary sea-level fall and were subsequently drowned and infilled during sea-level transgressions (Cooper et al., 1999; De Lecea et al., 2016). Sea level exerts important controls on the hydrological regime, sedimentation patterns, and ecological dynamics of coastal wetlands (McCarthy and Hancox, 2000). The impact of changing sea levels on wetland development and infilling should therefore be considered when examining the geochemical record from Pearly Beach.

Several geochemical indicators provide insight in the geomorphic evolution of the Pearly Beach wetland. Sediments deposited 30,000 – 15,000 cal yr BP consist primarily of quartz, containing 60 – 90% SiO_2 with minor amounts (<5%) of Al_2O_3 (Fig. 15a). Although grain size analyses were not conducted as part of this study, texturally this material comprises predominantly silt and fine sand. The low sedimentation rates observed during this period are attributed to the low sea levels prevailing during the LGM, which constrained the input of materials into the wetland to fluvial deposition from the upper catchment of the Haelkraal River. Consequently, this reduced sedimentation rate imposes limitations on the temporal resolution of the core for the LGM period, making it unlikely that abrupt or short-term climate events were adequately captured in the core. An increase in the relative proportion of Al_2O_3 from ~15,000 cal yr BP signals an increase in the accumulation of fine-grained material within the wetland. This shift in sediment characteristics is associated with a marked increase in sedimentation rate at ~11,000 cal yr BP and corresponds with a rise in global sea levels following deglaciation (Fig. 15f). Increasing sea levels at this time would have impacted coastal rivers by raising the base level of the riverbed, resulting in the increased deposition of fluvial material. An increase in base level also led to higher rates of organic matter preservation as reflected by an increase in %LOI at this time (Fig. 15b).

The $\delta^{13}C$ signatures of the organic material accumulated within Pearly Beach wetland vary between -22.4 and -27‰, indicating a predominately C_3 source (Fig. 15c). Based on the present data set, it is not possible to differentiate between terrestrial and aquatic sources of organic matter as nitrogen data could not be obtained. However, the $\delta^{13}C$ record from Pearly Beach reveals distinct shifts in organic matter source that likely reflect changes in dominant vegetation communities. From 30,000 – 15,000 cal yr BP, $\delta^{13}C$ values vary between -24 and -27‰, and are strongly characteristic of C_3 terrestrial plants which typically range between -21 and -32‰ (Fig. 6; Deines, 1980). The dominance of shrubs and trees suggests that relatively wet conditions prevailed during this period. Recent research has highlighted potential limitations in interpreting palaeo-pollen signals at 'wet' or 'dry' using modern analogues. The discussions surrounding lower temperatures and reduced CO_2 levels during the LGM raise questions about their influence on evapotranspiration and, consequently, the carbon isotope signals in plants (Prentice et al., 2017; Scheff et al., 2017). This could suggest that dominating C_3 vegetation may have been as a result of reduced CO_2 levels during the LGM rather than an increase in moisture during this period. A distinct shift to enriched $\delta^{13}C$ values between 15,200 and 14,500 cal yr BP points to a change in vegetation community, likely linked to an increase in contribution from C_4 plants (typically ranging from -9 to -17‰ (Deines, 1980)). This could suggest a shift to markedly drier conditions at Pearly Beach from ~14,500 cal yr BP onward, or a change in temperature and CO_2 levels during the post-Glacial warming.

Sea level reached present day levels around 8,000 – 7,000 cal yr BP (Ramsay and Cooper, 2002, Cooper et al., 2018). This led to the inundation of coastal valleys, with sand from the exposed continental shelf accumulating along the present coastline forming an early coastal dune barrier (Thwaites and Cowling, 1988; Cawthra et al., 2019). The presence of calcium carbonate in coastal sediments is often considered a strong indicator for marine intrusions associated with changes in sea level (e.g., Davies et al., 2015). At the Pearly Beach site, enrichment in calcium (i.e., Ca/Al) is predominantly attributed to the precipitation of calcium carbonate, serving as a proxy for changes in marine influence. A pronounced increase in marine influence is inferred from ~8,500 cal yr BP, coinciding with the stabilisation of sea level near to present-day levels (Fig. 15d). Interestingly, this is accompanied by a distinct increase in K/Al ratios, suggesting a possible change in the source sediment accumulating in the wetland or weathering regime (Fig. 15e). Potassium-bearing feldspathic sandstone is found in the upper catchment of the Haelkraal River (Thwaites and Cowling, 1988) and represents the likely source of this K-enriched material. This change in sediment composition corresponds with the timing of sea level rise, which may have promoted increased sediment accumulation within the wetland.

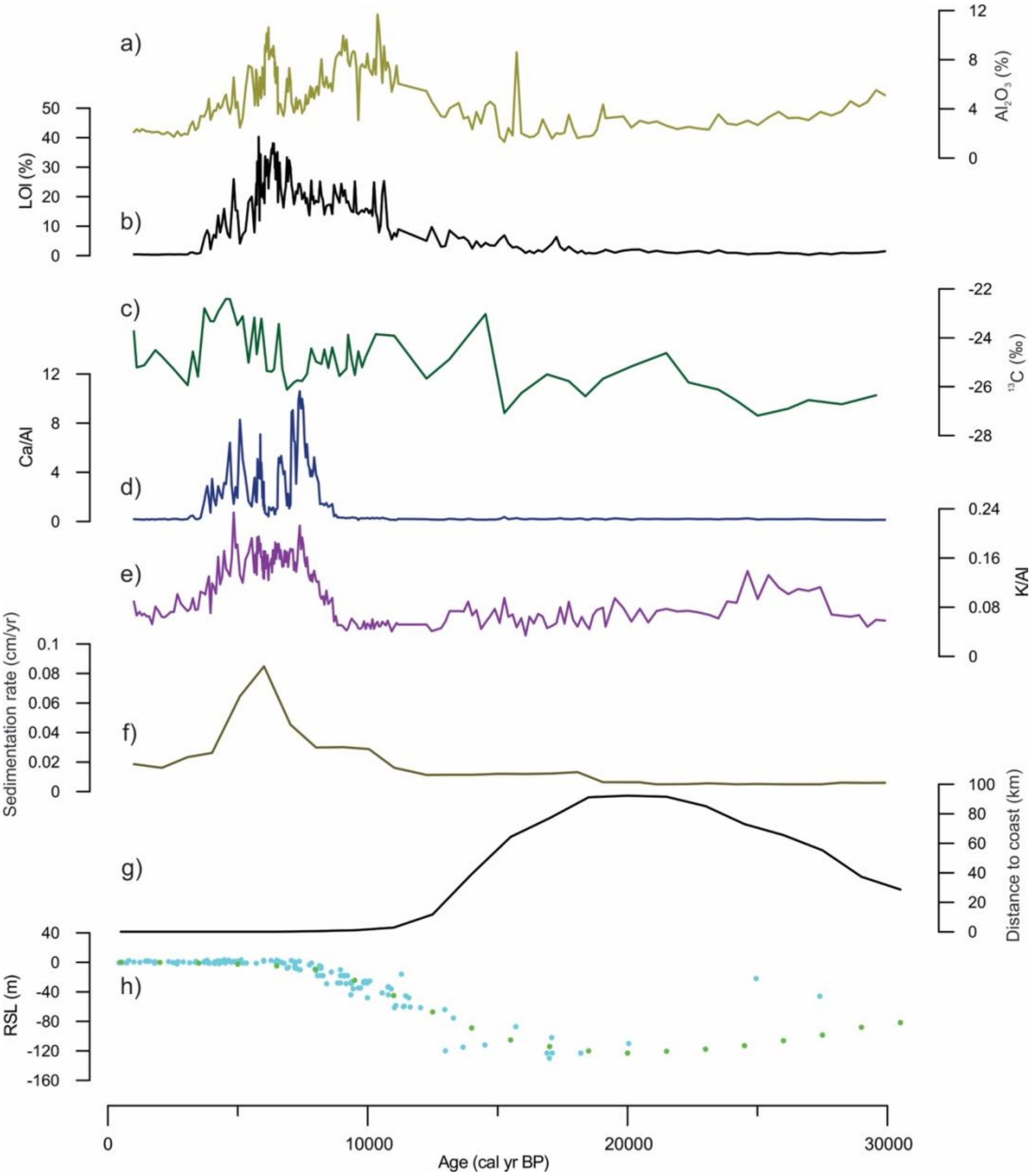

Figure 15: *Comparison between selected geochemical indicators from KSV-1 (a – e), where variations in δ^{13}C are relative to VPDB, with f) changes in sedimentation rate (calculated over 1,000 year intervals), g) reconstructed changes in coastline distance from Pinnacle Point (located near Mossel Bay on the southern Cape Coast) (Fisher et al., 2010), and h) changes in relative sea level derived from dating of shells and beachrock from the coast of South Africa (Ramsay and Cooper, 2002; Cooper et al, 2018; blue) and locally tuned sea level curve (Fisher et al., 2010; green) based on the globally-designed model of Waelbroeck et al. (2002).*

Figure 16 provides a more detailed overview of reconstructed changes in Holocene sea-level along the South African coastline. Two sea level curves have been proposed based on geological evidence found along the west (Compton, 2011; 2006) and east (Ramsay, 1996) coasts of the country, and later refined by Cooper et al., (2018). Evidence found along both coasts indicate that sea levels reached present-day levels between

7,000 and 7,500 cal yr BP. At this time, Pearly Beach wetland experienced a significant increase in marine influence, as reflected by strong enrichments in both Ca and Sr (Fig. 16b, c).

From 7,500 cal yr BP, the sea level curves for the west and east coast appear to deviate. For the west coast, there is evidence for a sea-level highstand (+3 m) around 7,000 – 6,500 cal yr BP (Fig. 16a). The timing of this event corresponds reasonably well with strong peaks in Sr/Al and Ca/Al evident in the record from Pearly Beach.

After 6,500 cal yr BP, sea levels along the west coast declined from ~6,500 cal yr BP to reach present-day levels, with a possible lowstand (-1 m) around 5,500 – 5,000 cal yr BP (Cooper et al., 2018). The Pearly Beach record shows a decline in marine influence, particularly between 6,500 and 6,000 cal yr BP, but there is evidence for moderate marine influence at the site between 6,000 and 6,500 cal yr BP. This is followed by an increase in marine influence from ~5,000 cal yr BP which corresponds with a rise in sea-level at this time, reaching a highstand (+2 m) at ~4500 cal yr BP. Thereafter, marine influence at Pearly Beach declined in response to falling sea-levels, which subsequently stabilised around present-day levels ~3,500 cal yr BP.

Variations in $\delta^{13}C$ are often used to infer marine influence in coastal environments because marine-derived organic carbon is typically characterised by significantly higher $\delta^{13}C$ values compared to terrestrial carbon sources (Lamb et al., 2006). At Pearly Beach, fluctuations in $\delta^{13}C$ do not appear to track variations in other marine indicators (Ca/Al and Sr/Al) or reconstructed changes in sea-level.

The record at Pearly Beach appears to respond to elevated sea levels along the west coast, corresponding to heightened marine influence in the Voëlvlei record between 7,500 to 6,500 cal yr BP (Fig. 16g; Strobel et al., 2021). Meanwhile, sites further eastward, such as Eilandvlei and Whale Rock, demonstrated a decrease in marine influence during this period, seemingly corresponding to lower sea levels along the east coast (Fig. 16e, f; Wündsch et al., 2018; Dyubele, 2023). Marine influence in the Pearly Beach and Voëlvlei records between 6,500 and 5,000 cal yr BP decrease along with declining west coast sea levels. During this period the Eilandvlei and Whale Rock records show a strong increase in marine influence due to rising sea levels along the east coast which reached a highstand (+4 m) at ~ 6,000 cal yr BP. The Voëlvlei and Pearly Beach records both reflect increases in marine influence between 5,000 and 4,000 cal yr BP, corresponding to the secondary highstand of west coast sea levels. During this period, decreased marine influence at Eilandvlei and Whale Rock correspond to declining sea levels along the east coast. After ~ 3,500 cal yr BP all sites show little marine influence corresponding to west and east coast levels stabilising at modern day levels.

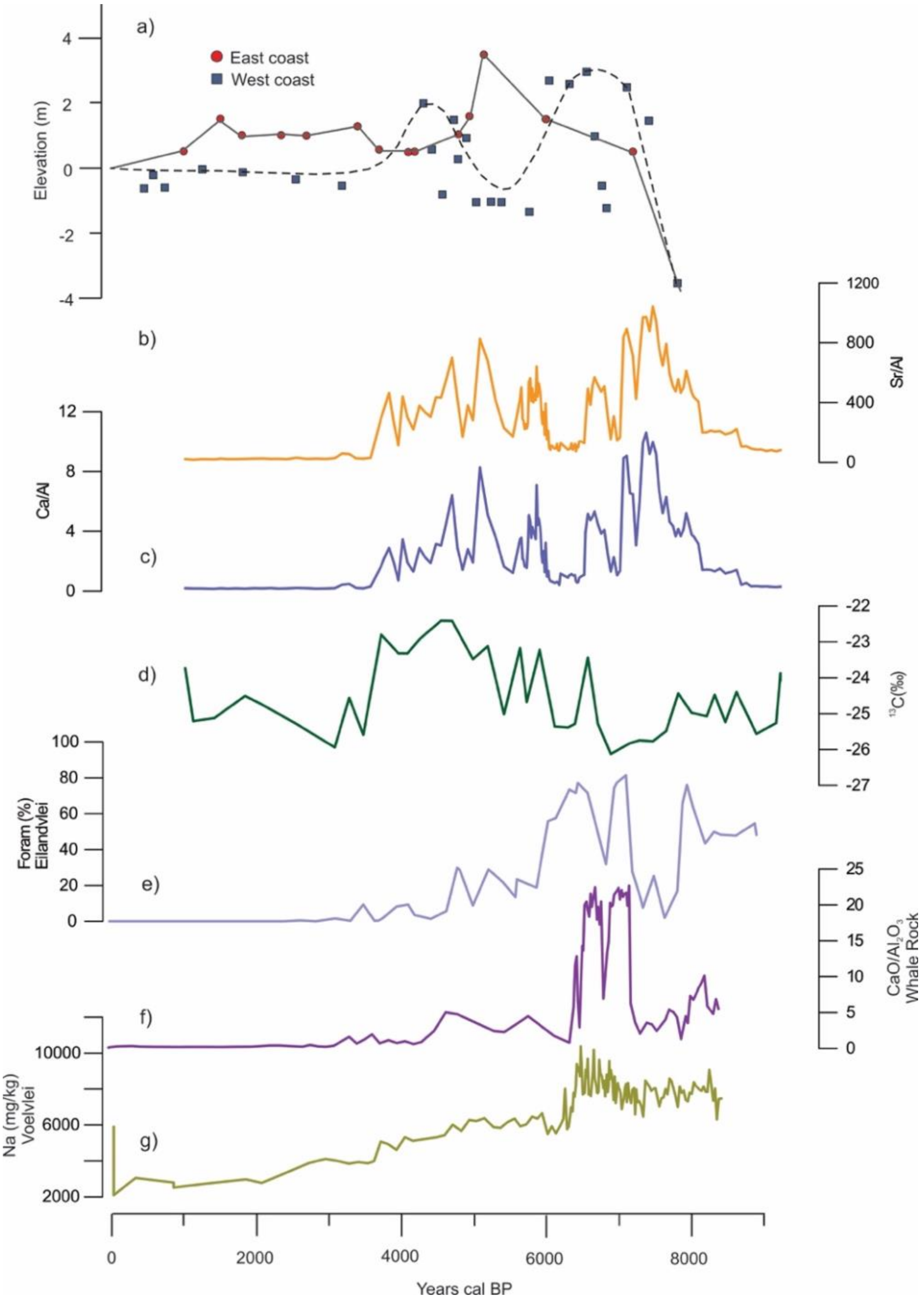

Figure 16: *Comparison between reconstructed variations in a) sea level along the east coast (red) and west coast (blue) of South Africa (Cooper et al., 2018) and indicators of marine influence at KSV-1 (b-d) over the last 10,000 cal yr BP. Regional comparisons of marine indicators from e) Eilandvlei (Wündsch et al., 2018), f) Whale Rock (Dyubele, 2023), and g) Voëlvlei (Strobel et al., 2021).*

6.2.2 Variations in depositional energy

Titanium and zirconium are often present in coastal sediments in the form of heavy minerals, TiO_2 and ZrO_2, respectively. These minerals are typically associated with coarse-grained sediments and can be used to infer changes in aeolian depositional energy, where increased energy conditions lead to enrichments of heavy minerals (Humphries, 2021). The variations in Ti/Al and Zr/Al observed in the Pearly Beach record exhibit similar trends and suggest a period of enhanced transport energy from 18,800 to 14,500 cal yr BP (Fig. 17a, b). The timing of these high-energy events is not clearly related to changes in sea level and occurred when sea level is estimated to have been between -80 and -120 m below present-day levels (Fig. 17e). Coastal sediments in South Africa are typically enriched in Ti and Zr with extensive, commercially viable heavy mineral deposits found along the east and west coast of the country (Rozendaal et al., 2017). Enrichment in Ti and Zr between 18,800 and 14,500 cal yr BP thus likely reflects the influx of sand from the exposed continental shelf into the wetland via aeolian processes. The gradual sloping Agulhas Bank means that large tracts of submerged land along the southern coastline were exposed during sea level regressions, providing a potential source of easily erodible sediment. A process involving aeolian transport and deposition is supported by corresponding increases in the Si/Al ratio. This, together with the enrichment of heavy minerals suggest that the period 18,000 to 14,500 cal yr BP was likely characterised by increased wind intensity (Fig. 17d). Changes in the sediment facies during this period also suggests a change in wetland input, where between 18,000 to 14,500 cal yr BP the sediment profile changes from dark brown sandy silts from fluvial inputs, to alternating dark and light brown sands with yellow sand pockets (Fig. 9A). The grain size distribution and textural characteristics of this material has yet to be investigated but would provide additional insight into their likely source.

Iron is often associated with heavy minerals (e.g., ilmenite, $FeTiO_3$), although such phases were not identified in any of the samples analysed. However, the upper catchment of the Haelkraal River contains siliceous ferricrete outcrops (Thwaites, 1988), which represents a potential source of iron. Hematite was identified in samples enriched in Fe and an increase in catchment erosion, possibly triggered by intense rainstorms could account for iron enrichments between 18,000 and 14,500 cal yr BP (Fig. 17c).

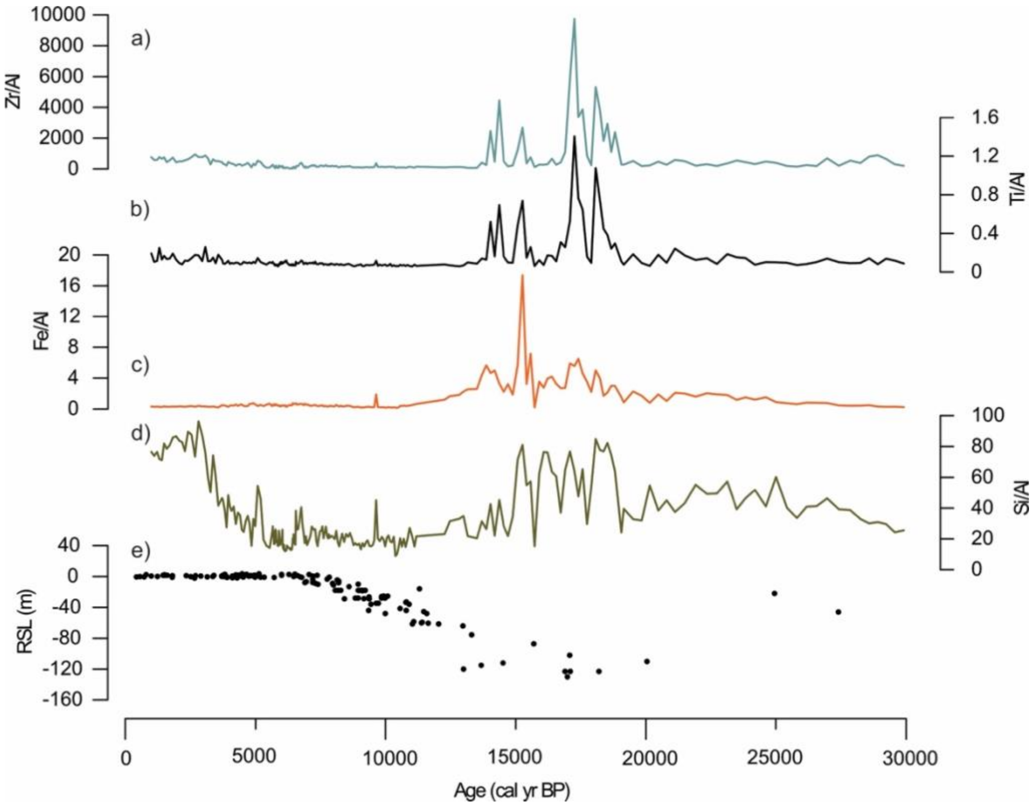

Figure 17: *Comparison between different geochemical indicators of transport energy at Pearly Beach. Sea level data from Ramsay and Cooper (2002) and Cooper et al. (2018)*

6.3 Regional climate reconstruction

Several studies indicate that the south western region of South Africa experienced relatively wet conditions during the LGM (Stowe and Sealy, 2015; Sealy et al., 2016; Thackeray and Fitchett, 2016; Quick et al., 2021). Increased moisture at this time has been associated with the more northward position of the westerly wind caused by an expansion in Antarctic sea ice (Chase et al., 2013; Chase et al., 2020). There is general agreement between available paleorecords that this brought more rainfall to the south-western Cape (Stowe and Sealy, 2015; Sealy et al., 2016; Thackeray and Fitchett, 2016; Quick et al., 2021). Depleted $\delta^{13}C$ signals in the Pearly Beach record (Fig. 18a) seemingly agree with this, were dominating C_3 terrestrial plants could suggest increased moisture at the site.

The geochemical record from Pearly Beach provides new insight into conditions that prevailed during the Last glacial-interglacial period, where an increase in wind intensity 18,000 – 14,500 cal yr BP at Pearly Beach is most likely to have been associated with intensification in Southern Hemisphere westerly winds. These winds are responsible for the arrival of frontal systems that bring rain and strong winds to the modern-day WRZ. This could indicate that increased precipitation brought on by frontal systems embedded in the westerly winds was likely associated with a strengthening in wind activity.

A fossil pollen record from a nearby wetland at Pearly Beach found evidence for considerable variation in temperature and moisture availability, particularly during glacial Termination I (~19,000 – 11,7000 cal yr

BP; Quick et al., 2021). A marked increase in coastal thicket pollen was recorded from ~18,500 to 15,000 cal yr BP, suggesting a substantial increase in moisture availability at this time (Fig. 18c). The authors attributed this shift to a slowdown in the AMOC (Fig. 18d), which resulted in a build-up of heat in the southeast Atlantic. The timing of increased moisture at Pearly Beach, as documented by Quick et al. (2021), corresponds well with a strengthening in wind/storm inferred from KSV-1. It is possible that a build-up of heat in the southeast Atlantic (reflected in Benguela SSTs; Fig. 18e) brought on by a slowdown in the AMOC increased moisture uptake in the frontal storms, resulting in stronger low-pressure systems and intensified storms.

The KSV-1 record indicates that this period of intense storm activity ended after ~14,500 cal yr BP. This coincided with a strengthening of the AMOC and lower Benguela SSTs (Fig. 18d, e). Coupled to this, increasing global temperatures during deglaciation lead to a decline in Antarctic sea ice extent (Fig. 18f). The southward shift of the westerlies reduced their influence at Pearly Beach, leading to drier conditions. This is indicated by the pronounced shift to higher $\delta^{13}C$ values at this time (Fig. 18b), as well as the sharp decline in coastal thicket (Fig. 18c).

A mid-Holocene shift to higher $\delta^{13}C$ values between 6,500 and 4,000 cal yr BP suggests a possible period of enhanced aridity at Pearly Beach (Fig. 18b). The Pearly Beach fossil pollen record (PB-1) also shows low levels of coastal thicket during this time (Fig. 18c). At around 6,000 cal yr BP there is a notable decline in sea ice extent which may resulted in a poleward shift in the westerlies and subsequent reduction of rain in the region (Fig. 18f). There is debate around the mid-Holocene experiencing dry conditions, with other records indicating increased moisture during this period (Chase et al., 2015b; Chase et al., 2019a).

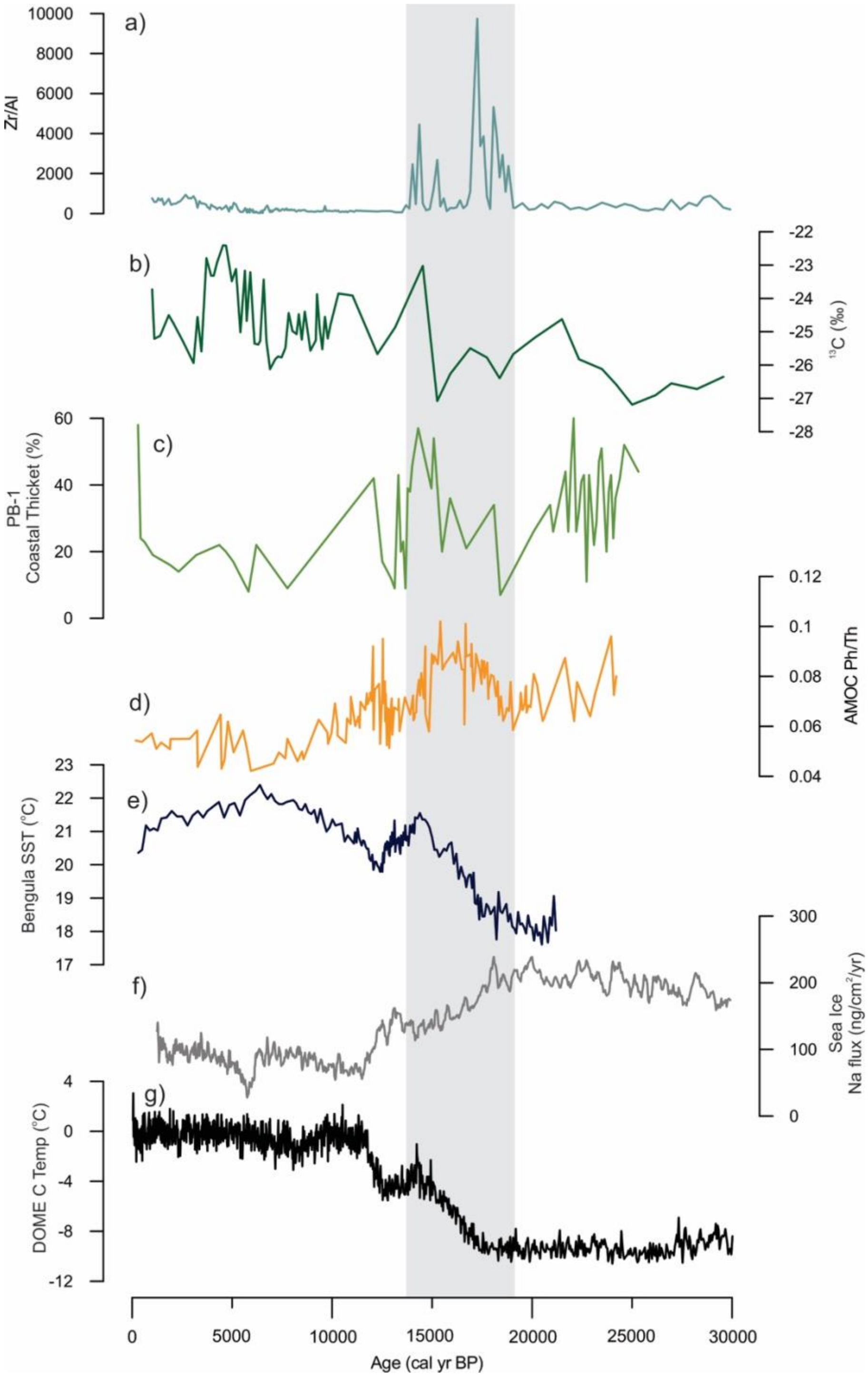

Figure 18: : *Comparisons between selected geochemical indicators from Pearly Beach (KSV-1) and other regional and global climate data sets. a) Heavy mineral deposits from KSV-1, b) Stable carbon isotope record from KSV-1, c) Coastal thicket pollen record from PB-1 (Quick et al., 2021), d) Atlantic overturning circulation strength (Ng et al., 2018), e) Sea surface temperature records of the Benguela current (Kim et al., 2002), f) Antarctic sea ice extent (Fischer et al., 2007), and g) Antarcitc temperature record from Dome C (Jouzel et al., 2007).*

6.4 Broader climatic context

Reconstructed changes in westerly wind dynamics at Pearly Beach should be considered in the context of broader climatic changes that occurred in southern Africa during the last glacial-interglacial transition. Although relatively few well-dated records from region covering this time period exist, there are several key records against which the geochemical data from Pearly Beach can be compared.

A marine core from Walvis Ridge in the south-east Atlantic provides one of the few available records of wind intensity in the region (Fig. 20c; Stuut et al., 2002). Based on grain size variations, this record suggests that trade-winds over the south-east Atlantic strengthened during glacial periods. In particular, a period of enhanced wind strength between 18,000 and 14,500 cal yr BP, coincides with major heavy mineral enrichments at Pearly Beach. An aeolian flux record from Mfabeni peatland has been argued to indicate that westerly storms influenced climate variability on the east coast of South Africa during the last glacial period (Fig. 20d; Humphries et al., 2017). Increased wind intensity at Mfabeni between 23,000 and 14,000 cal yr BP is attributed to the enhanced influence of westerly winds, which brought stronger or more intense storms to the east coast (Humphries et al., 2017). A reconstructed temperature record from Mfabeni based on branched glycerol dialkyl glycerol tetraethers (brGDGTs) indicates that air temperatures were lowest between ~16,000 – 15,000 cal yr BP (Fig. 20e; Fietz et al., 2023). This coincides with inferred storm intensity at Pearly Beach, and may be attributable to the passage of cold westerly-driven air masses across the country.

A similar cooling trend is evident in speleothem $\delta^{18}O$ records from Cold Air Cave (Makapansgat, Limpopo) and Cango Caves (Oudtshoorn, Western Cape) (Fig. 20f). At Cold Air Cave, major cooling events are observed at 18,600 and 17,600 cal yr BP, with a more moderate event at ~14,600 cal yr BP (Holmgren et al., 2003). At Cango Caves, there is evidence for major cooling between 18,600 and 15,500 cal yr BP (Talma and Vogel, 1990). The timing of these events, evident in records from across the country (Mfabeni, Cold Air Cave, and Cango Caves), suggest a general cooling trend in South Africa between ~18,500 and 14,500 cal yr BP. New geochemical data from Pearly Beach suggests that this cooling may have been linked to intensification of westerly winds at this time.

The Pearly Beach record suggests that westerly wind intensity/influence decreased after 14,500 cal yr BP. This was associated with reduced rainfall in the region and change in vegetation to more drought tolerant species. This shift in climatic conditions aligns well with a decrease in aeolian flux and shift to warmer conditions after 15,000 cal yr BP at Mfabeni (Fig. 19d). Speleothem records from Cold Air Cave and Cango Caves also indicate warming towards Holocene temperatures from around 15,000 cal yr BP (Fig. 19f). The onset of warming following deglaciation thus appears to only commence ~15,000 cal yr BP, despite an increase in global CO_2 and Antarctic temperatures from ~18,000 cal yr BP (Fig. 20g). The observed lag in warming over South Africa may have been due to the enhanced influence of the westerly winds during this period, which continued to push cold air masses across the interior of the country.

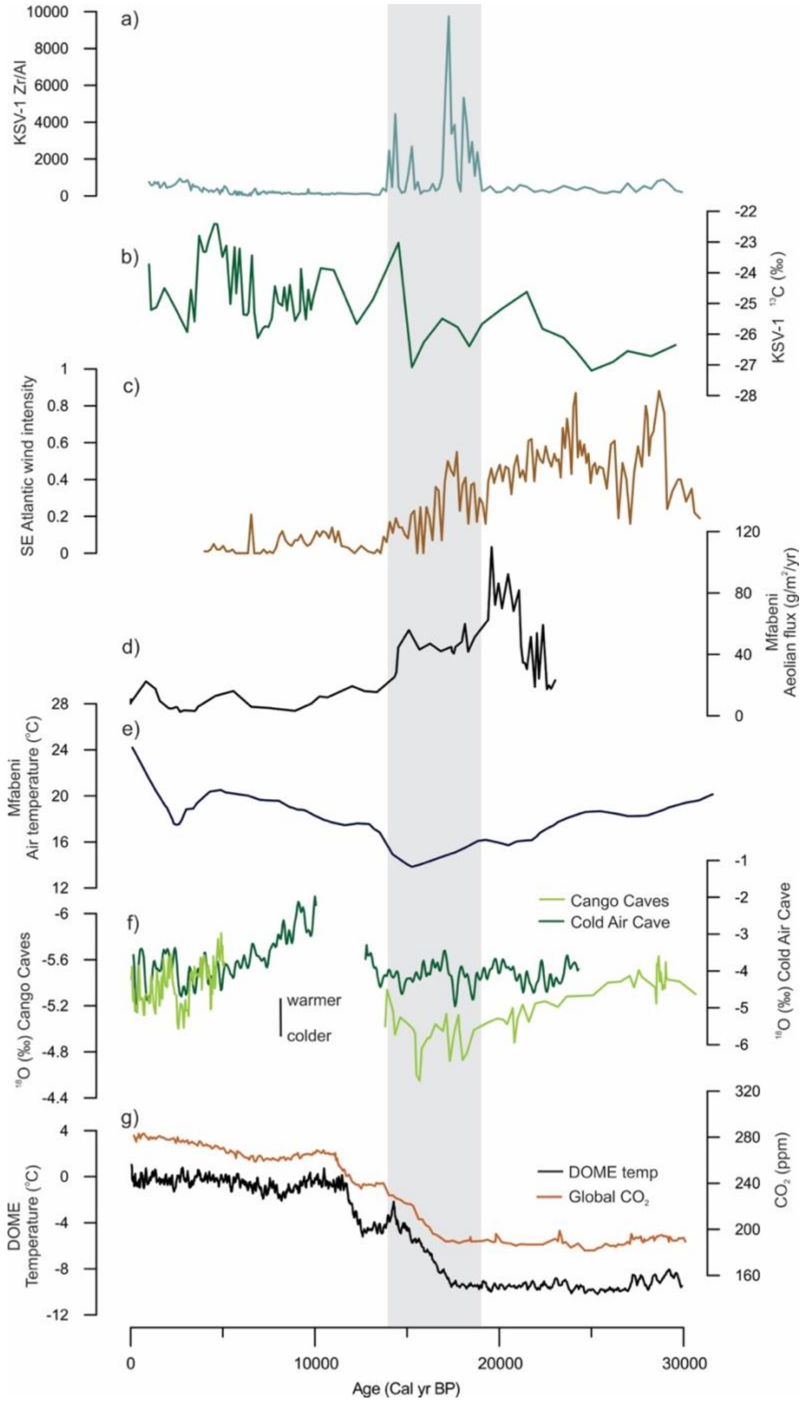

Figure 19: *Comparisons of records relevant to the broader climate dynamicsin southern Africa associated with the changes observed in the Pearly Beach record. a) Heavy mineral deposits in Pearly Beach, b) Stable carbon isotope record from Pearly Beach, c) Wind intensity data from Walvis Ridge (Stuut et al., 2002, d) Mfabeni aeoloian flux proxy (Humhries et al., 2017), e) Mfabeni temperature record (Fietz et al., 2023, f) Cango Cave $\delta^{18}O$ record (Talma and Vogel, 1990) and Cold Air Cave $\delta^{18}O$ record (Holmgren et al., 2003), g) Antactic DOME ice core (Jouzel et al., 2007) and Global CO_2 concentrations (Ahn and Brook, 2014; Monnin et al., 2001).*

Chapter 7: Conclusions

The sedimentary record from Pearly Beach wetland (KSV-1) provides valuable insights into the complex depositional processes and environmental changes that have influenced the region over the past 30,000 years. Through the analysis of geochemical proxies, the geomorphic evolution of the wetland and its response to both regional and global factors, including sea-level changes and climatic variations has been investigated.

The core from Pearly Beach reveals distinct lithostratigraphic changes that represent different depositional environments and sediment characteristics over time. Sedimentation rates, as well as variations in organic matter content (%LOI) and geochemical components (SiO_2, Al_2O_3, K_2O, Fe_2O_3, CaO, Sr, TiO_2, and Zr), provide evidence of past environmental changes and depositional processes. However, low sedimentation rates during the LGM and start of the following Glacial-interglacial period significantly restricts the temporal resolution of the Pearly Beach record. An increase in sedimentation rates and organic matter content began around 15,000 cal yr BP, coinciding with a rise in global sea levels following deglaciation. An increase in marine influence at this site is inferred at ~8,500 cal yr BP, corresponding to the stabilisation of sea level near present-day levels. Strong marine intrusions are evident between 7,000 and 6,500 cal yr BP, and generally correspond with indicators of marine influence at other nearby coastal sites, which appear to respond to reconstructed changes in sea level along the west coast of the country.

The analysis of heavy minerals (TiO_2 and ZrO_2) in the Pearly Beach core provides valuable insights into past sedimentary processes and environmental conditions during the period between 18,800 and 14,500 cal yr BP. During this period, marked enrichments in heavy minerals are used to infer high energy conditions prevailing in the coastal environment. These stronger, more intense storms are attributed to an intensification of Southern Hemisphere westerly winds. This hypothesis is supported by a nearby fossil pollen record (PB-1; Quick et al., 2021), which documented a substantial increase in coastal thicket pollen from ~18,500 to 15,000 cal yr BP. The heightened moisture availability during this period is attributed to a slowdown in the Atlantic Meridional Overturning Circulation (AMOC), leading to a build-up of heat in the southeast Atlantic. The increased moisture uptake in frontal storms, driven by a rise in sea surface temperatures in the Benguela Current region, likely contributed to the observed stronger low-pressure systems and intensified storms at Pearly Beach. Comparison with records from elsewhere in South Africa, such as speleothem $\delta^{18}O$ records from Cold Air Cave and Cango Caves, indicate a cooling trend over the country ~18,500 -14,500 cal yr BP, which may have been linked to the passage of stronger westerly-driven cold fronts across the country. The Pearly Beach record suggests that after 14,500 cal yr BP, the intensity and influence of westerly winds decreased, leading to reduced rainfall in the region and a shift in vegetation to more drought-tolerant species. This is reflected in a distinct shift to higher $\delta^{13}C$ values, which is linked to increased aridity and the expansion of drought-tolerant C_4 plants. This shift in climatic conditions coincides with a decrease in aeolian flux and a transition to warmer conditions at Mfabeni, Cold Air Cave and Cango Caves from around 15,000 cal yr BP. The observed lag in warming over South Africa, with global CO_2 and Antarctic temperatures increasing from 18,000 cal yr BP, may point to the continued influence of the westerly winds during this period, which brought cold air masses across the interior of the country.

To advance our understanding of past climatic and environmental changes in the southern Cape coast, it is imperative to explore additional research avenues. One essential aspect to explore is the integration of additional proxies to complement the existing geochemical indicators. Incorporating stable nitrogen isotope ($\delta^{15}N$) analyses would allow for a more comprehensive assessment of organic matter sources, differentiating between terrestrial and aquatic contributions. This could provide crucial information about changes in the hydrological regime and nutrient availability in the southern Coast over time. Pollen and microcharcoal analysis on KSV-1 would further contribute to our understanding of past vegetation dynamics and fire history in the region, providing valuable insights into changes in plant communities and past fire regimes. By examining the pollen assemblages, researchers could identify shifts in vegetation types and their responses to climatic changes. Additionally, conducting grain size analyses on the sediments would offer insights into the energy conditions during sediment deposition, further enhancing our understanding of the depositional processes and landscape evolution. Lastly, expanding the geographical scope of the study to include other coastal wetlands and terrestrial sites in the region would enable a broader comparison of climatic and environmental changes, helping to paint a more comprehensive picture of past climate dynamics in southern Africa.

References

Ahn, J. and Brook, E.J. 2014. Siple Dome ice reveals two modes of millennial CO2 change during the last ice age. *Nature Communications*, 5(1), p.3723.

Avery, G. 1974. Open station shell midden sites and associated features from the Pearly Beach area, south-western Cape. *The South African Archaeological Bulletin*, 29(115/116), pp.104-114.

Avery, G., Cruz-Uribe, K., Goldberg, P., Grine, F.E., Klein, R.G., Lenardi, M.J., Marean, C.W., Rink, W.J., Schwarcz, H.P., Thackeray, A.I., and Wilson, M.L. 1997. The 1992–1993 excavations at the Die Kelders Middle and Later Stone Age cave site, South Africa. *Journal of field archaeology*, 24(3), pp.263-291.

Baker, A., Pedentchouk, N., Routh, J., and Roychoudhury, A.N. 2017. Climatic variability in Mfabeni peatlands (South Africa) since the late Pleistocene. *Quaternary Science Reviews*, 160, pp.57-66.

Bamford, M. 2016. Early Holocene charcoals from Stratum 4d of Wonderwerk Cave, Northern Cape. *Quaternary International*, 404, p.186.

Bar-Matthews, M., Marean, C.W., Jacobs, Z., Karkanas, P., Fisher, E.C., Herries, A.I., Brown, K., Williams, H.M., Bernatchez, J., Ayalon, A., and Nilssen, P.J. 2010. A high resolution and continuous isotopic speleothem record of paleoclimate and paleoenvironment from 90 to 53 ka from Pinnacle Point on the south coast of South Africa. *Quaternary Science Reviews*, 29(17-18), pp.2131-2145.

Barker, S., Diz, P., Vautravers, M.J., Pike, J., Knorr, G., Hall, I.R., Broecker, W.S. 2009. Interhemispheric Atlantic seesaw response during the last deglaciation. *Nature*, 457, pp.1097-1102.

Barrable, A., Meadows, M.E., and Hewitson, B.C. 2002. Environmental reconstruction and climate modelling of the Late Quaternary in the winter rainfall region of the Western Cape, South Africa. *South African Journal of Science*, 98(11), pp.611-616.

Baxter, A. 1996. Late Quaternary Palaeoenvironments of the Sandveld, Western Cape Province, South Africa. Unpublished PhD Thesis, University of Cape Town, Cape Town.

Beal, L.M., De Ruijter, W.P.M., Biastoch, A., Zahn, R. 2011. On the role of the Agulhas system in ocean circulation and climate. *Nature*, 472, pp.429–436.

Benedict, C.R., Wong, W.W.L., Wong, J.H.H. 1980. Fractionation of the stable isotopes of inorganic carbon by seagrasses. *Plant Physiology*, 65, pp.512–517.

Bjørlykke, K. 2010. Sedimentary Geochemistry. In: K. Bjørlykke (Ed.), *Petroleum Geoscience: From Sedimentary Environments to Rock Physics*. Springer-Verlag Berlin, pp.87-111.

Blaauw, M. and Christen, J.A. 2011. Flexible paleoclimate age-depth models using an autoregressive gamma process.

Bolton, J.J. and Stegenga, H. 1990. The seaweeds of De Hoop Nature Reserve and their phytogeographical significance. *South African Journal of Botany*, 56(2), pp.233-238.

Botha, G., Haldorsen, S., and Porat, N. 2013. Geological history. In: Perissonoto R, Stretch D, Taylor RH (Eds.) *Ecology and conservation of estuarine ecosystems; Lake St Lucia as a global model*. Cambridge, Cambridge University Press, pp.47-61.

Braun, K., Bar-Matthews, M., Matthews, A., Ayalon, A., Cowling, R.M., Karkanas, P., Fisher, E.C., Dyez, K., Zilberman, T., Marean, C.W. 2019. Late Pleistocene records of speleothem stable isotopic compositions from Pinnacle Point on the South African south coast. *Quaternary Research*, 91(1), pp.265-288.

Braun, K., Bar-Matthews, M., Matthews, A., Ayalon, A., Zilberman, T., Cowling, R.M., Fisher, E.C., Herries, A.I., Brink, J.S., Marean, C.W. 2020. Comparison of climate and environment on the edge of the Palaeo-Agulhas Plain to the Little Karoo (South Africa) in Marine Isotope Stages 5–3 as indicated by speleothems. *Quaternary Science Reviews*, 235, p.105803.

Broecker, W.S. 1998. Paleocean circulation during the last deglaciation: a bipolar seesaw? *Paleoceanography*, 13, pp.119–121.

Brook, G.A., Scott, L., Railsback, L.B., Goddard, E.A. 2010. A 35 ka pollen and isotope record of environmental change along the southern margin of the Kalahari -pollen, charcoal and plant macrofossil evidence from a stalagmite and animal dung deposits in Wonderwerk Cave, South Africa. *Journal of Arid Environments*, 74, pp.870e884.

Caley, T., Kim, J.-H., Malaizé, B., Giraudeau, J., Laepple, T., Caillon, N., Charlier, K., Rebaubier, H., Rossignol, L., Castañeda, I.S., Schouten, S., Sinninghe Damsté, J. 2011. High-latitude obliquity as a dominant forcing in the Agulhas current system. *Climate of the Past*, 7, pp.1285–1296.

Calvert, S.E., Pedersen, T.F. 2007. Elemental proxies for palaeoclimatic and palaeoceanographic variability in marine sediments: interpretation and application. *Developments in Marine Geology*, 1, pp.567–644.

Campbell, B.M. 1986. Vegetation classification in a floristically complex area: The Cape Floristic Region. *South African Journal of Botany*, 52(2), pp.129-140.

Carr, A.S., Boom, A., Chase, B.M., Meadows, M.E., Grimes, H.L. 2015. Holocene sea level and environmental change on the west coast of South Africa: evidence from plant biomarkers, stable isotopes and pollen. *Journal of Paleolimnology*, 53, pp.415-432.

Carr, A.S., Chase, B.M., Mackay, A. 2016. Mid to Late Quaternary landscape and environmental dynamics in the Middle Stone Age of southern South Africa. In: Africa from MIS 6-2: Population Dynamics and Paleoenvironments, pp.23-47.

Carr, A.S., Thomas, D.S., Bateman, M.D., Meadows, M.E., Chase, B. 2006a. Late Quaternary palaeoenvironments of the winter-rainfall zone of southern Africa: palynological and sedimentological evidence from the Agulhas Plain. *Palaeogeography, Palaeoclimatology, Palaeoecology*, 239(1-2), pp.147-165.

Carr, A.S., Thomas, D.S.G., Bateman, M.D. 2006b. Climatic and sea level controls on late Quaternary eolian activity on the Agulhas Plain, South Africa. *Quaternary Research*, 65, pp.252-263.

Cawthra, H.C., Anderson, R.J., De Vynck, J.C., Jacobs, Z., Jerardino, A., Kyriacou, K., Marean, C.W. 2020. Migration of Pleistocene shorelines across the Palaeo-Agulhas Plain: Evidence from dated sub-bottom profiles and archaeological shellfish assemblages. *Quaternary Science Reviews*, 235, p.106-107.

Cawthra, H.C., Compton, J.S., Fisher, E.C., MacHutchon, M.R., Marean, C.W. 2015. Submerged terrestrial landscape features off the South African south coast. In: Harff, J., Bailey, G., Lüth, F. (Eds.), *Geology and Archaeology: Submerged Landscapes of the Continental Shelf*, vol. 411. Special Publication of the Geological Society of London, pp. 219-233.

Cawthra, H.C., Cowling, R.M., Andò, S., Marean, C.W. 2019. Geological and soil maps of the Palaeo-Agulhas Plain for the Last Glacial Maximum. *Quaternary Science Reviews*, 235, p.105858.

Chase, B. Boom, A., Carr, A., Chevalier, M., Quick, L., Verboom, A., Reimer, P. 2019a. Extreme hydroclimate gradients within the western Cape Floristic region of South Africa since the Last Glacial Maximum, 219, pp. 297–307.

Chase, B.M. and Quick, L.J., 2018. Influence of Agulhas forcing of Holocene climate change in South Africa's southern Cape. *Quaternary Research*, *90*(2), pp.303-309.

Chase, B.M., Boom, A., Carr, A.S., Carré, M., Chevalier, M., Meadows, M.E., Pedro, J.B., Stager, J.C., Reimer, P.J. 2015a. Evolving southwest African response to abrupt deglacial North Atlantic climate change events. *Quaternary Science Reviews*, 121, pp.132–136.

Chase, B.M., Boom, A., Carr, A.S., Meadows, M.E., Reimer, P.J. 2013. Holocene climate change in southernmost South Africa: rock hyrax middens record shifts in the southern westerlies. *Quaternary Science Reviews*, 82, pp.199-205.

Chase, B.M., Boom, A., Carr, A.S., Quick, L.J., Reimer, P.J. 2020. High-resolution record of Holocene climate change dynamics from southern Africa's temperate-tropical boundary, Baviaanskloof, South Africa. *Palaeogeography, Palaeoclimatology, Palaeoecology*, 539, p.109518.

Chase, B.M., Chevalier, M., Boom, A., Carr, A.S. 2017. The dynamic relationship between temperate and tropical circulation systems across South Africa since the last glacial maximum. *Quaternary Science Reviews*, 174, pp.54–62.

Chase, B.M., Faith, J.T., Mackay, A., Chevalier, M., Carr, A.S., Boom, A., Lim, S., Reimer, P.J. 2018. Climatic controls on Later Stone Age human adaptation in Africa's southern Cape. *Journal of Human Evolution*, 114, pp.35–44.

Chase, B.M., Lim, S., Chevalier, M., Boom, A., Carr, A.S., Meadows, M.E., Reimer, P.J. 2015b. Influence of tropical easterlies in southern Africa's winter rainfall zone during the Holocene. *Quaternary Science Reviews*, 107, pp.138–148.

Chase, B.M., Meadows, M.E. 2007. Late Quaternary dynamics of southern Africa's winter rainfall zone. *Earth-Science Reviews*, 84(3-4), pp.103–138.

Chase, B.M., Meadows, M.E., Carr, A.S., Reimer, P.J. 2010. Evidence for progressive Holocene aridification in southern Africa recorded in Namibian hyrax middens: Implications for African Monsoon dynamics and the "African Humid Period". *Quaternary Research*, 74, pp.36-45.

Chase, B.M., Quick, L.J., Meadows, M.E., Scott, L., Thomas, D.S.G., Reimer, P.J. 2011. Late glacial interhemispheric climate dynamics revealed in South African hyrax middens. *Geology*, 39, pp.19e22.

Chase, B.M., Scott, L., Meadows, M.E., Gil-Romera, G., Boom, A., Carr, A.S., Reimer, P.J., Truc, L., Valsecchi, V., Quick, L.J. 2012. Rock hyrax middens: a palaeoenvironmental archive for southern African drylands. *Quaternary Science Reviews*, 56, pp.107-125.

Chevalier, M., Chase, B.M. 2015. Southeast African records reveal a coherent shift from high- to low-latitude forcing mechanisms along the east African margin across last glacial–interglacial transition. *Quaternary Science Reviews*, 125, pp.117-130.

Chevalier, M., Chase, B.M. 2016. Determining the drivers of long-term aridity variability: a southern African case study. *Journal of Quaternary Science*, 31, pp.143-151.

Chivas, A.R., Garcia, A., van der Kaars, S., Couapel, M.J.J., Holt, S., Reeves, J.M., Wheeler, D.J., Switzer, A.D., Murray-Wallace, C.V., Banerjee, D., Price, D.M., Wang, S.X., Pearson, G., Edger, N.T., Beaufort, L., De Deckker, P., Lawson, E., Cecil, C.B. 2001. Sea-level and environmental changes since the last interglacial in the Gulf of Carpentaria, Australia: an overview. *Quaternary International*, 83–85, pp.19–46.

Climate Systems Analysis Group, U.C.T. 2012. Climate Information Portal (CIP). http://cip.csag.uct.ac.za/webclient/map. Accessed on: 15 March 2023.

Cockcroft, M.J., Wilkinson, M.J., Tyson, P.D. 1987. The application of a present-day climatic model to the late Quaternary in southern Africa. *Climatic Change*, 10, pp.161-181.

Coffin, R.B., Fry, B., Peterson, B.J., Wright, R.T. 1989. Carbon isotopic compositions of estuarine bacteria. *Limnology and Oceanography*, 34, pp.1305–1310.

Compton, J.S. 2001. Holocene sea-level fluctuations inferred from the evolution of depositional environments of the southern Langebaan Lagoon salt marsh, South Africa. *The Holocene*, 11(4), pp.395-405.

Compton, J.S. 2006. The mid-Holocene sea-level highstand at Bogenfels Pan on the southwest coast of Namibia. *Quaternary Research*, 66(2), pp.303-310.

Compton, J.S. 2011. Pleistocene sea-level fluctuations and human evolution on the southern coastal plain of South Africa. *Quaternary Science Reviews*, 30, pp.506-527.

Cooper, J. A. G., Green, A. N., Compton, J. S. 2018. Sea-level change in southern Africa since the Last Glacial Maximum. *Quaternary Science Reviews*, 201, pp.303-318.

Cooper, J. A. G., Wright, C. I., Mason, T. 1999. Geomorphology and sedimentology. In *Estuaries of South Africa*, ed. B. R. Allanson and D. Baird. Cambridge: Cambridge University Press, pp. 5–25.

Cowling, R. M. 1990. Diversity components in a species-rich area of the Cape Floristic Region. *Journal of Vegetation Science*, pp.699-710.

Cowling, R.M. and Bond, W.J., 1991. How small can reserves be? An empirical approach in Cape Fynbos, South Africa. *Biological Conservation*, *58*(3), pp.243-256.

Cowling, R. M., Holmes, P. M. 1991. Endemism and speciation in a lowland flora from the Cape Floristic Region. *Biological Journal of the Linnean Society*, 47(4), pp.367-383.

Cowling, R. M., Witkowski, E. T. F., Milewski, A. V., Newbey, K. R. 1994. Taxonomic, edaphic and biological aspects of narrow plant endemism on matched sites in Mediterranean South Africa and Australia. *Journal of Biogeography*, pp.651-664.

Cowling, R., Campbell, B., Mustart, P., McDonald, D., Jarman, M., Moll, E. 1988. Vegetation classification in a floristically complex area: the Agulhas Plain. *South African Journal of Botany*, 54, pp.290–300.

Davies, S. J., Lamb, H. F., Roberts, J. S. 2015. Micro-XRF Core Scanning in Paleolimnology: Recent Developments. In: Croudace, I., Rothwell, R.G. (Eds.), *Micro-XRF studies of sediment cores*, 17, Springer, pp.179–193.

De Lecea, A., Green, A.N. and Cooper, A., 2016. Environmental change during the Pleistocene and Holocene: Estuaries and lagoons of southern Africa. In *Quaternary environmental change in Southern Africa: Physical and human dimensions*. Cambridge University Press, pp. 219-233

Deacon, H. J., Jury, M. R., Ellis, F. 1992. Selective regime and time. In: Cowling, R. M. (Ed.), *The Ecology of Fynbos: Nutrients, Fire and Diversity*, Oxford University Press, Cape Town, pp. 6–22.

Deacon, J. 1978. Changing patterns in the Late Pleistocene/Early Holocene prehistory of southern Africa as seen from the Nelson Bay Cave stone artifact sequence. *Quaternary Research*, 10(1), pp.84-111.

Deacon, J., Lancaster, N. 1988. *Late Quaternary Palaeoenvironments of Southern Africa*, Oxford University Press, New York.

Deines, P. 1980. The isotopic composition of reduced organic carbon. In: Fritz, P., Fontes, J.C. (Eds.), *Handbook of Environmental Isotope Geochemistry. The Terrestrial Environment*, vol. 1. A. Elsevier, Amsterdam, pp. 329–406.

Dellwig, O., Hinrichs, J., Hild, A., Brumsack, H. J. 2000. Changing sedimentation in tidal flat sediments of the southern North Sea from the Holocene to the present: a geochemical approach. *Journal of Sea Research*, 44(3–4), pp.195-208.

Denys, L., de Wolf, H. 1999. Diatoms as indicators of coastal paleoenvironments and relative sea-level change. In: Stoermer, E.F., Smol, J.P. (Eds.), *The Diatoms: Applications for the Environmental and Earth Sciences*, Cambridge University Press, Cambridge, UK, pp.277.

Donnenfeld, Z., Hedden, S. and Crookes, C., 2018. A delicate balance: Water scarcity in South Africa.

du Plessis, N., 2021. Late Holocene environmental and climate dynamics along the southern Cape coast of South Africa: high resolution multi-proxy records from the wilderness embayment.

du Plessis, N., Chase, B. M., Quick, L. J., Haberzettl, T., Kasper, T., Meadows, M. E. 2020. Vegetation and climate change during the Medieval Climate Anomaly and the Little Ice Age on the southern Cape coast of South Africa: Pollen evidence from Bo Langvlei. *The Holocene*, 30(12), pp.1716-1727.

Dyubele, V. 2023. Geochemical Investigation Into Holocene Palaeoenvironmental Change Along The Southern Cape Coast, South Africa. Unpublished MSc thesis, University of the Witwatersrand, South Africa.

Ehleringer, J. R., Cerling, T. E., Helliker, B. R. 1997. C4 photosynthesis, atmospheric CO2, and climate. *Oecologia*, 112, pp.285-299.

Ellery, W. N., Grenfell, S. E., Grenfell, M. C., Powell, R., Kotze, D. C., Marren, P. M., Knight, J. 2016. Wetlands in southern Africa. In *Quaternary Environmental Change in Southern Africa*, ed. J. C. Compton, Cambridge University Press, pp.188-202.

Engelbrecht, F. A., Marean, Neumann, C. W., Cowling, R. M., Engelbrecht, C. J., Neumann, F. H., Scott, L., Nkoana, R., et al. 2019. Downscaling Last Glacial Maximum climate over southern Africa. *Quaternary Science Reviews*, 226, p. 105879.

Faith, J. T., Chase, B. M., Avery, D. M. 2018. Late Quaternary micromammals and the precipitation history of the southern Cape, South Africa. *Quaternary Research*, 91(2), pp.848-860.

Farmer, E. C., de Menocal, P. B., Marchitto, T. M. 2005. Holocene and deglacial ocean temperature variability in the Benguela upwelling region: implications for low-latitude atmospheric circulation. *Paleoceanography*, 20(2).

Farquhar, G. D., Ehleringer, J. R., Hubick, K. T. 1989a. Carbon isotope discrimination and photosynthesis. *Annual Review of Plant Physiology and Plant Molecular Biology*, 40, pp.503-537.

Farquhar, G. D., Hubick, K. T., Condon, A. G., Richards, R. A. 1989b. Carbon isotope fractionation and plant water-use efficiency. *Ecological Studies*, 68, pp.21-40.

Fietz, S., Baker, A., Miller, C. S., Naafs, B. D. A., Peterse, F., Finch, J., Humphries, M., Schefuß, E., Roychoudhury, A. N., Routh, J. 2023. Terrestrial temperature evolution of southern Africa during the late Pleistocene and Holocene: Evidence from the Mfabeni Peatland. *Quaternary Science Reviews*, 299, p.107870.

Fischer, H., Fundel, F., Ruth, U., Twarloh, B., Wegner, A., Udisti, R., Becagli, S., Castellano, E., Morganti, A., Severi, M., Wolff, E. 2007. Reconstruction of millennial changes in dust emission, transport and regional sea ice coverage using the deep EPICA ice cores from the Atlantic and Indian Ocean sector of Antarctica. *Earth and Planetary Science Letters*, 260(1-2), pp.340-354.

Flint, S.A., Hodgson, D.M., Sprague, A.R., Brunt, R.L., Van der Merwe, W.C., Figueiredo, J., Prélat, A., Box, D., Di Celma, C. and Kavanagh, J.P., 2011. Depositional architecture and sequence stratigraphy of the Karoo basin floor to shelf edge succession, Laingsburg depocentre, South Africa. *Marine and Petroleum Geology*, *28*(3), pp.658-674.

Foster, I., Walling, D. 1994. Using reservoir deposits to reconstruct changing sediment yields and sources in the catchment of the Old Mill Reservoir, South Devon, UK, over the past 50 years. *Hydrological Sciences Journal*, 39(4), pp.347-368.

Francke, A., Holtvoeth, J., Codilean, A. T., Lacey, J. H., Bayon, G., Dosseto, A. 2020. Geochemical methods to infer landscape response to Quaternary climate change and land use in depositional archives: A review. *Earth-Science Reviews*, 207, p. 103218.

Fritz, S. C. 2008. Deciphering climatic history from lake sediments. *Journal of Paleolimnology*, 39, pp.5-16.

Fry, B. 2006. *Stable isotope ecology*, Vol. 521, Springer, New York.

Gagan, M.K., Hendy, E.J., Haberle, S.G. and Hantoro, W.S., 2004. Post-glacial evolution of the Indo-Pacific warm pool and El Nino-Southern Oscillation. *Quaternary International*, *118*, pp.127-143.

Gebregiorgis, D., Giosan, L., Hathorne, E. C., Anand, P., Nilsson-Kerr, K., Plass, A., Lückge, A., Clemens, S. C., Frank, M. 2019. What can we learn from X-ray fluorescence core scanning data? A paleomonsoon case study. *Geochemistry, Geophysics, Geosystems*, 21(2), p.e2019GC008414.

Gibbard, P. and Cohen, K. M. 2008. Global chronostratigraphical correlation table for the last 2.7 million years. *Episodes*, 31, 243–247.

Goldblatt, P. 1997. Floristic diversity in the Cape flora of South Africa. *Biodiversity & Conservation*, 6, pp.359-377.

Gresse, P. G., Theron, J. N. 1992. The Geology of the Worcester Area: Explanations of Sheet 3319. 1:250 000. *Geological Survey of South*

Haberzettl, T., Kück, B., Wulf, S., Anselmetti, F., Ariztegui, D., Corbella, H., Fey, M., Janssen, S., Lücke, A., Mayr, C. 2008. Hydrological variability in southeastern Patagonia and explosive volcanic activity in the southern Andean Cordillera during Oxygen Isotope Stage 3 and the Holocene inferred from lake sediments of Laguna Potrok Aike, Argentina. *Palaeogeography, Palaeoclimatology, Palaeoecology*, 259(2), pp.213-229.

Hahn, A., Compton, J. S., Meyer-Jacob, C., Kirsten, K. L., Lucasssen, F., Perez Mayo, M., Schefuß, E., Zabel, M. 2016. Holocene paleo-climatic record from the South African Namaqualand mudbelt: A source to sink approach. *Quaternary International*, 404, pp.121-135.

Hahn, A., Schefuß, E., Ando, S., Cawthra, H. C., Frenzel, P., Kugel, M., Meschner, S., Mollenhauer, G., Zabel, M. 2017. Southern Hemisphere anticyclonic circulation drives oceanic and climatic conditions in late Holocene southernmost Africa. *Climate of the Past*, 13(6), pp.649-665.

Hahn, A., Schefuß, E., Groeneveld, J., Miller, C., Zabel, M. 2021. Glacial to interglacial climate variability in the southeastern African subtropics (25°S–20°S). *Climate of the Past*, 17, pp.345-360.

Haines, E. B. 1976. Stable carbon isotope ratios in biota, soils and tidal water of a Georgia salt marsh. *Estuarine and Coastal Marine Science*, 4, pp.609–616.

Harrison, M. S. J. 1984. A generalised classification of South African summer rain-bearing synoptic systems. *Journal of Climatology*, 4, pp.547-560.

Scheff, J., Seager, R., Liu, H. and Coats, S., 2017. Are glacials dry? Consequences for paleoclimatology and for greenhouse warming. *Journal of Climate*, *30*(17), pp.6593-6609.

Heydorn, A.E.F. and Tinley, K.L., 1980. *Estuaries of the Cape. Part. 1, Synopsis of the Cape Coast, Natural Features, Dynamics and Utilization*. National Research Institute for Oceanology.

Higginson, M. J., Gornitz, V. 2009. Geochemical proxies (non-isotopic). *Encyclopedia of Paleoclimatology and Ancient Environments*, pp.341-353.

Higgs, C. G. 2017. Geochemical Insights Into the Influence of Holocene Sea Level Change on the Evolution of the Mkhuze River Delta, Lake St Lucia, Northern KwaZulu-Natal (Masters dissertation, University of the Witwatersrand, Faculty of Science, School of Chemistry).

Hogg, A., Heaton, T., Hua, Q., Palmer, J., Turney, C., Southon, J., Bayliss, A., Blackwell, P., Boswijk, G., Bronk Ramsey, C., Petchey, F., Reimer, P., Reimer, R., Wacker, L. 2020. SHCal20 Southern Hemisphere calibration, 0–55,000 years cal BP. *Radiocarbon*, 62(4), pp.759-778.

Holmgren, K., Lee-Thorp, J.A., Cooper, G.R.J., Lundblad, K., Partridge, T.C., Scott, L., Sithaldeen, R., Talma, A.S., Tyson, P.D., 2003. Persistent millennial-scale climatic variability over the past 25,000 years in southern Africa. *Quaternary Science Reviews*. 22, pp. 2311-2326.

Humphries, M., Green, A., Higgs, C., Strachan, K., Hahn, A., Pillay, L., Zabel, M. 2020. High-resolution geochemical records of extreme drought in southeastern Africa during the past 7000 years. *Quaternary Science Reviews*, 236, p.106294.

Humphries, M.S. 2021. Elemental proxy evidence for late Quaternary palaeoenvironmental change in southern African sedimentary records: interpretation and applications. *South African Journal of Geology*, 2021, 124(4), pp.1033-1046.

Humphries, M.S., Benitez-Nelson, C.R., Bizimis, M., Finch, J.M. 2017. An aeolian sediment reconstruction of regional wind intensity and links to larger scale climate variability since the last deglaciation from the east coast of southern Africa. *Global and Planetary Change*, 156, pp.59-67.

Humphries, M.S., Kirsten, K.L., McCarthy, T.S. 2019. Rapid changes in the hydroclimate of southeast Africa during the mid-to late-Holocene. *Quaternary Science Reviews*, 212, pp.178-186.

Hunter, I.T. 1987. The Weather of the Agulhas Bank and the Cape South Coast. Unpublished M.Sc thesis, University of Cape Town, Cape Town.

Jacobs, Z., Duller, G.A., Wintle, A.G., Henshilwood, C.S. 2006. Extending the chronology of deposits at Blombos Cave, South Africa, back to 140 ka using optical dating of single and multiple grains of quartz. *Journal of Human Evolution*, 51(3), pp.255-273.

Jacobs, Z., Jones, B.G., Cawthra, H.C., Henshilwood, C.S., Roberts, R.G. 2020. The chronological, sedimentary and environmental context for the archaeological deposits at Blombos Cave, South Africa. *Quaternary Science Reviews*, 235, p.105850.

Jones, M.G.W., van Nieuwenhuizen, G.D.P., Day, J.A. 2000. Cape Action Plan for the Environment: Selecting Priority Wetlands for Conservation: The Agulhas Plain as a Case Study. Freshwater Research Unit, Zoology Department, University of Cape Town, Cape Town.

Jouzel, J., Masson-Delmotte, V., Cattani, O., Dreyfus, G., Falourd, S., Hoffmann, G., Minster, B., Nouet, J., Barnola, J.M., Chappellaz, J., Fischer, H. 2007. Orbital and millennial Antarctic climate variability over the past 800,000 years. *Science*, 317(5839), pp.793-796.

Julius, M.L., Theriot, E.C. 2010. The diatoms: a primer, in: Smol, J.P., Stoermer, E.F. (Eds.), The Diatoms: Applications for the Environmental and Earth Sciences. Cambridge University Press, New York, pp.8–22.

Jury, M., Rouault, M., Weeks, S., Schormann, M. 1997. Atmospheric boundary-layer fluxes and structure across a land-sea transition zone in south-eastern Africa. *Boundary-Layer Meteorology*, 83, pp.311–330.

Jury, M.R., Valentine, H.R., Lutjeharms, J.R.E. 1993. Influence of the Agulhas Current on summer rainfall along the southeast coast of South Africa. *Journal of Applied Meteorology*, 32, pp.1282–1287.

Kim, J.-H., Schneider, R.R. 2002. Low-latitude control of interhemispheric sea- surface temperature contrast in the tropical Atlantic over the past 21 kyrs: the possible role of SE trade winds. *Clim. Dyn.*, 23, pp.337-347.

Kim, J.-H., Schneider, R.R., Mulitza, S., Müller, P.J. 2003. Reconstruction of SE trade-wind intensity based on sea-surface temperature gradients in the Southeast Atlantic over the last 25 kyr. *Geophys. Res. Lett.*, 30, pp.2144.

Kristen, I., Fuhrmann, A., Thorpe, J., Rohl, U., Wilkes, H. and Oberhansli, H., 2007. Hydrological changes in southern Africa over the last 200 Ka as recorded in lake sediments from the Tswaing impact crater. *South African Journal of Geology*, *110*(2-3), pp.311-326.

Kirsten, K. 2014. Late Holocene diatom community responses to climate variability along the southern Cape coastal plain, South Africa. University of Cape Town.

Kirsten, K.L., Haberzettl, T., Wündsch, M., Frenzel, P., Meschner, S., Smit, A.J., Quick, L.J., Mäusbacher, R., Meadows, M.E. 2018. A multiproxy study of the ocean-atmospheric forcing and the impact of sea-level changes on the southern Cape coast, South Africa during the Holocene. *Palaeogeography, Palaeoclimatology, Palaeoecology*, 496, pp.282-291.

Kirsten, K.L., Kasper, T., Cawthra, H.C., Strobel, P., Quick, L.J., Meadows, M.E., Haberzettl, T. 2020. Holocene variability in climate and oceanic conditions in the winter rainfall zone of South Africa—inferred from a high resolution diatom record from Verlorenvlei. *Journal of Quaternary Science*, 35(4), pp.572-581.

Kirsten, K.L., Meadows, M.E. 2016. Late-Holocene palaeolimnological and climate dynamics at Princessvlei, South Africa: evidence from diatoms. *The Holocene*, 26(9), pp.1371-1381.

Knight, J. 2020. An Environmental History of Southern Africa. In *Oxford Research Encyclopedia of African History*.

Knight, J., Grab, S.W. 2016. The context of Quaternary environmental change in southern Africa. *Quaternary environmental change in southern Africa: physical and human dimensions*. Cambridge University Press, Cambridge, pp.1-17.

Kraaij, T., Hanekom, N., Russell, I.A., Randall, R.M. 2009. Agulhas National Park State of Knowledge. Unpublished Internal Report, South African National Parks, 51.

Kruger, A. 2004. Climate of South Africa: climate controls. WS45. South African Weather Service. Pretoria, South Africa.

Kutzbach, J., Liu, X., Liu, Z., Chen, G. 2008. Simulation of the evolutionary response of global summer monsoons to orbital forcing over the past 280,000 years. *Clim Dyn*, 30, pp.567-579.

Kutzbach, J.E. 1981. Monsoon climate of the early Holocene: climate experiment with the Earth's orbital parameters for 9000 years ago. *Science*, 214, pp.59-61.

Kylander, M. E., Ampel, L., Wohlfarth, B., Veres, D. 2011. High-resolution X-ray fluorescence core scanning analysis of Les Echets (France) sedimentary sequence: new insights from chemical proxies. *Journal of Quaternary Science*, 26, pp.109-117.

Lamb, A.L., Wilson, G.P., Leng, M.J. 2006. A review of coastal palaeoclimate and relative sea-level reconstructions using δ13C and C/N ratios in organic material. *Earth-Science Reviews*, 75(1-4), pp.29-57.

Leng, M.J., Lamb, A.L., Heaton, T.H., Marshall, J.D., Wolfe, B.B., Jones, M.D., Holmes, J.A., Arrowsmith, C. 2006. Isotopes in lake sediments. Springer Netherlands, pp.147-184.

Lim, S., Chase, B.M., Chevalier, M., Reimer, P.J. 2016. 50,000 years of vegetation and climate change in the southern Namib Desert, Pella, South Africa. *Palaeogeography, Palaeoclimatology, Palaeoecology*, 451, pp.197-209.

Lindesay, J.A. 1998. Present Climates of Southern Africa, in: Hobbs, J.E., Lindesay, J.A., Bridgman, H.A. (Eds.), *Climates of the Southern Continents: Present, Past and Future*. John Wiley & Sons, New York, pp.5-62.

Low, A.B. and Rebelo, A.G., 1996. *Vegetation of South Africa, Lesotho and Swaziland. Department of Environmental Affairs and Tourism, Pretoria*.

Lutjeharms, J., Monteiro, P., Tyson, P., Obura, D. 2001. The oceans around southern Africa and regional effects of global change. *South African Journal of Science*, 97, pp.119-130.

Mackie, E.A.V., Leng, M.J., Lloyd, J.M., Arrowsmith, C. 2005. Bulk organic δ13C and C/N ratios as palaeosalinity indicators within a Scottish isolation basin. *Journal of Quaternary Science*, 20, pp.303-312.

Mahlalela, P.T., Blamey, R.C., Reason, C.J.C. 2019. Mechanisms behind early winter rainfall variability in the southwestern Cape, South Africa. *Climate Dynamics*, 53, pp.21-39.

Malan, J.A. 1989. Bredasdorp Group, in: Johnson, M.R. (Ed.), *Catalogue of South African Lithostratigraphic units*, 1st ed. SA Committee for Stratigraphy.

Malan, J.A. 1990. The stratigraphy and sedimentology of the Bredasdorp Group, Southern Cape Province. Unpublished M.Sc. thesis, University of Cape Town.

Marean, C.W., Bar-Matthews, M., Bernatchez, J., Fisher, E., Goldberg, P., Herries, A.I., Jacobs, Z., Jerardino, A., Karkanas, P., Minichillo, T., Nilssen, P.J. 2007. Early human use of marine resources and pigment in South Africa during the Middle Pleistocene. *Nature*, 449(7164), pp.905-908.

Marean, C.W., Cawthra, H.C., Cowling, R.M., Esler, K.J., Fisher, E., Milewski, A., Potts, A.J., Singels, E., De Vynck, J. 2014. Stone age people in a changing South African greater Cape Floristic Region. *Fynbos: ecology, evolution, and conservation of a megadiverse region*, 18, pp.164-199.

Marean, C.W., Cowling, R.M., Franklin, J. 2020. The Palaeo-Agulhas Plain: Temporal and spatial variation in an extraordinary extinct ecosystem of the Pleistocene of the Cape Floristic Region. *Quaternary Science Reviews*, 235, p.106161.

Marker, M.E., Holmes, P.J. 2010. The geomorphology of the Coastal Platform in the southern Cape. *South African Geographical Journal*, 92, pp.105-116.

McCarthy, T.S., Hancox, P.J. 2000. Wetlands. In *The Cenozoic of Southern Africa*, ed. T.C. Partridge and R.R. Maud. Oxford: Oxford University Press, pp.218–235.

McDermott, F. 2004. Palaeo-climate reconstruction from stable isotope variations in speleothems: a review. *Quaternary Science Reviews*, 23(7-8), pp.901-918.

McManus, J.F., Francois, R., Gherardi, J.-M., Keigwin, L.D., Brown-Leger, S. 2004. Collapse and rapid resumption of Atlantic meridional circulation linked to deglacial climate changes. *Nature*, 428, pp.834e837.

Metwally, A.A., Scott, L., Neumann, F.H. 2014. Holocene palynology and palaeoenvironments in the Savanna Biome at Tswaing Crater, central South Africa. *Palaeogeography, Palaeoclimatology, Palaeoecology*, 402, pp.125–135.

Meyers, A.P., Teranes, L.J. 2001. Sediment organic matter. In: Last, M.W., Smol, P.J. (Eds.) *Tracking Environmental Change Using Lake Sediments*, vol. 2. Berlin: Springer, pp.239–269.

Meyers, P.A. 1994. Preservation of elemental and isotopic source identification of sedimentary organic matter. *Chemical Geology*, 114(3-4), pp.289–302.

Meyers, P.A. 2003. Application of organic geochemistry to paleolimnological reconstruction: a summary of examples from the Laurentian Great Lakes. *Organic Geochemistry*, 34(2), pp.261–289.

Meyers, P.A., 1997. Organic geochemical proxies of paleoceanographic, paleolimnologic, and paleoclimatic processes. Organic Geochemistry 27, 213-250.

Meyers, P.A., Lallier-Vergès, E. 1999. Lacustrine sedimentary organic matter records of Late Quaternary paleoclimates. *Journal of Paleolimnology*, 21(3), pp.345–372.

Midgley, G.F., Hannah, L., Millar, D., Rutherford, M.C., Powrie, L.W. 2002. Assessing the vulnerability of species richness to anthropogenic climate change in a biodiversity hotspot. *Global Ecology and Biogeography*, 11, pp.445-451.

Miller, C., Hahn, A., Liebrand, D., Zabel, M., Schefuß, E. 2019. Mid- and low latitude effects on eastern South African rainfall over the Holocene. *Quat. Sci. Rev.*, 229, p.106088.

Miller, C., Hahn, A., Liebrand, D., Zabel, M., Schefuß, E. 2020. Mid- and low latitude effects on eastern South African rainfall over the Holocene. *Quaternary Science Reviews*, 229, p.106088.

Monnin, E., Indermühle, A., D€allenbach, A., Flückiger, J., Stauffer, B., Stocker, T.F., Barnola, J.M. 2001. Atmospheric CO2 concentrations over the last glacial termination. *Science*, 291, pp.112e114.

Mucina, L., Rutherford, M.C. 2006. The vegetation of South Africa, Lesotho and Swaziland, *Strelitzia*. South African National Biodiversity Institute, Pretoria.

Mustart, P.J., Cowling, R.M., Albertyn, J. 2003. Southern Overberg South African Wild Flower Guide 8. Botanical Society of South Africa, Cape Town.

Myers, N., Mittermeier, R.A., Mittermeier, C.G., da Fonseca, G.A.B., Kent, J. 2000. Biodiversity hotspots for conservation priorities. *Nature*, 403, pp.853-858.

Nesbitt, H.W., Markovics, G. 1980. Chemical processes affecting alkalis and alkaline earths during continental weathering. *Geochimica et Cosmochimica Acta*, 44(11), pp.1659-1666.

Ng, H.C., Robinson, L.F., McManus, J.F., Mohamed, K.J., Jacobel, A.W., Ivanovic, R.F., Gregoire, L.J., Chen, T. 2018. Coherent deglacial changes in western Atlantic Ocean circulation. *Nature communications*, 9(1), p.2947.

Norström, E., Bringensparr, C., Fitchett, J.M., Grab, S.W., Rydberg, J., Kylander, M. 2018. Late-Holocene climate and vegetation dynamics in eastern Lesotho highlands. *The Holocene*, 28(9), pp.1483-1494.

Parkington, J. 2003. Middens and moderns: shellfishing and the middle stone age of the western Cape, South Africa. *South Afr. J. Sci.*, 99, pp.243.

Partridge, T.C., Maud, R.R. 1987. Geomorphic evolution of southern Africa since the Mesozoic. *South African Journal of Geology*, 90, pp.179-208.

Partridge, T.C., Maud, R.R. 2000. Macro-Scale Geomorphic Evolution of Southern Africa, in: Partridge, T.C., Maud, R.R. (Eds.), *The Cenozoic of South Africa*. Oxford University Press, Oxford, pp.3-18.

Pate, J.S. 2001. Carbon isotope discrimination and plant water-use efficiency: case scenarios for C3 plants, in: Unkovich, M., Pate, J., McNeill, A., Gibbs, D.J. (Eds.), *Stable Isotope Techniques in the Study of Biological Processes and Functioning of Ecosystems*. Kluwer Academic Publishers, Dordrecht, pp.19-37.

Prentice, I.C., Cleator, S.F., Huang, Y.H., Harrison, S.P. and Roulstone, I., 2017. Reconstructing ice-age palaeoclimates: Quantifying low-CO2 effects on plants. *Global and Planetary Change*, *149*, pp.166-176.

Quick, L.J., Carr, A.S., Meadows, M.E., Boom, A., Bateman, M.D., Roberts, D.L., Reimer, P.J., Chase, B.M. 2015. A late Pleistocene-Holocene multi-proxy record of palaeoenvironmental change from Still Bay, southern Cape Coast, South Africa. *Journal of Quaternary Science*, 30, pp.870–885.

Quick, L.J., Chase, B.M., Carr, A.S., Chevalier, M., Grobler, B.A., Meadows, M.E. 2021. A 25,000 year record of climate and vegetation change from the southwestern Cape coast, South Africa. *Quaternary Research*, 105, pp.82–99.

Quick, L.J., Chase, B.M., Meadows, M.E., Scott, L., Reimer, P.J. 2011. A 19.5 kyr vegetation history from the central Cederberg Mountains, South Africa: palynological evidence from rock hyrax middens. *Palaeogeogr. Palaeoclimatol. Palaeoecol.*, 309, pp.253–270.

Quick, L.J., Chase, B.M., Wuendsch, M., Kirsten, K.L., Chevalier, M., Maeusbacher, R., Meadows, M.E., Haberzettl, T. 2018. A high-resolution record of Holocene climate and vegetation dynamics from the southern Cape coast of South Africa: pollen and microcharcoal evidence from Eilandvlei. *Journal of Quaternary Science*, 33(5), pp.487–500.

Quick, L.J., Meadows, M.E., Bateman, M.D., Kirsten, K.L., Mäusbacher, R., Haberzettl, T., Chase, B.M. 2016. Vegetation and climate dynamics during the last glacial period in the fynbos-afrotemperate forest ecotone, southern Cape, South Africa. *Quaternary International*, 404, pp.136–149.

Ramsay, P.J. 1996. 9000 years of sea-level change along the southern African coastline. *Quaternary International*, 31, pp.71–75.

Ramsay, P.J., Cooper, J.A.G. 2002. Late Quaternary sea-level change in South Africa. *Quaternary Research*, 57(1), pp.82–90.

Reason, C.J.C., Landman, W., Tennant, W. 2006. Seasonal to decadal prediction of southern African climate and its links with variability of the Atlantic ocean. *Bulletin of the American Meteorological Society*, 87, pp.941–955.

Rebelo, A.G., Boucher, C., Helme, N., Mucina, L., Rutherford, M.C. 2006. Fynbos biome. In: Mucina, L., Rutherford, M.C. (Eds.), *The Vegetation of South Africa, Lesotho and Swaziland*. South African National Biodiversity Institute, Pretoria, pp.221–299.

Rebelo, A.G., Cowling, R.M., Campbell, B.M., Meadows, M.E. 1991. Plant communities of the Riversdale Plain. *South African Journal of Botany*, 57, pp.10–28.

Rice, D.L., Hanson, R.B. 1984. A kinetic model for detritus nitrogen: role of the associated bacteria in nitrogen accumulation. *Bulletin of Marine Science*, 35, pp.326–340.

Rowberry, M.D., McCarthy, T.S., Thompson, M., Nomnganga, A., Moyo, L. 2011. The spatial and temporal characterisation of flooding within the floodplain wetland of the Nyl River, Limpopo Province, South Africa. *Water SA*, 37, pp.445–451.

Rozendaal, A., Philander, C., Heyn, R. 2017. The coastal heavy mineral sand deposits of Africa. *South African Journal of Geology*, 120(1), pp.133–152.

SAWS, 2001. Annual report - weathersa. Available at: *https://www.weathersa.co.za/Documents/AnnualReports/SAWS-Annual-Report-10-11.pdf* (Accessed: 20 March 2023).

Schidlowski, M., Hayes, J.M., Kaplan, I.R. 1983. Isotopic inferences of ancient biochemistries: carbon, sulphur, hydrogen and nitrogen. In: Scholf, J.W. (Ed.), *Earth's Earliest Biosphere, Its Origin and Evolution*. Princeton University Press, Princeton, pp.149–186.

Schleser, G.H. 1995. Parameters determining carbon isotope ratios in plants. In: Frenzel, B., Stauffer, B., Weib, M. (Eds.), *Problems of Stable Isotopes in Tree-Rings, Lake Sediments and Peat Bogs as Climate Evidence for the Holocene*. Fischer Verlag, Stuttgart, pp.71–96.

Scott, L. and Neumann, F.H., 2018. Pollen-interpreted palaeoenvironments associated with the Middle and Late Pleistocene peopling of Southern Africa. *Quaternary International*, *495*, pp.169-184.

Scott, L., Bousman, C.B., Nyakale, M. 2005. Holocene pollen from swamp, cave and hyrax dung deposits at Blydefontein (Kikvorsberge), Karoo, South Africa. *Quat. Int.*, 129, pp.49–59.

Scott, L., Lee-Thorp, J.A. 2004. Holocene climatic trends and rhythms in southern Africa, in: Battarbee, R.W., Gasse, F., Stickley, C.E. (Eds.), *Past Climate Variability through Europe and Africa*. Springer Netherlands, Netherlands, pp.69–91.

Scott, L., Manzano, S., Carr, A.S., Cordova, C., Ochando, J., Bateman, M.D., Carrión, J.S. 2021. A 14000 year multi-proxy alluvial record of ecotone changes in a Fynbos-Succulent Karoo transition in South Africa. *Palaeogeography, Palaeoclimatology, Palaeoecology*, 569, p.110331.

Scott, L., Neumann, F.H., Brook, G.A., Bousman, C.B., Norström, E., Metwally, A.A. 2012. Terrestrial fossil Pollen evidence of climate Change during the last 26 Thousand Years in Southern Africa. *Quat. Sci. Rev.*, 32, pp.100–118.

Scott, L., Nyakale, M. 2002. Pollen indications of Holocene palaeoenvironments at Florisbad spring in the central Free State, South Africa. *Holocene*, 12, pp.497–503.

Scott, L., Thackeray, J.F. 1987. Multivariate analysis of late Pleistocene and Holocene pollen spectra from Wonderkrater, Transvaal, South Africa. *South African Journal of Science*, 83(2), p.93.

Scott, L., Thackeray, J.F. 2015. Palynology of Holocene deposits in excavation 1 at Wonderwerk cave, northern Cape (South Africa). *Afr. Archaeol. Rev.*, 32, pp.839–855.

Scott, L., Woodborne, S. 2007. Pollen analysis and dating of late Quaternary faecal deposits (hyraceum) in the Cederberg, Western Cape, South Africa. *Review of Paleobotany and Palynology*, 144, pp.123–134.

Sealy, J., Lee-Thorp, J., Loftus, E., Faith, J.T., Marean, C.W. 2016. Late Quaternary environmental change in the Southern Cape, South Africa, from stable carbon and oxygen isotopes in faunal tooth enamel from Boomplaas Cave. *Journal of Quaternary Science*, 31, pp.919–927.

Sealy, J., Naidoo, N., Hare, V.J., Brunton, S., Faith, J.T. 2020. Climate and ecology of the palaeo-Agulhas Plain from stable carbon and oxygen isotopes in bovid tooth enamel from Nelson Bay Cave, South Africa. *Quaternary Science Reviews*, 235, p.105974.

Smith, B.N., Epstein, S. 1971. Two categories of 13C/12C ratios for higher plants. *Plant Physiology*, 47, pp.380–384.

Snyder, N.P., Allen, J.R., Dare, C., Hampton, M.A., Schneider, G., Wooley, R.J., Alpers, C.N., Marvin-DiPasquale, M.C. 2004. Sediment grain-size and loss-on-ignition analyses from 2002 Englebright Lake coring and sampling campaigns.

Stats SA, 2011. Census 2011 Municipal Report Western Cape. Pretoria: Statistics South Africa.

Stocker, T.F. 1998. The seesaw effect. *Science*, 282, pp.61–62.

Stocker, T.F., Johnsen, S.J. 2003. A minimum thermodynamic model for the bipolar seesaw. *Paleoceanography*, 18.

Stowe, M.-J., Sealy, J. 2015. Terminal Pleistocene and Holocene dynamics of southern Africa's winter rainfall zone based on carbon and oxygen isotope analysis of bovid tooth enamel from Elands Bay Cave. *Quaternary International*, pp. 57-67.

Strobel, P., Bliedtner, M., Carr, A.S., Frenzel, P., Klaes, B., Salazar, G., Struck, J., Szidat, S., Zech, R., Haberzettl, T. 2021. Holocene sea level and environmental change at the southern Cape – an 8.5 kyr multi-proxy paleoclimate record from Lake Voëlvlei, South Africa. *Climate of the Past*, 17(4), pp.1567–1586.

Strobel, P., Bliedtner, M., Carr, A.S., Struck, J., du Plessis, N., Glaser, B., Meadows, M.E., Quick, L.J., Zech, M., Zech, R., Haberzettl, T. 2022. Reconstructing Late Quaternary precipitation and its source on the southern Cape coast of South Africa: A multi-proxy paleoenvironmental record from Vankervelsvlei. *Quaternary Science Reviews*, 284, p.107

Strobel, P., Kasper, T., Frenzel, P., Schittek, K., Quick, L.J., Meadows, M.E., Mäusbacher, R., Haberzettl, T. 2019. Late Quaternary palaeoenvironmental change in the year-round rainfall zone of South Africa derived from peat sediments from Vankervelsvlei. *Quaternary Science Reviews*, 218, pp.200–214.

Stuut, J.B.W., Prins, M.A., Schneider, R.R., Weltje, G.J., Jansen, J.F., Postma, G. 2002. A 300-kyr record of aridity and wind strength in southwestern Africa: inferences from grain-size distributions of sediments on Walvis Ridge, SE Atlantic. *Marine Geology*, 180(1-4), pp.221–233.

Talbot, M.R., Johannessen, T. 1992. A high resolution palaeoclimatic record for the last 27,500 years in tropical West Africa from the carbon and nitrogen isotopic composition of lacustrine organic matter. *Earth Planet. Sci. Lett.*, 110, pp.23–37.

Talma, A.S., Vogel, J.C. 1992. Late Quaternary palaeotemperatures derived from a speleothem from Cango Caves, Cape Province, South Africa. *Quaternary Research*, 37, pp.203–213.

Thackeray, J.F. 1988. Molluscan fauna from Klasies River, South Africa. *The South African Archaeological Bulletin*, pp.27–32.

Thackeray, J.F., Fitchett, J.M. 2016. Rainfall seasonality captured in micromammalian fauna in Late Quaternary contexts, South Africa. *Palaeontologia Africana*, 51, pp.1–9.

Thwaites, R.N., Cowling, R.M. 1988. Soil-vegetation relationships on the Agulhas plain, South Africa. *Catena*, 15(3-4), pp.333–345.

Tinley, K.L. 1985. Coastal dunes of South Africa (South African National Scientific Programmes Report No. 109). Pretoria: CSIR.

Truc, L., Chevalier, M., Favier, C., et al. 2013. Quantification of climate change for the last 20,000 years from Wonderkrater, South Africa: Implications for the long-term dynamics of the Intertropical Convergence Zone. *Palaeogeography, Palaeoclimatology, Palaeoecology*, 386, pp.575–587.

Tyson, P.D. 1986. Climatic Change and Variability in Southern Africa. Oxford University Press, Cape Town.

Tyson, P.D. 1999. Atmospheric circulation changes and palaeoclimates of southern Africa. *South African Journal of Science*, 95, pp.194–201.

Tyson, P.D., Preston-Whyte, R.A. 2000. The Weather and Climate of Southern Africa. Oxford University Press, Cape Town.

Tyson, R.V. 1995. Sedimentary Organic Matter: Organic Facies and Palynofacies. Chapman and Hall, London.

Valsecchi, V., Chase, B.M., Slingsby, J.A., Carr, A.S., Quick, L.J., Meadows, M.E., Cheddadi, R., Reimer, P.J. 2013. A high-resolution 15,600-year pollen and microcharcoal record from the Cederberg Mountains, South Africa. *Palaeogeogr. Palaeoclimatol. Palaeoecol.*, 387, pp.6–16.

van Zinderen Bakker, E.M. 1976. The evolution of late Quaternary paleoclimates of Southern Africa. *Palaeoecology of Africa*, 9, pp.160–202.

Vogel, J.C. 1978. Isotopic assessment of dietary habits of ungulates. *South African Journal of Science*, 74, pp.298–301.

Wündsch, M., Haberzettl, T., Cawthra, H.C., Kirsten, K.L., Quick, L.J., Zabel, M., Frenzel, P., Hahn, A., Baade, J., Daut, G., Kasper, T. 2018. Holocene environmental change along the southern Cape coast of South Africa – Insights from the Eilandvlei sediment record spanning the last 8.9 kyr. *Global and Planetary Change*, 163, pp.51–66.

Wündsch, M., Haberzettl, T., Kirsten, K.L., Kasper, T., Zabel, M., Dietze, E., Baade, J., Daut, G., Meschner, S., Meadows, M.E., Mäusbacher, R. 2016. Sea level and climate change at the southern Cape coast, South Africa, during the past 4.2 kyr. *Palaeogeography, Palaeoclimatology, Palaeoecology*, 446, pp.295–307.

Zhao, X., Dupont, L., Schefuß, E., Meadows, M.E., Hahn, A., Wefer, G. 2016. Holocene vegetation and climate variability in the winter and summer rainfall zones of South Africa. *The Holocene*, 26(6), pp.843–857.

Zinke, J., Loveday, B.R., Reason, C.J.C., Dullo, W-C., Kroon, D. 2014. Madagascar corals track sea surface temperature variability in the Agulhas Current core region over the past 334 years. *Scientific Reports*, 4, p. 4393.

Zolitschka, B., Francus, P., Ojala, A.E.K., Schimmelmann, A. 2015. Varves in lake sediments – a review. *Quaternary Science Reviews*, 117, pp.1–41.

Appendix A: XRF Data

Average Depth (cm)	Age (cal yr BP)	LOI (%)	SiO_2 (%)	Al_2O_3 (%)	Fe_2O_3 (%)	Na_2O (%)	CaO (%)	MgO (%)	K_2O (%)	MnO (%)	TiO_2 (%)	P_2O_5 (%)	S (%)	Total	Rb (PPM)	Sr (PPM)	Zr (PPM)
12	1000	0.418	91.47	2.11	0.51	0	0.15	1.19	0.12	0.002	0.18	0.1	0.1	95.8	3	12	425
14	1111	0.442	98.44	2.35	0.5	0	0.15	1.35	0.1	0.002	0.11	0.15	0.191	103.2	5	11	360
16	1220	0.434	93.56	2.16	0.5	0	0.14	1.16	0.1	0.002	0.11	0.09	0.17	98.0	5	12	337
18	1310	0.400	95.67	2.35	0.48	0	0.14	1.3	0.1	0.002	0.26	0.13	0.188	100.4	4	13	477
20	1402	0.372	91.1	2.26	0.45	0	0.13	1.33	0.1	0.001	0.13	0.13	0.192	95.6	3	12	392
22	1492	0.394	100.64	2.17	0.55	0	0.15	1.32	0.09	0.003	0.16	0.12	0.201	105.2	4	14	432
24	1590	0.372	96.46	2.17	0.46	0	0.13	1.28	0.09	0.002	0.13	0.11	0.159	100.8	3	12	254
26	1706	0.350	95.77	2.09	0.45	0	0.14	1.21	0.07	0.001	0.13	0.11	0.176	100.0	4	12	312
28	1828	0.328	103.55	2.13	0.5	0	0.13	1.32	0.11	0.003	0.18	0.11	0.144	108.0	5	13	413
30	1955	0.343	104.54	2.13	0.49	0	0.15	1.28	0.1	0.001	0.12	0.11	0.162	108.9	5	14	245
32	2075	0.395	92.52	1.95	0.51	0	0.13	1.2	0.08	0.002	0.08	0.1	0.169	96.6	4	13	253
34	2184	0.402	92.42	1.97	0.47	0	0.15	1.16	0.08	0.002	0.07	0.11	0.167	96.4	3	12	258
36	2288	0.460	92.06	2.11	0.45	0	0.13	1.23	0.09	0.001	0.11	0.12	0.187	96.3	5	13	313
38	2409	0.451	99.43	1.96	0.5	0.96	0.13	1.15	0.09	0.002	0.1	0.1	0.156	104.4	3	11	325
40	2541	0.400	85.84	1.73	0.5	3.78	0.14	0.87	0.08	0.003	0.11	0.08	0.071	93.1	4	14	352
42	2676	0.463	90.33	2.17	0.48	0	0.16	1.23	0.14	0.002	0.17	0.12	0.202	94.8	5	13	540
44	2812	0.440	99.77	1.83	0.57	0	0.11	1.13	0.1	0.004	0.14	0.05	0.098	103.7	4	12	373
46	2953	0.385	98.3	1.99	0.49	1.09	0.13	1.24	0.1	0.002	0.1	0.11	0.152	103.6	3	12	403
48	3070	0.447	82.68	1.92	0.47	0	0.14	1.13	0.09	0.001	0.22	0.11	0.229	87.0	3	14	439
50	3173	1.080	88.85	2.62	0.57	0	0.42	1.34	0.13	0.003	0.13	0.15	0.391	94.6	7	41	476
52	3271	1.084	85.08	2.98	0.61	0	0.53	1.37	0.18	0.003	0.15	0.16	0.399	91.5	6	44	232
54	3367	0.777	95.86	2.28	0.54	0	0.18	1.41	0.11	0.003	0.15	0.12	0.207	100.9	3	16	373
56	3466	0.718	84.22	2.46	0.49	0	0.17	1.29	0.12	0.002	0.1	0.11	0.226	89.0	4	16	327

Average Depth (cm)	Age (cal yr BP)	LOI (%)	SiO_2 (%)	Al_2O_3 (%)	Fe_2O_3 (%)	Na_2O (%)	CaO (%)	MgO (%)	K_2O (%)	MnO (%)	TiO_2 (%)	P_2O_5 (%)	S (%)	Total	Rb (PPM)	Sr (PPM)	Zr (PPM)
58	3567	0.996	80.65	3.42	0.55	0	0.39	1.44	0.23	0.002	0.27	0.19	0.444	87.1	5	27	460
61	3714	6.060	88.99	3.38	1.23	0.54	2.1	1.49	0.22	0.012	0.19	0.21	0.853	98.4	20	266	391
62	3751	7.035	91.18	3.59	1.31	0	2.84	1.58	0.23	0.013	0.14	0.26	1.031	101.1	22	334	323
64	3824	8.590	85.74	3.99	1.34	0	4.26	1.59	0.3	0.013	0.15	0.35	1.321	97.7	31	490	308
66	3888	7.081	74.99	4.82	1.34	1	3.4	1.69	0.4	0.012	0.21	0.34	1.609	89.8	25	340	277
68	3951	2.193	85.27	3.11	0.69	0	0.83	1.52	0.14	0.005	0.16	0.15	0.57	92.4	8	94	365
70	4012	4.826	79.75	3.43	1.08	1	4.4	1.37	0.26	0.01	0.13	0.3	1.113	92.8	22	400	359
72	4078	7.081	83.99	3.88	1.4	0	2.73	1.46	0.28	0.015	0.16	0.27	1.19	94.2	24	308	356
74	4159	6.109	89.17	3.84	1.26	0	1.86	1.44	0.25	0.013	0.15	0.22	1.044	98.2	19	224	318
76	4244	13.645	74.66	4.45	1.96	0	4.75	1.4	0.46	0.024	0.19	0.36	1.652	89.9	33	446	254
78	4322	7.876	84.52	4.02	1.23	0	3.38	1.59	0.3	0.015	0.17	0.28	1.329	96.8	24	357	310
80	4399	10.963	85.3	4.25	1.74	0	2.96	1.72	0.35	0.026	0.15	0.23	1.481	98.2	25	342	346
82	4473	15.916	70.97	4.84	2.13	2.14	5.64	1.5	0.53	0.035	0.18	0.41	2.062	90.4	37	557	276
84	4544	10.335	71.71	5.16	1.51	2.56	5.82	1.7	0.47	0.023	0.24	0.42	1.922	91.5	34	591	352
86	4614	7.415	74.05	4.2	1.15	1.45	7.06	1.53	0.37	0.015	0.18	0.39	1.592	92.0	31	614	341
88	4697	6.119	71.49	3.61	1.04	0	8.57	1.36	0.3	0.013	0.15	0.39	1.411	88.3	30	669	375
90	4770	14.956	73	4.33	2.11	1.68	4.62	1.39	0.44	0.03	0.19	0.35	1.759	89.9	34	483	307
92	4843	25.966	57.46	6.57	3.34	3.61	3.49	1.92	0.98	0.061	0.26	0.38	3.024	81.1	29	297	178
94	4915	15.443	76.18	4.09	2.3	0	4.25	1.22	0.46	0.036	0.19	0.31	1.665	90.7	30	413	364
96	4985	15.273	73.09	4.57	2.02	1.38	3.25	1.59	0.53	0.027	0.19	0.25	1.783	88.7	26	340	290
98	5082	4.132	76.88	2.49	0.74	0	7.63	1.04	0.21	0.006	0.16	0.33	0.9	90.4	23	544	351
100	5190	7.146	85.44	3.27	1.29	0	6.15	1.36	0.25	0.016	0.15	0.3	1.043	99.3	26	586	395
102	5300	8.444	61.48	5.57	1.61	3.14	7.4	1.49	0.56	0.026	0.22	0.43	2.177	84.1	34	607	303

Average Depth (cm)	**Age (cal yr BP)**	**LOI (%)**	**SiO_2 (%)**	**Al_2O_3 (%)**	**Fe_2O_3 (%)**	**Na_2O (%)**	**CaO (%)**	**MgO (%)**	**K_2O (%)**	**MnO (%)**	**TiO_2 (%)**	**P_2O_5 (%)**	**S (%)**	**Total**	**Rb (PPM)**	**Sr (PPM)**	**Zr (PPM)**
104	5417	18.269	65.9	7.52	3.09	2.38	4.57	1.58	0.81	0.039	0.26	0.4	2.632	89.2	39	456	160
106	5539	20.021	58.82	7.34	3.81	3.46	3.31	1.62	0.9	0.051	0.33	0.3	2.491	79.9	35	336	165
108	5638	7.916	70.63	5.07	1.41	1.5	6.52	1.33	0.44	0.018	0.21	0.39	1.971	87.5	30	565	326
110	5656	11.041	68.28	4.29	1.65	1.83	5.67	1.33	0.45	0.021	0.2	0.27	1.48	85.5	37	568	307
112	5673	17.463	64.18	5.3	2.02	1.32	4.19	1.45	0.53	0.028	0.22	0.37	2.627	82.2	35	404	290
114	5687	18.804	73.73	5.21	2.35	1.37	4.04	1.45	0.52	0.031	0.21	0.37	2.638	91.9	30	383	278
116	5701	20.724	68.62	7.2	3.15	0	4.4	1.82	0.77	0.045	0.28	0.42	3.03	89.7	36	423	236
118	5717	24.456	64.97	6.95	2.75	3.83	4.28	1.9	0.63	0.039	0.24	0.33	2.462	88.4	40	473	228
120	5731	17.266	67.05	6.97	2.36	1	4.03	1.54	0.59	0.031	0.22	0.42	2.666	86.9	37	417	213
122	5747	31.882	60.88	6.08	2.61	0	6.79	1.47	0.75	0.037	0.18	0.53	3.755	83.1	32	424	71
124	5761	27.450	67.84	4.6	1.71	2.2	8.65	1.44	0.49	0.024	0.14	0.54	2.673	90.3	39	652	184
126	5779	24.001	60.75	4.26	1.93	2.25	7.35	1.37	0.46	0.025	0.15	0.45	2.3	81.3	42	633	250
128	5794	29.767	65.53	5.58	2.11	2.11	7.36	1.57	0.6	0.03	0.18	0.51	2.961	88.5	41	606	206
130	5807	40.281	54.08	5.39	2.2	3.45	8.56	1.36	0.67	0.034	0.18	0.5	3.085	79.5	51	704	165
132	5821	30.745	58.32	5.58	2.38	2.24	8.27	1.22	0.67	0.042	0.18	0.59	3.504	79.5	44	593	125
134	5838	11.943	60.95	6.21	2.27	3.69	8.71	1.88	0.72	0.038	0.18	0.64	3.701	89.0	55	749	122
136	5853	34.511	58.03	6.6	2.31	0.3	8.52	1.92	0.73	0.039	0.17	0.73	4.465	83.8	58	727	121
138	5866	27.274	53.84	5.04	1.56	3.61	13.23	1.69	0.59	0.034	0.15	0.79	3.791	84.3	52	853	167
140	5879	34.310	56.93	6.52	2.11	0.49	10.67	2.12	0.76	0.043	0.18	0.74	4.169	84.7	56	761	93
142	5894	19.957	69.44	4.85	1.47	2.21	8.74	1.76	0.5	0.027	0.18	0.52	2.455	92.2	40	679	292
144	5909	24.063	65.63	5.04	1.73	2.47	8.6	1.48	0.52	0.033	0.19	0.56	2.796	89.0	43	674	266
146	5924	23.051	66.91	5.72	1.73	2.19	8.24	1.72	0.59	0.032	0.2	0.51	2.523	90.4	44	672	280
148	5937	23.316	69.02	6.37	2.14	1.64	5.99	1.55	0.61	0.039	0.24	0.48	2.783	90.9	40	540	236

Average Depth (cm)	Age (cal yr BP)	LOI (%)	SiO_2 (%)	Al_2O_3 (%)	Fe_2O_3 (%)	Na_2O (%)	CaO (%)	MgO (%)	K_2O (%)	MnO (%)	TiO_2 (%)	P_2O_5 (%)	S (%)	Total	Rb (PPM)	Sr (PPM)	Zr (PPM)
150	5951	22.337	67.75	7.39	1.86	1.79	5.22	1.66	0.66	0.035	0.33	0.43	2.635	89.8	43	501	265
152	5967	23.352	68.42	6.7	2.05	3.01	6.65	1.8	0.68	0.039	0.25	0.48	2.729	92.8	44	598	249
154	5981	19.474	75.72	6.89	2.13	1.64	3.25	1.57	0.56	0.039	0.32	0.37	2.551	95.0	29	336	299
156	5994	24.745	58.56	5.68	1.74	2.16	6.79	1.49	0.62	0.033	0.21	0.49	2.633	80.4	40	592	224
158	6011	20.219	77.5	7.08	2.08	1.93	2.57	1.93	0.57	0.035	0.28	0.35	2.699	97.0	27	290	304
160	6028	17.783	75.54	5.14	1.76	1.06	2.59	1.47	0.49	0.021	0.23	0.27	2.058	88.6	26	286	269
162	6041	29.099	74.41	8.43	3.08	2.82	2.65	2.5	0.81	0.041	0.33	0.42	3.255	98.7	25	226	168
164	6057	33.688	73.78	9.18	3.34	3.01	2.28	2.68	1	0.038	0.38	0.39	2.816	98.9	26	202	130
166	6071	31.997	68.03	9.05	3.03	2.74	2.24	2.45	0.91	0.033	0.39	0.41	2.927	92.2	35	266	144
168	6086	27.039	78.9	8.63	2.91	2.82	1.93	2.56	0.8	0.03	0.37	0.4	2.634	99.4	32	246	249
170	6101	28.535	71.66	9.87	3.1	1.73	2.24	2.2	0.9	0.036	0.45	0.36	2.803	92.5	37	258	197
172	6118	28.894	70.97	10.14	2.94	2.03	2.07	2.32	0.93	0.032	0.49	0.39	2.703	95.0	39	248	165
174	6135	31.234	66.87	9.88	3.14	2.69	2.11	2.58	0.98	0.035	0.5	0.32	2.357	89.1	40	247	139
176	6151	32.518	61.03	8.85	3.19	1.69	2.05	2.47	0.93	0.032	0.46	0.32	2.231	81.0	42	286	198
178	6166	29.536	72.29	9.67	2.76	2.94	2.04	2.38	0.82	0.031	0.45	0.35	2.34	93.7	32	208	134
180	6182	22.758	76.26	10.62	2.24	2.21	1.61	2.04	0.84	0.025	0.56	0.31	1.89	98.6	43	221	226
182	6199	26.582	71.23	8.04	1.96	1.77	3.47	1.93	0.74	0.025	0.35	0.4	2.517	89.9	34	274	206
194	6302	36.147	68	8.86	3.42	3.38	2.96	2.81	0.9	0.034	0.28	0.57	3.604	91.2	23	198	69
196	6318	36.450	68.01	8.85	3.21	1.09	3.43	2.78	0.77	0.033	0.28	0.62	4.183	93.3	22	211	79
198	6334	34.571	67.43	8.49	2.94	0.99	3.4	2.81	0.81	0.033	0.27	0.59	3.584	91.3	22	208	67
200	6350	38.075	59.7	8.26	3.14	1.31	3.49	2.64	0.91	0.033	0.29	0.55	3.446	80.3	29	275	85
202	6367	38.066	67.19	9.12	3.21	0.38	3.62	2.23	0.9	0.038	0.28	0.55	3.882	91.4	23	204	51
204	6385	38.027	64.47	8.78	3.09	1.63	3.38	3.23	0.94	0.031	0.28	0.59	3.402	86.4	27	241	69

Average Depth (cm)	Age (cal yr BP)	LOI (%)	SiO_2 (%)	Al_2O_3 (%)	Fe_2O_3 (%)	Na_2O (%)	CaO (%)	MgO (%)	K_2O (%)	MnO (%)	TiO_2 (%)	P_2O_5 (%)	S (%)	Total	Rb (PPM)	Sr (PPM)	Zr (PPM)
206	6398	35.309	65.43	8.22	3.07	0	3.23	2.26	0.79	0.032	0.26	0.57	3.719	83.9	29	267	86
208	6412	35.117	76.88	8.24	4	4.03	2.03	3.21	0.82	0.05	0.25	0.45	3.124	103.1	20	161	61
210	6426	29.614	76.39	6.65	3.76	2.81	1.42	2.52	0.71	0.053	0.24	0.34	2.473	94.9	26	199	196
212	6442	34.532	74.24	7.78	3.64	2.65	1.76	2.95	0.92	0.048	0.23	0.41	2.763	94.6	25	206	96
214	6458	25.827	79.15	6.1	3.06	2.1	2.02	2.29	0.62	0.042	0.21	0.38	2.681	96.0	22	227	213
216	6476	29.100	75.28	6.63	3.19	2.13	2.35	2.3	0.67	0.057	0.21	0.43	3.266	93.2	24	247	148
219	6528	35.091	67.41	7.39	3.81	2.68	2.98	2.29	0.86	0.06	0.22	0.55	3.899	88.3	24	251	60
220	6545	18.111	78.08	3.6	2.01	1.25	5.19	1.22	0.39	0.033	0.17	0.38	2.067	94.4	17	247	158
222	6578	24.310	64.69	4.37	1.84	2.23	8.37	1.48	0.51	0.038	0.17	0.6	2.923	84.3	36	570	213
224	6613	31.617	65.52	4.45	2.13	2.44	7.82	1.45	0.45	0.04	0.18	0.57	3.065	88.1	30	453	214
226	6642	23.648	66.62	4.35	1.95	2.07	8	1.6	0.48	0.036	0.17	0.58	2.732	85.9	37	588	241
228	6670	21.602	68.69	4.06	1.8	2.74	8.02	1.62	0.43	0.034	0.17	0.56	2.631	88.1	37	611	304
230	6716	19.150	74.67	3.66	1.82	2.02	6.09	1.53	0.34	0.031	0.17	0.42	1.936	92.7	30	502	344
232	6762	16.313	78.64	3.42	1.7	1.22	4.87	1.3	0.32	0.027	0.18	0.34	1.612	93.6	26	428	360
234	6806	20.877	67.14	4.01	1.87	2.52	6.07	1.66	0.44	0.031	0.2	0.43	2.219	84.4	35	539	314
236	6852	23.639	69.18	5.21	1.97	2.37	4.79	1.79	0.51	0.029	0.19	0.45	2.904	89.4	33	426	224
238	6894	33.305	62.85	6.46	3.31	0	3.12	1.39	0.7	0.05	0.26	0.41	3.542	82.1	24	265	129
240	6937	25.163	66.35	5.39	2.26	1.96	4.52	1.41	0.5	0.038	0.23	0.49	3.147	86.3	35	438	227
242	6981	32.377	66.12	7.32	3.06	0	2.88	2.35	0.77	0.044	0.27	0.51	3.78	83.3	25	286	168
244	7024	29.940	63.9	6.37	2.73	0	3.18	1.51	0.71	0.041	0.25	0.37	3.404	79.1	24	281	161
246	7072	23.931	50.77	4.49	1.41	4.1	14.77	1.8	0.49	0.033	0.19	0.84	3.313	78.9	49	995	206
248	7117	21.478	52.57	4.14	1.39	4.71	13.88	1.81	0.46	0.034	0.17	0.73	2.485	79.9	48	977	215
250	7162	17.420	58.42	3.69	1.13	2.66	8.94	1.26	0.33	0.021	0.15	0.52	1.841	79.0	39	776	204

Average Depth (cm)	Age (cal yr BP)	LOI (%)	SiO_2 (%)	Al_2O_3 (%)	Fe_2O_3 (%)	Na_2O (%)	CaO (%)	MgO (%)	K_2O (%)	MnO (%)	TiO_2 (%)	P_2O_5 (%)	S (%)	Total	Rb (PPM)	Sr (PPM)	Zr (PPM)
252	7201	18.894	59.49	3.9	1.35	2.86	9.36	1.75	0.38	0.027	0.17	0.53	2.109	81.9	37	735	265
254	7245	21.822	71.54	4.9	1.78	2.91	5.56	1.71	0.43	0.028	0.19	0.44	2.375	91.9	37	551	263
256	7293	21.072	59.63	4.01	1.58	3.11	8.79	1.38	0.4	0.031	0.19	0.52	2.233	81.9	41	765	245
258	7341	24.359	46.59	4.56	1.44	4.98	16.75	1.7	0.55	0.036	0.17	0.86	2.853	80.5	54	1170	163
260	7386	24.353	40.86	4.72	1.37	4.7	18.52	1.58	0.64	0.039	0.17	0.98	3.2	73.6	54	1214	174
262	7433	22.370	51.5	4.32	1.26	3.94	14.69	1.63	0.48	0.033	0.16	0.81	2.702	81.5	47	1003	173
264	7477	19.126	51.64	3.65	1.21	0	13.48	1.07	0.45	0.03	0.15	0.62	2.294	72.3	47	1007	198
266	7523	19.884	55.31	3.89	1.28	4.22	13.22	1.88	0.45	0.036	0.15	0.69	2.283	81.1	46	973	232
268	7566	21.352	62.95	3.96	1.44	3.14	9.8	1.87	0.4	0.033	0.16	0.61	2.506	84.4	43	797	215
270	7616	17.825	59.37	5.14	1.27	2.23	9.92	1.41	0.48	0.028	0.17	0.63	2.502	80.6	49	880	229
272	7663	19.511	59.14	4.37	1.31	3.06	10.19	1.16	0.45	0.028	0.16	0.53	2.166	80.4	48	916	237
274	7711	15.979	70.86	4.49	1.29	0	7.7	1.38	0.39	0.027	0.16	0.55	1.932	86.8	40	702	301
276	7758	13.652	65.6	5.28	1.21	3.31	8.5	1.44	0.43	0.024	0.18	0.6	2.442	86.6	40	708	238
278	7794	19.303	66.98	5.83	1.47	2.55	7.93	1.62	0.46	0.029	0.19	0.62	2.685	87.7	44	732	272
280	7829	25.463	64.27	4.95	1.47	2.28	7.61	1.24	0.42	0.03	0.18	0.56	2.389	85.4	42	727	265
282	7865	19.025	66.66	5.68	1.52	2.15	7.74	1.69	0.44	0.033	0.19	0.58	2.616	86.7	42	699	255
284	7903	20.175	63.35	5.15	1.67	2.23	7.87	1.33	0.44	0.035	0.2	0.55	2.395	82.8	41	682	232
286	7940	17.519	60.11	4.84	1.39	3.22	9.36	1.43	0.43	0.031	0.18	0.59	2.388	84.0	44	784	262
289	8015	18.630	67.01	5.73	1.5	3.45	8.02	1.68	0.45	0.033	0.2	0.56	2.416	88.6	42	711	266
290	8045	18.247	65.6	5.83	1.46	2.24	7.88	1.77	0.45	0.029	0.19	0.58	2.575	86.0	41	674	253
292	8109	18.213	73.33	5.14	2.05	1.38	5.98	1.39	0.4	0.037	0.19	0.46	2.007	90.4	35	552	261
294	8167	25.158	68.06	6.79	2.04	0	3.56	1.45	0.43	0.031	0.24	0.46	2.788	85.8	30	359	228
296	8224	20.433	68.54	8.04	2.01	0	4.29	1.78	0.48	0.031	0.26	0.56	3.499	86.0	37	428	211

Average Depth (cm)	Age (cal yr BP)	LOI (%)	SiO_2 (%)	Al_2O_3 (%)	Fe_2O_3 (%)	Na_2O (%)	CaO (%)	MgO (%)	K_2O (%)	MnO (%)	TiO_2 (%)	P_2O_5 (%)	S (%)	Total	Rb (PPM)	Sr (PPM)	Zr (PPM)
298	8280	18.765	67.35	6.08	1.91	0.53	3.2	1.05	0.38	0.03	0.22	0.36	2.449	81.1	28	342	234
300	8334	13.964	76.61	5.78	1.46	0.85	2.83	1.55	0.31	0.02	0.19	0.4	2.317	90.0	27	315	258
302	8408	16.804	67.14	6.6	1.66	1.63	3.69	1.57	0.45	0.024	0.21	0.45	2.734	83.4	31	365	236
304	8483	17.201	74.82	5.71	1.76	0.87	2.5	1.3	0.31	0.025	0.2	0.4	2.227	90.1	26	283	249
306	8566	17.343	73.39	6.08	1.9	1.11	2.91	1.17	0.35	0.026	0.23	0.4	2.418	90.0	29	320	270
308	8635	14.106	73.47	5.44	1.63	2.82	2.87	1.59	0.33	0.021	0.19	0.33	1.935	88.7	29	320	256
310	8708	24.000	82.54	7.19	1.61	0.92	1.14	1.9	0.26	0.021	0.22	0.39	1.688	96.2	15	200	215
312	8774	21.153	73.28	8.15	1.51	1.38	1.65	2.16	0.34	0.019	0.22	0.49	2.403	89.2	17	232	223
314	8841	19.708	81.57	8.38	1.56	1.97	1.01	1.83	0.27	0.018	0.23	0.44	1.634	97.3	16	204	224
316	8913	17.951	77.71	8.62	1.77	1.71	1.07	2.07	0.28	0.019	0.27	0.44	1.654	94.0	14	194	233
318	8985	24.366	79.87	8.37	1.63	1.23	0.95	1.87	0.27	0.018	0.27	0.41	1.559	94.9	14	190	244
320	9054	20.205	74.36	9.96	1.4	1.94	1.18	2.07	0.31	0.016	0.35	0.49	1.654	92.1	16	199	235
322	9119	22.200	84.97	8.73	1.49	2.37	0.92	1.93	0.25	0.018	0.24	0.39	1.345	102.7	15	190	224
324	9185	17.998	82.41	9.65	1.39	2.09	0.97	2.02	0.26	0.016	0.27	0.42	1.428	100.9	15	187	248
326	9246	18.386	79.03	7.86	1.52	1.41	0.86	1.69	0.23	0.018	0.25	0.38	1.577	94.8	14	171	253
328	9312	16.367	80.6	7.47	1.56	1.32	0.79	1.58	0.26	0.017	0.24	0.31	1.321	95.5	12	157	239
330	9380	14.952	73.12	8.43	1.79	1.58	1.03	1.65	0.33	0.018	0.26	0.37	1.725	90.3	14	171	209
332	9449	14.772	74.99	8.7	1.44	2.36	1.05	1.76	0.32	0.014	0.28	0.41	1.828	93.2	13	161	277
334	9508	25.211	77.23	8.57	1.54	1.84	0.94	1.91	0.3	0.015	0.28	0.4	2.143	95.2	10	140	234
336	9569	14.697	78.13	7.25	1.39	1.38	0.78	1.55	0.24	0.014	0.25	0.35	1.686	93.0	10	138	253
338	9639	14.056	79.01	3.09	4.3	1.5	0.15	0.91	0.09	0.021	0.16	0.18	1.327	90.7	3	14	304
340	9708	14.860	84.35	7.34	1.37	1.38	0.69	1.69	0.21	0.016	0.21	0.33	1.448	99.0	10	131	260
342	9782	15.441	79.94	7.64	1.31	1.55	0.77	1.5	0.23	0.014	0.26	0.37	1.572	95.2	11	134	261

Average Depth (cm)	Age (cal yr BP)	LOI (%)	SiO_2 (%)	Al_2O_3 (%)	Fe_2O_3 (%)	Na_2O (%)	CaO (%)	MgO (%)	K_2O (%)	MnO (%)	TiO_2 (%)	P_2O_5 (%)	S (%)	Total	Rb (PPM)	Sr (PPM)	Zr (PPM)
344	9858	14.725	89.3	7.41	1.25	1.04	0.7	1.64	0.27	0.014	0.22	0.35	1.228	103.4	11	128	271
346	9923	15.948	82.11	7.37	1.25	2.06	0.73	1.79	0.21	0.014	0.24	0.36	1.623	97.8	10	135	242
348	9986	15.778	72.84	8.5	1.22	2.38	0.93	1.75	0.29	0.014	0.29	0.44	1.797	90.5	12	141	266
350	10049	14.421	85.9	7.32	1.11	1.01	0.67	1.79	0.24	0.012	0.21	0.36	1.283	99.9	10	121	240
352	10115	15.436	87.75	6.98	1.21	0.61	0.64	1.66	0.2	0.015	0.21	0.32	1.365	101.0	10	123	254
354	10182	13.497	69.81	6.75	1.09	1.43	0.77	1.38	0.26	0.013	0.25	0.32	1.61	83.7	9	122	264
356	10245	24.876	80.88	8.05	1.08	1.22	0.73	1.88	0.23	0.011	0.22	0.41	1.821	96.5	9	112	249
358	10313	14.728	82.1	6.8	1.14	0.86	0.7	1.64	0.23	0.014	0.21	0.35	1.64	95.7	10	123	268
360	10378	12.596	59.19	11.69	1.56	3.17	1.24	2.25	0.42	0.02	0.32	0.63	2.2	82.7	11	125	232
362	10436	7.900	61	10.67	1.33	2.79	0.98	1.66	0.33	0.016	0.3	0.54	2.151	81.8	8	98	238
364	10493	10.191	69.34	8.87	1.32	1.62	0.84	1.92	0.28	0.014	0.24	0.45	2.223	87.1	10	98	229
366	10562	21.351	70.64	6.11	1.8	1.34	0.7	1.57	0.22	0.018	0.2	0.34	1.872	84.8	9	121	164
368	10628	25.328	76.81	9.1	2.69	1.91	0.89	2.2	0.31	0.027	0.27	0.48	2.548	97.2	16	190	210
370	10699	18.148	81.24	7.15	2.37	1.64	0.64	1.86	0.23	0.022	0.23	0.4	2.246	98.0	12	133	206
372	10768	9.520	64.97	7.8	2.31	3.07	0.59	1.69	0.29	0.018	0.22	0.45	2.51	83.9	7	68	149
374	10843	8.044	81.34	7.19	2.23	2.23	0.4	1.63	0.23	0.016	0.23	0.38	2.125	98.0	6	57	215
376	10924	5.491	82.73	5.4	1.83	0	0.28	1.2	0.14	0.011	0.15	0.29	1.807	93.8	4	38	196
378	11021	7.654	75.24	6.19	2.39	1.83	0.32	1.41	0.19	0.016	0.16	0.34	1.947	90.0	5	43	190
380	11109	6.545	63.85	7.52	3.26	2.11	0.37	1.16	0.26	0.022	0.25	0.43	2.467	81.7	6	49	178
382	11182	8.971	74.3	6.05	2.96	2.29	0.47	1.33	0.2	0.018	0.17	0.39	2.412	90.6	5	57	236
398	12263	5.046	71.46	5.45	4.93	2.07	0.37	1.21	0.18	0.028	0.19	0.33	2.534	88.8	5	40	147
400	12466	9.737	81.61	4.58	5.62	1.75	0.28	1.23	0.12	0.031	0.14	0.25	1.963	97.6	6	45	147
404	12826	3.046	63.72	3.41	4.62	1.64	0.18	0.77	0.1	0.02	0.09	0.21	1.912	76.7	4	16	112

Average Depth (cm)	Age (cal yr BP)	LOI (%)	SiO_2 (%)	Al_2O_3 (%)	Fe_2O_3 (%)	Na_2O (%)	CaO (%)	MgO (%)	K_2O (%)	MnO (%)	TiO_2 (%)	P_2O_5 (%)	S (%)	Total	Rb (PPM)	Sr (PPM)	Zr (PPM)
406	12987	3.316	65.91	3.34	5.6	1.64	0.21	0.89	0.12	0.026	0.1	0.26	2.191	80.3	4	20	100
408	13151	8.559	50.02	4.05	7.68	3.18	0.34	0.78	0.19	0.038	0.18	0.32	3.56	70.3	5	35	71
412	13501	5.862	51.67	4.48	8.65	2.09	0.28	0.62	0.21	0.042	0.17	0.39	3.31	71.9	7	27	78
414	13696	6.258	57.07	3.22	10.48	1.93	0.19	0.86	0.15	0.048	0.2	0.29	2.888	77.3	7	19	352
416	13865	5.049	49.94	3.35	14.06	2.87	0.26	0.79	0.19	0.066	0.19	0.33	3.387	75.4	9	19	222
418	14026	2.422	56.65	2.35	8.12	1.62	0.16	0.74	0.1	0.033	0.54	0.24	2.104	72.7	3	14	1531
420	14185	4.856	47.02	3.75	13.9	2.03	0.21	0.7	0.18	0.063	0.27	0.32	2.349	70.8	10	22	470
422	14362	2.965	72.02	2.81	6.86	1.57	0.15	0.96	0.08	0.046	0.86	0.34	1.567	87.3	4	18	3307
424	14537	4.380	67.68	4.24	6.98	1.59	0.23	1.02	0.15	0.038	0.3	0.32	2.339	84.9	6	26	553
426	14705	3.509	56.83	4.59	10.99	2.16	0.28	0.87	0.19	0.062	0.2	0.4	3.453	80.0	9	27	201
428	14887	3.413	82.73	4.26	5.87	0	0.25	0.97	0.21	0.047	0.18	0.31	1.553	96.4	8	22	252
430	15076	5.452	70.17	1.73	7.3	0	0.13	0.82	0.06	0.035	0.37	0.18	1.707	82.5	3	12	558
432	15260	6.886	60.58	1.32	17.03	2.09	0.18	0.76	0.08	0.074	0.43	0.19	2	84.7	12	13	936
434	15415	4.214	75.87	2.44	5.87	2.11	0.17	0.95	0.1	0.023	0.16	0.22	1.829	89.7	3	14	234
436	15578	2.769	59.79	1.84	9.78	2.38	0.16	0.74	0.08	0.039	0.21	0.2	1.892	77.1	6	14	367
438	15733	3.027	74.02	8.6	1.4	1.31	0.89	1.61	0.26	0.013	0.24	0.43	1.811	90.6	11	141	273
440	15911	2.175	71.37	2.02	5.32	0	0.15	0.85	0.08	0.024	0.11	0.15	1.541	81.6	3	12	151
442	16078	0.943	79.67	1.84	3.77	0	0.12	0.93	0.04	0.015	0.06	0.13	1.267	87.8	1	9	132
444	16226	1.585	73.32	1.7	4.98	2.23	0.13	0.7	0.07	0.022	0.13	0.09	1.141	84.5	2	8	139
446	16394	0.871	63.28	1.76	5.47	0	0.14	0.56	0.06	0.022	0.13	0.15	1.425	73.0	2	10	308
448	16560	1.878	70.11	2.04	4.95	0	0.14	0.88	0.09	0.022	0.1	0.14	1.391	79.9	2	9	146
450	16734	1.326	66.25	3.15	6.32	2.28	0.21	0.76	0.13	0.036	0.43	0.26	2.361	82.2	4	15	356
452	16904	2.539	87.52	2.38	4.82	0	0.16	1.06	0.07	0.024	0.27	0.18	1.379	97.9	3	14	684

Average Depth (cm)	**Age (cal yr BP)**	**LOI (%)**	**SiO_2 (%)**	**Al_2O_3 (%)**	**Fe_2O_3 (%)**	**Na_2O (%)**	**CaO (%)**	**MgO (%)**	**K_2O (%)**	**MnO (%)**	**TiO_2 (%)**	**P_2O_5 (%)**	**S (%)**	**Total**	**Rb (PPM)**	**Sr (PPM)**	**Zr (PPM)**
454	17088	4.065	68.71	1.58	6.93	0	0.12	0.75	0.05	0.026	0.37	0.21	1.723	80.5	2	12	2441
456	17262	6.326	73.49	2.03	8.38	0	0.16	0.98	0.07	0.035	1.26	0.36	2.053	88.8	4	12	5232
458	17410	2.951	52.91	1.96	9.46	1.78	0.2	0.77	0.1	0.038	0.66	0.26	2.068	70.2	4	14	1751
460	17575	1.804	76.21	2.06	7.07	1.68	0.15	0.97	0.07	0.028	0.59	0.23	1.537	90.6	3	14	2108
462	17742	3.107	59.09	3.53	9.21	1.81	0.25	0.9	0.2	0.039	0.25	0.25	2.621	78.2	6	18	799
464	17905	1.910	72.6	2.39	3.92	1.72	0.16	0.91	0.09	0.014	0.1	0.19	1.955	84.0	3	10	150
466	18074	0.973	77.82	1.62	6.01	1.31	0.14	0.82	0.05	0.024	0.77	0.16	1.189	89.9	2	11	2282
468	18238	1.654	75.32	1.71	5.04	0	0.15	0.8	0.07	0.02	0.56	0.17	1.198	85.0	3	10	1726
470	18377	0.728	77.03	1.77	2.25	1.3	0.11	0.81	0.06	0.007	0.35	0.13	1.086	84.9	2	8	850
472	18527	0.954	82.47	1.77	2.8	1.7	0.11	0.84	0.05	0.01	0.3	0.17	0.964	91.2	2	8	1372
474	18674	0.742	78.88	1.87	4.19	1.3	0.16	0.94	0.08	0.016	0.2	0.16	1.357	89.2	2	10	543
476	18814	0.878	82.73	2.29	5.07	1.75	0.19	0.99	0.11	0.021	0.3	0.17	1.437	95.1	4	12	1443
478	19060	1.581	59.63	4.35	4.87	1.89	0.31	1.03	0.22	0.018	0.21	0.28	2.805	75.6	4	20	328
480	19152	2.047	72.91	3.25	2.06	1.45	0.19	1.07	0.1	0.007	0.11	0.18	1.766	83.1	4	16	240
482	19513	1.041	61.58	3.32	5.62	1.68	0.31	1.19	0.2	0.022	0.27	0.25	2.921	77.4	4	17	458
484	19840	1.738	61.27	3.39	4.29	2.05	0.26	1.07	0.17	0.016	0.14	0.24	2.571	75.5	3	16	170
486	20148	2.020	77.11	2.49	1.48	1.55	0.14	1.06	0.09	0.004	0.07	0.14	1.384	85.5	3	13	151
488	20476	2.058	66.25	3.04	4.27	2.18	0.24	1.04	0.15	0.015	0.24	0.22	2.151	79.8	3	16	381
490	20795	1.118	72.51	2.84	2.2	1.31	0.2	1.09	0.1	0.007	0.12	0.18	1.819	82.4	3	16	204
492	21117	1.662	63.37	2.98	4.62	2.04	0.23	1.02	0.14	0.017	0.32	0.23	2.427	77.4	4	17	464
494	21494	1.088	64.77	2.64	3.91	1.34	0.19	1	0.13	0.013	0.2	0.19	2.036	76.4	2	11	349
496	21912	0.858	73.77	2.36	2.8	1.5	0.17	1.03	0.11	0.01	0.13	0.16	1.776	83.8	2	12	135
498	22344	1.319	70.84	2.54	3.85	1.39	0.21	1	0.12	0.014	0.16	0.17	1.869	82.2	2	11	207

Average Depth (cm)	Age (cal yr BP)	LOI (%)	SiO_2 (%)	Al_2O_3 (%)	Fe_2O_3 (%)	Na_2O (%)	CaO (%)	MgO (%)	K_2O (%)	MnO (%)	TiO_2 (%)	P_2O_5 (%)	S (%)	Total	Rb (PPM)	Sr (PPM)	Zr (PPM)
500	22732	1.574	67.67	2.41	3.39	1.57	0.17	0.84	0.11	0.012	0.09	0.15	1.856	78.3	2	11	124
502	23129	0.909	75.33	2.32	3.13	1.48	0.17	1.09	0.1	0.011	0.19	0.17	1.61	85.6	3	13	220
504	23497	1.788	79.11	3.56	3.14	1.23	0.23	1.04	0.14	0.013	0.24	0.18	1.524	90.4	5	18	515
506	23835	0.969	73.91	2.81	3.14	1.14	0.22	0.94	0.16	0.011	0.18	0.19	1.559	84.3	4	12	326
508	24197	0.959	79.27	2.7	2.44	1.33	0.2	0.97	0.15	0.009	0.09	0.15	1.333	88.6	4	11	222
510	24618	0.508	71.05	3.05	3.44	1.48	0.29	0.85	0.27	0.013	0.14	0.16	1.604	82.3	10	17	386
512	25007	0.703	91.77	2.69	1.79	0	0.17	1.04	0.16	0.008	0.12	0.12	0.879	98.7	8	12	282
514	25425	0.734	75.7	3.32	1.85	2.03	0.24	0.84	0.28	0.007	0.14	0.16	0.958	85.5	11	13	171
516	25811	1.116	71.55	3.77	1.75	1.57	0.26	0.95	0.27	0.006	0.12	0.19	1.385	81.8	13	20	144
518	26182	0.802	75.37	3.25	2.01	1.2	0.22	1.01	0.21	0.007	0.12	0.12	0.997	84.5	6	14	220
520	26566	0.757	77.01	3.29	1.94	0	0.24	0.97	0.23	0.008	0.15	0.14	1.094	85.1	7	12	164
522	26967	0.305	81.08	3.09	1.76	1.14	0.25	0.98	0.21	0.006	0.19	0.16	1.086	90.0	7	14	564
524	27418	0.818	83.59	3.76	1.32	1.29	0.25	1.18	0.27	0.006	0.17	0.15	0.889	92.9	10	14	206
526	27852	0.498	75.85	3.46	1.1	1.34	0.19	1.04	0.15	0.003	0.14	0.18	0.814	84.3	5	14	496
528	28244	0.980	70.76	3.8	1.23	1.71	0.21	0.93	0.16	0.003	0.16	0.17	1.034	80.2	5	14	392
530	28581	0.859	78.47	4.62	1.7	1.53	0.25	1.39	0.19	0.006	0.29	0.22	1.304	90.0	4	20	980
532	28908	0.912	73.34	4.2	0.99	1.75	0.21	1.18	0.18	0.003	0.15	0.2	1.268	83.5	4	19	988
534	29231	1.023	76.29	4.56	0.95	1.37	0.21	1.28	0.14	0.002	0.28	0.19	1.005	86.3	2	19	779
536	29564	1.128	75.93	5.53	1.22	1.98	0.28	1.31	0.21	0.005	0.29	0.23	1.184	88.2	6	22	442
538	29910	1.508	73.9	5.11	0.95	1.51	0.26	1.28	0.19	0.003	0.2	0.21	0.925	84.5	4	21	280

Appendix B: Isotope Data

Depth	Age	δ13C (VPDB)	Depth	Age	δ13C (VPDB)
12	1000	-23.73	**296**	8224	-25.07
16	1111	-25.21	**300**	8334	-24.47
20	1402	-25.12	**304**	8483	-25.23
28	1828	-24.51	**308**	8635	-24.40
32	2075	-24.76	**316**	8913	-25.56
40	2541	-25.29	**324**	9185	-25.26
48	3070	-25.94	**326**	9246	-23.88
52	3271	-24.56	**330**	9380	-24.90
56	3466	-25.59	**334**	9508	-25.52
60	3714	-22.79	**338**	9639	-24.55
68	3951	-23.32	**342**	9782	-25.20
72	4078	-23.32	**346**	9923	-24.77
76	4244	-22.93	**358**	10313	-23.85
84	4544	-22.41	**378**	11021	-23.92
88	4697	-22.42	**398**	12263	-25.67
96	4985	-23.48	**408**	13151	-24.87
100	5190	-23.12	**424**	14537	-23.03
104	5417	-25.02	**432**	15260	-27.08
108	5638	-23.17	**440**	15911	-26.26
120	5731	-24.67	**452**	16904	-25.49
144	5909	-23.22	**462**	17742	-25.77
172	6118	-25.36	**470**	18377	-26.39
194	6302	-25.38	**478**	19060	-25.67
206	6398	-25.28	**486**	20148	-25.17
222	6578	-23.44	**494**	21494	-24.62
230	6716	-25.28	**498**	22344	-25.83
238	6894	-26.12	**504**	23497	-26.12
250	7162	-25.82	**508**	24197	-26.57
256	7293	-25.74	**512**	25007	-27.19
264	7477	-25.77	**518**	26182	-26.90
272	7663	-25.48	**522**	26967	-26.55
280	7829	-24.44	**528**	28244	-26.72
288	8015	-24.98	**536**	29564	-26.35